SYNTHESIS AND PHOTOPHYSICS OF DENDRONIZED NANOMATERIALS

by

ROLANDE R. HODEL

A dissertation submitted to the Graduate Faculty in Chemistry
in partial fulfillment of the requirements for the degree of
Doctor of Philosophy, City University of New York

2005

INFORMATION TO USERS

The quality of this reproduction is dependent upon the quality of the copy submitted. Broken or indistinct print, colored or poor quality illustrations and photographs, print bleed-through, substandard margins, and improper alignment can adversely affect reproduction.

In the unlikely event that the author did not send a complete manuscript and there are missing pages, these will be noted. Also, if unauthorized copyright material had to be removed, a note will indicate the deletion.

ProQuest Information and Learning Company
300 North Zeeb Road
P.O. Box 1346
Ann Arbor, MI 48106-1346

This manuscript has been read and accepted for the
Graduate Faculty in Chemistry in satisfaction of the
dissertation requirement for the degree of Doctor of Philosophy.

04/25/05
Date

Chair of Examining Committee

April 25, 2005
Date

Executive Officer

Dr. Harry D. Gafney

Dr. Robert Engel

Dr. Klaus Grohmann

Dr. Neil McKelvie

Supervision Committee

THE CITY UNIVERSITY OF NEW YORK

THE CITY UNIVERSITY OF NEW YORK

Abstract

SYNTHESIS AND PHOTOPHYSICS OF DENDRONIZED NANOMATERIALS

by

Rolande R. Hodel

Advisor: Professor Dr. Harry D. Gafney

Quantum dots (QDs) refer to a size domain in which the physical properties of a material are a function not only of its composition, but also its size. Generally size is controlled through the introduction of a surfactant. Traditionally, n-trioctylphosphine oxide (TOPO) is added to limit the extent of aggregation of the semiconductor cadmium selenide (CdSe). However, TOPO binds strongly to the QDs surface. This research was undertaken using octadecene (ODE) as the coating agent. Here, we describe the synthesis of CdSe quantum dots in ODE, and show that a narrow range of dot sizes is accessible. We also demonstrate that the surface of ODE coated QDs, unlike their TOPO coated counterparts, can be modified by means of a phase transfer reaction. Furthermore, the weaker binding of ODE to the dots presents the opportunity for covalently attaching aliphatic and aromatic thiol functionalized dendrimer wedges, called dendrons. Change in photophysics caused by the attachment of thiol dendrons is measured using absorption, emission intensity and lifetime. The composition of dendronized QDs of a specific size was determined by thermogravimetric analysis, and elemental analysis is our final goal.

ACKNOWLEDGEMENTS

I would like to express my sincere appreciation to Professor Harry D. Gafney, my thesis advisor, for his hands off guidance and generous wisdom supporting my research and the existence of this thesis. I thank my committee members, Professor Grohmann, Professor Engel, Professor McKelvie for their efforts and valuable discussions at many times during the course of my program. Dendron synthesis was performed in part at City College, CUNY under the supervision of Professor Balogh-Nair.

I thank José Zambrano and Dr. Julie Colis for the lifetime measurements. Thank you to members of Dr. Gafney's research group, in particular Dr. Dehipawalage Sunil, Elena Ferloni, and Shantha Amarasinghe for engaging in discussions, which often clarified my thoughts and furthered this project in important ways. Thank you to Dr. Cliff Soll of the Hunter College/CUNY Mass Spectrometry Facility for providing mass spectroscopy data. Dr. Gopal for support with the NMR, Dr. Bonnie Gersten for the TEM picture, and Dr. Shlomit Chappel for running x-ray diffraction. Very special thanks to Dr. Cherice Evans for her efforts proofreading this thesis.

Dedicated to:

My mother, Erna Fischer, thank you for who you are. Thank you for your passion and love.

And to my dear partner Betti K. Lewis for her loving support, her cheering and her unwavering belief in the success of this thesis.

And to my Forum leader and coaches at Landmark Education Corporation, for having created the possibility to make this dream come true.

TABLE OF CONTENTS

Part III Experimental

LIST OF TABLES

LIST OF FIGURES

LIST OF SCHEMES

Statement of Problem:

The primary focus of this dissertation is to determine if the photophysical properties of CdSe QDs can be improved by replacing an organic coating with an organic matrix, specifically, covalently bound aliphatic and aromatic thiol dendrons. CdSe QDs are commonly synthesized in trioctylphosphine oxide (TOPO) that serves as the reaction solvent and as coating for the QDs. The disadvantage of TOPO is that it is bound strongly to the cadmium ion and thus resists being displaced by thiol dendrons. To solve the problem of residual coating, CdSe QDs will be synthesized in octadecene that will again act simultaneously as solvent and coating. Photophysical measurements such as absorption and photoluminescence spectroscopy will demonstrate whether ODE is a suitable coating for the synthesis of CdSe QDs. Nuclear magnetic resonance measurements will be employed to prove the extent of coating replacement by the dendron.

To preserve a small size for the QDs and to keep them from agglomerating, QDs must be coated at all times. This passivation of the surface states may stabilize the QD, enhance photoluminescence and reduce nonradiative decay pathways, thereby increasing the quantum efficiency of emission from the QD. Thus, one part of this work is the synthesis of Fréchet-type polybenzylether dendrons of different generation for later attachment to CdSe QDs. The main work will be to determine how to attach the dendrons successfully to the QD and to investigate photophysical changes.

Part I Introduction

1. Introduction

Since Richard P. Feynman (Nobel Laureate in Physics, 1965) first predicted the field of nanotechnology more than half a century ago in his famous 1959 Cal Tech lecture entitled, "There is Plenty of Room at the Bottom", nanotechnology has become a major player in science.[1] Nanotechnology is the process of generating, manipulating and deploying nanomaterials, which are materials possessing sizes on the order of a few nanometers, or 1/1,000,000,000 of a meter. This technology represents an area in science holding significant promise, since nanomaterials, hundreds of times smaller than human cells, offer properties different from molecular and bulk species. In fact, the particle size range for nanomaterials is similar to that of the macrocomponents in cells. Therefore, the impact nanotechnology will have on communications, information storage, and material sciences is anticipated to be comparable to that of the *nuclear revolution* of the 1930s,[2] or the *molecular revolution* in the life sciences in the 1980s.[3-5] At the same time, understanding the principles of nanotechnology may provide an infrastructure which can be extended to give insights into critical biologic systems related to diagnostics, disease control, correction of genetic disorders, and longevity.[6,7]

The classical approach to nanoscale materials, referred to as the *top down* approach, has been to utilize traditional engineering principles that remove unwanted domains from macroscopic materials by grinding, casting, lathing or using small-scale

lithography. This strategy offers very little control over critical molecular features such as atomic position or final size of the nanoparticle. On the other hand, the manipulating and positioning of individual atoms and molecules has now been realized. Heinrich Rohrer (Nobel Laureate, 1986)[8] used a scanning tunneling microscope (STM) tip to resolve atomic-scale features on the surface of even the poor, conducting material silicon, Si(111). Himpsel et al. pushed the envelope further, distinguishing different oxidation states in non-conducting nanostructures of CaF_2 and CaF on Si (111).[9] In 1989, Don Eigler created the now well-known display made of 35 xenon atoms on a nickel surface spelling out "IBM" and demonstrating that atom positioning can be controlled precisely. This was achieved at high vacuum and near liquid helium temperature. Today, atoms can be positioned under ambient conditions,[10] something necessary if these processes should ever find commercial applications.[11] Furthermore, Franz Himpsel and co-workers have recently been able to create 2D arrays of gold atoms on silicon that resemble the bit structure of a standard CD-ROM, but at the nano- instead of micro-scale, and to write to these arrays by removing individual clusters of gold atoms.[11] With this advancement, Himpsel and co-workers have realized the storage of 1 bit of information in a 5 x 4 atom unit cell, which is very close to the 5 x 5 x 5 atom volume that Feynman predicted.[1]

In recent years, the excitement generated by nanotechnology has lead to an ever-expanding use of the term. Today nanotechnology includes any material with significant features less than 100 nanometers in size.[12] With this new expanded definition, *nanotechnology* is no longer limited to making nanoscale productive systems, as envisioned by Feyman, but now includes anything with small features, *i.e.*, fine particles,

thin coatings, large molecules, or even 'big things' with 'tiny holes' such as doped zeolites, glasses, clays, alumina or silica.[13] Therefore, many areas of chemistry, materials science, microelectronics, and biotechnology can now be categorized as nanotechnology.

The work in this dissertation is concerned with one specific area of nanotechnology, namely that of semiconductor nanocrystals referred to as quantum dots (QDs). The application of energy, usually in the form of photons, to a semiconductor can excite an electron from the valence band to the conducting band if the excitation energy is close to or greater than the band gap energy. The excitation of the electron leaves a hole, or positive charge, in the valence band. The hole, in turn, is coupled to the excited electron via a Coulomb interaction, thereby slightly lowering the total energy of the system. This electron-hole pair is referred to as an *exciton.* In quantum dots (QDs), the overall size of the material is smaller than the exciton Bohr radius. The size of the nanoparticle limits the number of energy levels, and leads to transitions with smaller half-widths. This situation, referred to as quantum confinement, leads to changes in the absorptive and emissive behavior of the semiconductor material.[14]

In 1982 Rossetti and Brus[15] reported the first preparation of a group II-VI semiconductor nanoparticle, namely cadmium sulfide (CdS), with a mean particle diameter of greater than 20 nm. These authors also investigated the band-edge luminescence properties, reported in the same paper. However, quantum confinement effects, such as a change in the band gap as a function of particle size, were not observed since the size range of the particles was larger than the exciton Bohr radius.[16] Ten years

later, Bawendi and coworkers at the Massachusetts Institute of Technology (MIT)[17] reported the organometallic synthesis of nearly mono-dispersed, high quality quantum dots (QDs) of cadmium sulfide (CdS), cadmium selenide (CdSe), and cadmium telluride (CdTe). However, this breakthrough synthesis required reaction temperatures above the flash point of *n*-trioctylphosphine oxide (TOPO), the coating for the quantum dots as well as the reaction solvent. Furthermore, highly toxic dimethyl cadmium and dimethyl selenium precursors were employed in this synthesis. Today, TOPO coated CdSe quantum dots are produced commercially (Evident Technologies, Applied NanoWorks). However, with a cost of $40/mg of material, using these QDs for additional studies is prohibitively expensive.

Recently, Peng et al.[18-20] reported a much improved, versatile, and environmentally friendly synthesis. Studying the Bawendi synthesis, Peng found that hexylphosphonic acid (HPA), an impurity in TOPO, plays a major role.[21] Once the dependence on hexylphosphonic acid was discovered, Peng and coworkers were able to develop a broad array of possible precursors and solvents for the synthesis of high-quality CdSe QDs. "High-quality" refers to QDs being comprised of crystalline particles with narrow size distribution, good photo stability, and surface properties that allow for high luminescence quantum yields.[22] Research has shown that surface passivation of free valences at the particle surface can be achieved by epitaxial overcoating QDs with inorganic materials. This suppresses the radiationless recombination and causes an increase in luminescence quantum yield. Similar results have yet to be achieved when passivating the surface with organic materials. The first goal of this thesis is to synthesize

reliably and repeatedly high-quality CdSe QDs starting with cadmium oxide (CdO) and a combination of reagents identified by Peng, *et al.*[18] The details of this synthesis will be presented in Chapter 9.

CdSe QDs are stronger emitters, with a 5-15 % luminescence quantum yield,[23] than, for example, are many organic fluorescent dyes.[24,25] Using wavelength matched fluorescent latex spheres as a standard, the fluorescence intensity of a single CdSe QD was found to be equivalent to that of approximately 20 rhodamine molecules.[26] However, to increase the utility of the CdSe quantum dots for biotechnology and lighting applications, the strength of emission needs to be increased. Different approaches to accomplish this have been reported. In an effort to increase luminescent output, Guyot-Sionnest and Hines developed an improved method to synthesize CdSe QDs with an inorganic coating of zinc sulfide (ZnS). Abbreviated CdSe/ZnS, these QDs are referred to as core/shell nanocrystals.[27] As observed previously by Brus,[15] the ZnS coating enhances the fluorescence quantum yields of the nanocrystal by 40-60%. Zinc sulfide (ZnS), zinc selenide (ZnSe) and other coating materials such as those listed in Chapter 2.3 (Table 2.3) also serve as coatings to prevent agglomeration and crystal growth.[28] Most applications require small particles with narrow size distribution. To prevent agglomeration and crystal growth the QDs have to be coated or embedded in a matrix. Inorganic coatings generate a core/shell type QD. One way to synthesize core/shell QDs is by adding alternating dimethylzinc (Me_2Zn) and bis(trimethylsilyl)sulfide ($[TMS]_2S$) to a solution of CdSe QDs.[27]

CdSe QDs are synthesized in an *n*-trioctylphosphine oxide (TOPO) and *n*-trioctylphosphine (TOP) solution. TOPO/TOP serves a dual function as reaction solvent and as organic coating, which prevents the QDs from agglomerating. The luminescence quantum yield of TOPO/TOP coated CdSe QDs does not exceed 5-15% of the theoretically possible 100% as compared to a rhodamine G6 standard.[23] Attempts to modify the QD surface by first removing TOPO using pyridine as the interim coating before attaching organic thiols was only partially successful.[29] Thermogravimetric analyses (TGA) indicate incomplete removal of the TOPO coating. Experiments show that after the introduction of the new coating (pyridine), 10-15% of TOPO remains bound on the QD surface. These TGA results were confirmed by quantitative proton nuclear magnetic resonance spectroscopy (NMR) studies. Bawendi reasons that since only 30% of all possible surface cadmium binding sites are passivated with TOPO before the TOPO coating is exchanged, the 10-15% remaining TOPO ligands after that exchange reaction may take the form of bridging positions binding over several cadmium atoms which would account for stronger bonding strength observed.[30] It is known that the oxygen in TOPO is datively bound to Cd^{+2}, and the phosphorus in TOP is covalently bound to Se^{-2}.[31] However, despite the difficulties, many attempts to increase luminescence quantum yield by modifying the organic coating surface of CdSe QDs have been undertaken starting out from TOPO/TOP coated QDs, but to date, with limited success. One exception is the recent report of the use of an organic coating, namely long chain primary amines, to result in an increased luminescence quantum yield similar to that found with core/shell QDs.[27,32,33]

To improve systematically the luminescence output and quantum yield through surface modification, and to facilitate complete surface exchange, the work presented here is performed exclusively using CdSe QDs coated and dissolved in octadecene (ODE).[20] With only a double bond to donate electron density to the positively charged cadmium ion, ODE may be considered to be more weakly bound to the QD than TOPO/TOP. One indication of this weak binding constant is the fact that CdSe/TOPO/TOP coated QDs can be easily precipitated from ODE by adding TOPO to an ODE solution of ODE coated CdSe quantum dots. The successful exchange is readily apparent through a dramatic change in the solubility of the QDs. TOPO/TOP coated QDs dissolve in polar solvents, such as chloroform, and not in non-polar solvents like hexane as is preferred by their ODE coated counterparts. TOPO/TOP coated QDs precipitate using acetone or butanol, while ODE coated QDs precipitate from a chloroform/methanol mixture.[20]

The term "dendrimer" derives from the Greek words "dendron" meaning tree, and "meros" meaning part, and was introduced in 1984 by Donald A. Tomalia.[34,35] Dendrimers are well-defined hyper-branched globular macromolecules constructed around a core unit. During synthesis, each successive reaction step, or series of the same alternating reaction steps, leads to an additional generation of branching. The initial method of dendrimer synthesis was Tomalia's divergent approach.[36] However, in 1989, Fréchet *et al.* synthesized dendrimers by a convergent method.[37] The convergent approach has definite advantages over the divergent method, since the latter method starts with the core unit and adds each additional generation, risking structural defects that

cannot easily be repaired. The convergent method, on the other hand, starts on the periphery of the dendrimer and works towards the core. The number of synthetic steps per generation stays constant, but defects can be eliminated by column chromatography if necessary. The same principle is true for dendrons, since the difference between a dendron and a dendrimer is that the former has a focal point instead of a core and is shaped like slices of a round pie while the latter is the whole pie.

Since the primary focus of this dissertation is to manipulate the photophysical properties of CdSe QDs by the attachment of various types of dendrons to the OD, the synthesis and characterization of the dendronized QDs were performed (cf. Chapter 7). Characterization included UV-Visible absorption spectroscopy, photoluminescence (PL) spectroscopy, nuclear magnetic resonance spectroscopy (NMR), transmission electron spectroscopy (TEM), thermogravimetric analyses (TGA), and X-ray powder diffraction (XPD). Finally, an attempt to determine the number of dendrons of different generations that are attached per QD is presented along with a discussion of the effect of dendron size on luminescence of the QDs in Chapter 8.

2. Nanomaterials

2.1 Bulk Semiconductor Materials

Semiconductors are crystalline materials with properties between a pure conductor (such as gold or copper) and an insulator (such as rubber or teflon). Semiconductors can be pure crystals like silicon or may be composed of elements from the periodic groups of II-VI, III-V, or IV-VI. Since the conduction can be tuned by temperature, controlled doping with a conducting material, or other external stimuli, semiconductors are widely used in the electronics and computer industries.

Although the composition of semiconductors vary, all semiconductors require an external stimulus such as voltage or photon flux to conduct electricity. The advantage of a required stimulus is that it allows one greatly to alter the electrical conductivity of the material in a controlled manner. In a bulk semiconductor, the large number of atoms, typically on the order of 10^5 leads to many degenerate energy levels, which effectively form bands, rather than discrete energy levels. At ambient temperature and in the ground state, electrons are located in the lower energy continuum, known as the valence band, while the higher energy continuum (*i.e.*, conduction band) is unoccupied. These two bands are separated by an energy gap (E_g), the magnitude of which is a characteristic property of the bulk macro crystalline material and is typically between 0.3 eV and 3.8 eV.[38]

Figure 2.1. A depicts the energy levels in a molecule. Each pair of bonding electrons in a molecule adds one bonding and one antibonding molecular orbital to the energy diagram. Figure 2.1 A shows three bonding molecular orbitals (MO) and three antibonding MO's. When a molecule is excited an electron moves from the highest occupied molecular orbital (HOMO) to the lowest unoccupied molecular orbital (LUMO) as indicated with a solid line arrow pointing up. Eventually the molecule relaxes and the electron returns back to the ground state, represented with the dashed arrow pointing down. The energy levels in a molecule are distinct when compared to the closely spaced energy levels that form the two continuum bands of a semiconductor material, as shown in Figure 2.1. B. These two bands are separated by the band gap energy E_g.[39] When energy is supplied in the form of heat, voltage or photons, electrons from the valence band that gain enough energy move across the band gap to the conducting band. As mentioned before, this excitation leaves a hole or positive charge in the valence band. Since a Coulomb attraction exists between the excited electron and the valence hole, the electron and hole form a "bound" pair known as an exciton.

In a bulk semiconductor of known composition, the band gap energy is fixed. Naturally, the excited electrons stay only briefly in the conduction band before returning to the valence band. As the excited electrons return to the valence band, electromagnetic radiation corresponding to the energy of the band gap is emitted. The band gap and, therefore, the transition are fixed which, in turn, defines the emission wavelength for the system. The band gap spacing is a characteristic property of the semiconductor and is related to the distance between any given electron/hole pair, *i.e.*, the Bohr radius.

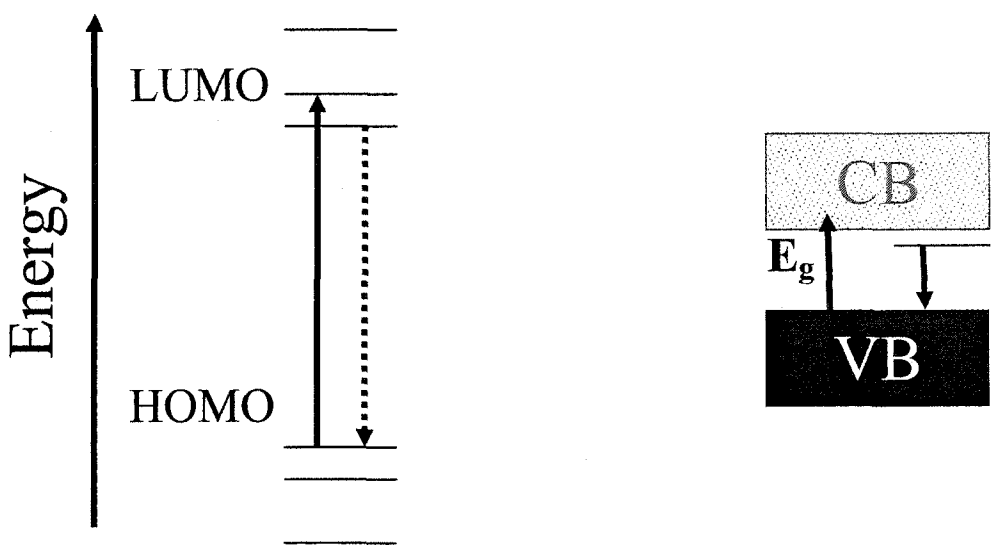

Figure 2.1. (**A**) Molecular orbital diagram with highest occupied molecular orbital (HOMO) and lowest unoccupied molecular orbital (LUMO). Energy levels are discrete. (**B**) Semiconductor energy diagram with valence band (VB) and conducting band (CB). Energy levels are continuous.[40]

The Bohr radius of the bulk exciton is given by

$$\alpha_B = \frac{\hbar^2 \varepsilon}{e^2}\left[\frac{1}{m_e^*} + \frac{1}{m_h^*}\right] \quad (1)$$

where α_B is the Bohr radius, ε is the bulk optical dielectric coefficient, ħ is the Planck's constant divided by 2π. m_e^* and m_n^* are the effective masses of the electron and hole, respectively, and e is the charge on the electron.[38] Selected elemental and compound bulk semiconductors and their optical characteristics are summarized in Table 2.1.

Table 2.1. Selected elemental and compound bulk semiconductors and their optical characteristics. *Eg* is the band gap of the bulk semiconductor in (eV.) and λ T is the approximate photoconduction threshold wavelength in (nm). Adapted from[13]. CdS, CdSe, CdTe band-gap energy *Eg* in (nm).[17]

Semiconductor	*Eg* (eV)	λ T (nm)
Elemental		
Si	1.12	1107
Ge	0.66	1879
Oxides		
TiO_2 (rutile)	3.00	413
TiO_2 (anatase)	3.15	394
ZnO	3.35	370
WO_3	3.2	388
MoO_3	2.9	428
Fe_2O_3	2.2	564
SnO_2	3.8	326
Chalcogenides		
CdS	2.42 (512 nm)	512
CdSe	1.70 (716 nm)	729
CdTe	1.50 (827 nm)	827
ZnS	3.2	388
ZnSe	2.58	481
PbS	0.50	2480
HgS	0.50	2480
HgTe	0.14	8857
Groups III-V		
GaAs	1.43	867
GaP	2.24	554
InAs	0.33	3758
InP	1.29	960

Nanocrystal research was originally motivated by the desire to understand better the bulk structural and electronic properties of semiconductor materials by looking at their properties on the molecular scale.[41] Quantum dots are one type of nanomaterial with a characteristic size of 1-10 nm in diameter. As will be shown in the next section, quantum dots display a wealth of energy transitions. Their band gap energy can be manipulated by changing the size of the quantum dot, offering the opportunity of a much wider range of emission wavelengths.

2.2 Nanomaterials

In 1996, Paul Alivisatos published the first review article on semiconductor nanocrystals.[40] There he described efforts made to understand novel bonding geometries and the state of knowledge about structure and composition of colloidal semiconductor nanocrystal surfaces. Since this time, additional reviews have been published. A selection of which are discussed here. Wise[42] focuses his review on the influence of surface effects on QD properties by proposing to study semiconductors of group IV-VI, such as lead sulfide (PbS) and lead selenide (PbSe). He noted that certain nonlinear optical properties of quantum dots would be most enhanced in the strong confinement limit (*i.e.*, where $R / \alpha_B << 1$ with R being the radius of the quantum dot and α_B the Bohr radius of the bulk exciton given by equation 1). The most common materials of the group II-VI and III-V semiconductors do not reach strong enough confinement, since R / α_B is only 0.16. However, according to Wise, PbS and PbSe quantum dots fall within the strong quantum confinement limit with $R / \alpha_B = 0.04$. This fact led to electronic spectra with energy

spacings that allow for the investigation of quantum effects without the influence of the bulk surface states. The review by O'Brien[38] focused on the preparation of nanoparticles. In particular, the review discussed synthetic methods such as arrested precipitation in solution[23,43] and matrix assisted synthesis in various types of matrices including zeolites,[44,45] micelles,[46] glasses,[47,48] and films.[49] The molecular precursor method described by Bawendi and coworkers was the first published organometallic synthesis of CdS, CdSe, and CdTe quantum dots.[17] The main advantages of this method are the degree of control over particle size and its versatility in allowing for chemically altering the surface of a QD. The same year, Rajeshwar published a review on semiconductor-based composite materials that also included a chapter on nanomaterials.[13] Today the importance of nanomaterials is reflected in the increasing number of journals dedicated solely to nanotechnology, the large number of national and international conferences, the creation of nanotech science centers, and the increasing number and value of government grants. Most recently, Rotello reviewed the status of nanocrystal research and outlined the new opportunities afforded through the use of nanocrystalline material today. His focus was on the ability to control nanoparticle properties within the synthetic design by allowing for the formation of self-assembled monolayer systems.[50] By manipulating the synthetic procedures, control from the molecular to the microscopic level can be provided. Table 2.2 lists some of the semiconductor nanomaterials routinely synthesized today.

There are two major effects that are responsible for the uniqueness of quantum dots as compared to their bulk counterparts. First, in nanocrystals the number of surface

atoms is a large fraction of the total, making it useful in catalysis and biological applications. Second, quantum size effects transform the intrinsic properties of the nanocrystals. The actual size of the particle determines the electronic and physical properties of the material. For example, in cadmium sulfide (CdS), a widely used material to study quantum size effects, the band gap can be tuned from 2.5 to 4.0 eV., while the excitation lifetime ranges from several nanoseconds down to picoseconds[51]. Never before seen physical changes are manifested by a fourfold drop in melting temperature of CdS quantum dots from 1600°C to 400°C[52,53] which may eventually lend itself to applications such as lead free solder.[54] Another example of the uniqueness of quantum dots is the focusing of the intensity of light to the point that the photons interact with each other, resulting in nonlinear optical effects. As a result, switches based on the focusing of energy within quantum dots are now being developed, since they are potentially much faster than currently used switches. Therefore, quantum dots are hugely versatile and are finding applications in optoelectronics,[55-57] photovoltaic devices,[39,58] biolabeling,[7,26,59,60] biocatalyst,[61] drug delivery,[62] tunable lasers,[63-66] and telecommunication devices such as optical amplifiers and waveguides.[67,68]

Table 2.2. Examples of semiconductors QDs, size range, stabilizer used and references.

Semiconductor	d (nm)	Stabilizer	References
Cd_3As_2, Cd_3P_2	10.0-30.0	AOT reverse micelles	69,22
Cd_3P_2, Zn_3P_2	1.0-2.0	Hexametaphosphate	70
CdS	1.3-4.0	Thiols, Sulfonic acids	22
CdS	1.2-17.0	TOPO/TOP, Polyphosphate	17,22
CdSe	2.0-4.0	Thiols	22,71
CdTe	2.0-4.0	Thiols, TOPO/TOP	17,22,72
Fe_2O_3	6.0-15.0	Alkylamine	73
GaAs	3.5-4.5	Quinoline	74,75
Ge	5.8-6.8	Silica matrix	76,77
HgI_2	1.0-2.6	Acetonitrile, no additional stabilizer	78
HgS, HgTe	2.0-5.0	Polyphosphate, Thiols	22
InAs, InP	3.0-6.0	TOPO/TOP	22,79
MoS_2, WS_2	1.0-3.5	No additional stabilizer	80
PbS	1.0-<20	Poly(vinyl alcohol) Alkanethiols	42,81
PbSe	3.0-13.0	1-Octadecene	82
Si	1.0-2.0	Octanethiol	83,84
SnO_2	4.0-20.0	In glass	85
TiO_2 (anatase)	4.0-5.0	No additional stabilizer	22
ZnO, ZnS	1.0-10.0	1-Thioglycerol	22,86

Nanoparticles of the group I-VII (e.g., AgBr), II-VI (e.g., CdSe), III-V (e.g., GaAs), and IV (e.g., Si) semiconductors are known. The band-gap energy of nanomaterials shifts to lower energy when compared to the band gap of the bulk material. The energy $E(R)$ of the first electronic transition band-gap for a particle of radius (R) can be approximated by

$$E(R) = E_g + \frac{\hbar^2 \pi^2}{2R^2}\left[\frac{1}{m_e^*} + \frac{1}{m_h^*}\right] - \frac{1.8e^2}{\varepsilon R} \qquad (2)$$

In equation (2), E_g is the energy band-gap of the bulk semiconductor, ε is the bulk optical dielectric coefficient, $\hbar$ is Planck's constant divided by 2π, m_e^* and m_h^* are the effective mass of the electron and hole, respectively, and e is the charge of the electron. Equation (2) shows the dependence of the band-gap energy with particle size. The negative term considers Coulombic attractions, which, at a certain radius, are balanced by the kinetic energy. However, this equation ignores two important effects: the coupling of electronic states to vibrations and the structure of the particle's surface.[87]

Today, manipulating the size of a QD is well understood. Spherical QDs can be synthesized reliably and repeatedly with any particle size and narrow size-distribution. Nucleation and growth are critical factors and are influenced by choice of reagents and reaction temperature.[23] By varying the monomer concentration in the starting reaction solution, *i.e.*, the concentration of Cd^{2+} in the synthesis of a CdS quantum dot, size, shape and size/shape distribution can be influenced. For instance, Peng et al.[88] found that an excess of monomer produces rice-shaped QDs. Similarly, the formation of extremely high aspect ratio CdSe nanorods (30:1), as well as arrow-, teardrop-, tetrapod-, and

branched tetrapod-shaped nanocrystals of CdSe, was achieved by the growth of the nanoparticles in a mixture of hexylphosphonic acid and trioctylphosphine oxide. Thus, the most influential factors in shape control were found to be the ratio of surfactants, injection volume, and time-dependent monomer concentration.[89]

However, understanding how to manipulate the particle surface in a way that allows for control over photophysical properties is less understood. As will be demonstrated in the following section, inorganic and organic coatings have been investigated in great numbers in an attempt to improve the luminescence quantum yield. While inorganic coatings have achieved significant increases of 40-60% in the emission quantum yield, a similar success with organic coatings has been found for only a single organic functionality. Organic coated quantum dots with strong emission have been a synthetic goal for many years, because of the increased potential for further synthetic manipulation of the material. The recent attempts to find new organic coatings for quantum dots are summarized in the following section.

2.3 Cadmium Selenide Quantum Dots Coating

The quantum yield (Φ_{em}) of a system is defined as the ratio of emitted intensity I_{em} divided by the absorbed intensity, I_{abs}. The quantum efficiency of a system

$$\Phi_{em} = \frac{I_{em}}{I_{abs}} = \frac{k_{radiative}}{k_{radiative} + k_{nonradiative}} \quad (3)$$

is the ratio of the rate constant of radiative decay over the sum of the rate constants of the radiative plus the nonradiative decays determined by the number of nonradiative transitions in the system. The more nonradiative transitions that exist in the system, the smaller the quantum yield since nonradiative transitions compete with the radiative rate, *i.e.*, the emission of electomagnetic radiation. The electron/hole recombinations that occur nonradiatively are thought to be surface transitions and, therefore, are greatly influenced by the surface chemistry and electronic environment, *i.e.*, solvent effects. Highly luminescent quantum dots with high values of Φ_{em} are increasingly sought after for use in light-emitting devices and biolabeling.[7,90] However, how modifications of the surface of QDs changes the photoluminescence (PL) are not fully understood.[91,92] It is known that coating quantum dots can greatly enhance photoluminescence (PL) and quantum yield (Φ_{em}) and decrease the lifetime.[93] For example, passivating CdSe QDs with several atomic layers of an inorganic wide band gap semiconductor, such as ZnS, ZnSe or CdS can increase QY by 40-60%.[23,94] A wide variety of so called core/shell quantum dots have been reported and Table 2.3 lists some of these core/shell systems and the methods of their preparation.

Table 2.3. Examples of core/shell type semiconductor quantum dot composites. The core semiconductor is identified within parentheses. Adapted from [13] and references therein[a].

(Core) Shell	Preparative Route	Reference(s)[a]
(CdSe)ZnS	Chemical solution growth in inverse micelles	151
(ZnS)CdSe	Chemical solution growth in inverse micelles	151
(CdSe)ZnSe	Chemical solution growth in inverse micelles	152
(ZnSe)CdSe	Chemical solution growth in inverse micelles	152
(CdSe)ZnS	Injection of organometallic precursors in hot solvent	153,154a
(CdSe)ZnSe	Above method combined with electrospray	154b,c
(CdSe)ZnS	Above method combined with electrospray	154d
(CdSe)CdS	Injection of organometallic precursors in hot solvent	150
(InP)$ZnCdSe_2$	Injection of organometallic precursors in hot solvent	155
(CdTe)CdS	Organometallic colloidal synthesis	156
(Ge) silane	Chemical solution growth	157
(Ge) silica	Chemical solution growth	157
(Si) silica	Pyrolysis/oxidation	158
(CdS)HgS	Colloidal solution growth	159a
(CdS)PbS	Chemical solution growth	160
(CdS)S	Hybrid electrochemical solution growth	161
$(TiO_2)MoO_3$	Modified sol-gel	162

The resulting brighter emission is due to changes in the surface chemistry of the core dot. The surface of non-coated QDs consists of atoms that are not fully coordinated and, therefore, have free unbound electrons. Furthermore, the surface atoms act like defects. Both unbound electrons and surface defects allow for nonradiative electron

energy transitions at the surface, thereby lowering (Φ_{em}). The inorganic coating reduces the occurrence of nonradiative transitions with increasing defect-free passivation.[22] The electron hole is confined to the QD core, while the electrons are delocalized throughout the core/shell structure. It has been proposed that this phenomenon is explained by the increase in photostablity of core/shell QDs.[95] Photooxidation requires a hole trapped on the surface, a phenomenon less likely in a core/shell QD. The inorganic coating also neutralizes surface defects by tying up "dangling" bonds, further increasing photoluminescence output. Recently, quantum dots with double inorganic shells CdSe/CdS/ZnS and CdSe/ZnSe/ZnS were reported to deliver up to an 80% QY.[96] Earlier attempts using a CdS/HgS/CdS core-shell-shell material produced only decreased quantum yields.[97,98]

Colloidally prepared quantum dots are free floating and can be attached to a variety of organic coatings via metal coordination to the organic functional group, such as thiols, amines, nitriles, phosphines, phosphine oxides, phosphonic acids, and carboxylic acids. The surface chemistry can be used to alter effectively the properties of the QD including brightness and excited state lifetime. Table 2.4 lists a variety of semiconductor QDs coated in different polymer matrices and references. However, organic coatings are not limited to polymers. Small molecules with any of the functional groups previously mentioned will coat a QD and influence its photophysics. Table 2.5 lists some of the many organic coated QDs that have been prepared and described.

Table 2.4. A selection of semiconductor quantum dot nanocomposites, listed with their respective polymer coating, and adapted from reference [16] and references therein [f]. Note that today poly(amidoamine) (PAMAM) is considered a dendrimer rather than a polymer and would be listed elsewhere [g].

Semiconductor QD(s)	Polymer Matrix	Reference(s) [f]
CdS	*N*-poly(vinylcarbazole) (PVK)	163a,b
ZnS	Poly(ethylene oxide)	164
CdSe	Poly(*p*-phenylene) vinylene (PPV)	165a,b
CdS	Polypyridine (functionalized)	166
CdSe	PVK-oxadiazole derivative	167
CdS	Poly(vinyl alcohol)	168
CdSe or CdS	Poly(2-methoxy,5-(2'-ethyl)-hexyloxy-PPV)	169a,b,c
CdSe or (CdSe)ZnS	Phosphine-functionalized block copolymer	170a,b
CdS	Polydiacetylene	171
Si	Polystyrene	172
CdSe or (CdSe)ZnS	PPV	173a,b
CdS	Chelating polymer (Chelex)	174
CdS	Polyamine dendrimer (PAMAM)	175a,b [g]
CdSe	Poly (3-hexylthiophene)	176
PbS	Polyacrylamide	177
CdS	Polystyrene-maleic anhydride	178
(ZnS)Mn	Poly(acrylic acid) or poly(methyl methacrylate)	179
CdTe or HgTe	Poly(diallyldimethylammonium chloride)	180a,b
(CdS)ZnS, (CdSe)ZnS	Poly(lauryl methacrylate)	154e
CsTe	Polypyrrole	180e

If increased photoluminescence is the goal, currently the only successful organic coating are organics with amine functionalization.[18,19,23,99] As previously mentioned, the QY for CdSe in a TOPO/TOP coating does not exceed 5-15%. The quantum efficiency, however, can be improved to 40-60% by surface passivation with organic alkylamine coatings such as hexadecylamine (HDA) or dioctylamine,[99] and dodecylamine.[100] Thus, organic coatings can achieve the same high luminescence quantum efficiencies as inorganic coated core/shell QDs.[100]

Strictly speaking, there are organic coated QDs, such as CdSe/TOPO, and functionalized QDs such as CdSe coated for example with an organic thiol. The later are synthesized using a process refered to as surface modification or surface functionlization. The difference between coated ODs and surface functionalized QDs lies in the type of synthesis. If the organic material to be attached to the surface is present during the synthesis of the QD, then the organic material is commonly refered to as coating. When that organic coating of a QD is subsequently replaced by an organic material, such as a alkylthiol or alkylamine, the process is refered to as surface modification and the QD refered to as a functionalized QD.

Chen[101] demonstrated the effect of a coating on the properties of the QD. CdSe QDs synthesized in TOPO/TOP solution are hydrophobic and dissolve in organic solvents such as chloroform and toluene. Exchanging the TOPO/TOP coating with mercaptobenzoic acid oriented with the carboxylic acid functionality on the periphery and the thiol group attached to the QD, hydrophilic, water soluble CdSe QDs are

obtained. Because of the different solubility, these quantum dots can now be applied with specific patterns on glass matrices via self-assembled-monolayer techniques. Some of the common organic coatings for QDs are listed in Table 2.5.

Rotello[50] reviewed nanoparticle building blocks such as monolayer-protected clusters (MPC) and mixed monolayer-protected clusters MMPC's synthesized by the Schiffrin reaction.[102] In the Schiffrin reaction, dodecanethiol is added to organic-phase $AuCl_4^-$ followed by reduction with sodium borohydride, which leads to thiol-coated gold nanoparticles ranging in size between 1 and 3 nanometers. Monolayer functionalized nanoparticles show different stabilities depending on type and amount of coating. The monolayer also acts as a shield to prevent agglomeration and increased particle size, and provides a scaffold for the attachment of functional molecular entities that, in turn, can become building blocks of larger entities.

Table 2.5. Selected semiconductor QDs and nanoparticles functionalized with organic ligands and references.

Semiconductor/ Nanomaterial	Organic Coating	References
Au	Porphrin-alkanethiolate	103
Au	Thiolated poly(ethyleneglycol)	104
CdSe	Alkanethiols, glutathione, tiopronin, thiolates poly(ethylene glycol), p-mercaptophenol, aromatic alkanethiols, phenyl alkanethiols, (γ-mercaptopropyl)-trimethoxysilane.	105
CdSe	Poly(ethylene glycol)	46
CdSe	Thiolated PAMAM dendrons	106
CdSe	Thioglycolic acid	69
CdSe	DNA	107
CdSe	Chelated Dithiothreitol (DTT)	108
CdTe	2-Mercaptoethanol, 1-thioglycerol, 2,3-dimercapto-1-propanol, 2-mercaptoethylamine, L-cysteine, 2-(dimethylamino)ethanethiol,	72
Pd	C6 and C12 Alkanethiols	109
CdSe	Mercaptoacetic acid	26
ZnS	Mercaptoacetic acid	86

Murray synthesized a range of thiolated gold nanoparticles using 4-mercaptophenol and other thiolated ligands. He successfully applied known organic reactions such as place exchange, polymerizations, S_N2 and coupling to further modify and functionalize the surface. These modified nanoparticles exhibited increased stability in comparison to CdS quantum dots. These monolayer protected gold particles were generally air- and solvent stable.[110] Pietro synthesized a series of analogs similar to Murphy's thiolated gold nanoparticles, but with CdS instead of Au.[111] Pietro then measured the rate of decomposition of differently substituted thiophenols and correlated the decomposition rates with the appropriate substituent Hammett parameter (σ), demonstrating the influence of the para substituent on the stability of the QD. He also demonstrated that the decomposition rate to form a disulfide) correlates with the excitonic fluorescence intensity with the faster rate of decomposition correlating with higher emission intensity. From this, he proposes a mechanism of photodecomposition that results in the formation of bulk CdS, and an organic byproduct that is the disulfide of the thiolated coating. His proposed mechanism implies electronic contact between the QD core and substituents on the organic coating and demonstrates the influence of the organic coating on the photophysics of the QD.[100]

Mercaptoacetic acid (MAA) has been used to functionalize QDs. The thiol covalently binds to the QD surface and the carboxylic acid functional group of MAA offers the opportunity to further modify the particle (cf. Scheme 2.3.1) However, MAA undergoes photo-oxidation and is not stable, and it does not reproducibly functionalize QDs.[112] The stability of QDs increases slightly with increasing alkyl chain length.[112]

Unfortunately, even mercaptoundecanoic acid (MUA) used in conjunction with CdSe is not robust enough to withstand the necessary reaction conditions for generating thiolated gold particles. Reiss[90] reported findings of 60-85% photoluminescence intensity using MUA coated CdSe/ZnSe QDs. The increased QY, however, stems from the use of core/shell QDs rather than the influence of the organic coating. Mirkin[107] took advantage of the inherent lability of short chain mercaptopropionic acid (MPA). Instead of coupling DNA to the carboxylic acid functionality of MPA he replaced MPA with DNA by covalently coupling the thiol functionality of the proteins to the core/shell QD surface, however, observing a 26 % drop in photoluminescence.

Leblanc[69] has recently demonstrated that thioglycolic acid capped CdSe QDs sandwiched between two layers of organophosphorus hydrolase (OPH) within a sensing assembly produces higher photoluminescence than the same QDs in solution. OPH is an enzyme often used to digest neurotoxins since OPH catalyzes the breakdown of the P-O, P-S, P-F, and P-CN bond often found in neurotoxins. The lower QD luminescence in solutions, when compared to the same QD in a sensing assembly, can be understood when one considers that the solvent cage introduces surface traps (*i.e.*, electron and hole traps) in quantum dots which lower the quantum yield of emission. However, the increase in photoluminescence can be used to design detecting devices for organophosphorus neurotoxins.

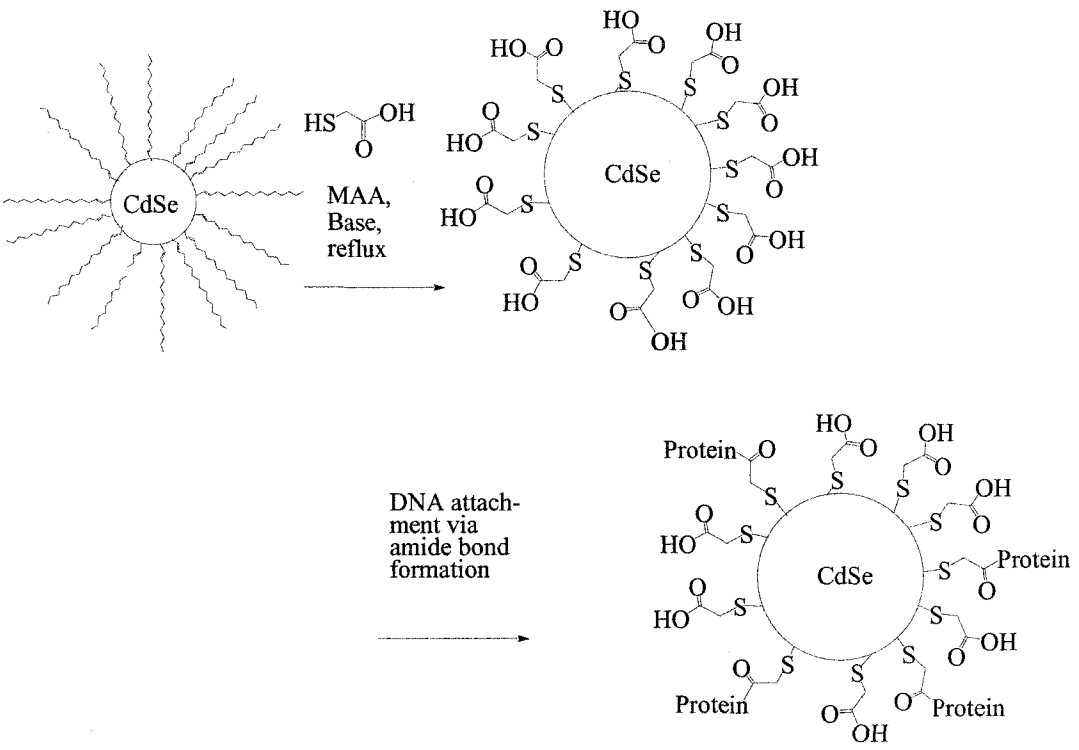

Scheme 2.1. Abbreviated scheme to functionalize coated QDs with further surface modification by attaching proteins.

One notices in Table 2.4 that PAMAM is still listed amongst polymer coatings. Today PAMAM is classified as a dendrimer. Dendrimer and dendron functionalized coated QDs are discussed next, in Chapter 4 after a detailed excursion into the history and synthesis of dendrimers and dendrons in Chapter 3.

3. Dendrimers and Dendrons

Dendrimers are a type of ordered polymer. As previously noted, the term "dendrimer" derives from the Greek word "dendron" meaning tree and "meros" meaning part. It was first postulated in the 1940s by macromolecular pioneer Paul Flory[113,114] who received a Nobel Prize in 1974 for his theoretical and experimental achievements in the physical chemistry of macromolecules. Fritz Vögtle[115] began synthesizing small-branched molecules in the 1980s, but it was Donald A. Tomalia[34] and George R. Newkome[116] who both published the synthesis of their respective "starbust" multigenerational dendrimers in 1985. These two papers laid the groundwork for this new area of organic macromolecules.

Dendrimers are well-defined, hyper-branched, globular macromolecules constructed around a core unit rather than the chain-like structures of conventional polymers. During the synthesis of a dendrimer, each successive reaction step or series of the same reaction steps leads to an additional generation of branching. The molecular weight of the dendrimer is easily controlled by the iterative sequence of reaction steps. Thus, the final product has a distinct molecular weight instead of the broad weight distribution commonly observed in polymers. The highest molecular weight dendrimer being synthesized today has a nine allyl unit core.[117,118] Since each of the allyl units has 3 connection points, it follows that a generation one dendrimer has 27 branches, which grow to 243 branches in generation three. Six more generations later at generation nine, 177,147 functional groups cover a 13 nm diameter spherical molecule. Even with a

fraction of functional groups described above, dendrimers have inspired various applications for the attachment of antibodies,[119,120] as contrast agents,[121,122] as drug delivery agents,[123,124] in catalysis[125], and in light-harvesting devices.[126,127]

DAB, a poly(propylene imine) dendrimer, first reported by Müelhaupt[128] and De Brabander,[129] is now commercially available. DAB is an abbreviation for the dendrimer core, the 1,4-diaminobutane. The repeat unit is a propylamine group, abbreviated –Am-, and the number designates the number of amine functionalities that doubles with each generation on the periphery of the dendrimer. For instance, DAB–Am–4 is the name for a dendrimer with a diaminobutane core (DAB), with polyamine repeat units (–Am-) and 4 primary amines. Thus, DAB–Am–4, DAB–Am–8, DAB–Am–16, DAB–Am–32, and DAB–Am–64 are dendrimers of generation one through five (cf. Figure 3.1.). Only in DAB does the number in the name designate the number of peripheral amine groups rather than the number of generation. The cost for the fifth generation DAB–Am–64 is $163/g. Since DAB-Am-64 has a molecular weight of 7,168 g/mol, the cost for the dendrimer is $1168/mmol. Production of the fifth generation DAB–Am–64 requires 10 synthetic steps (cf. Scheme 3.1). Thus, the fifth generation DAB-Am-64 dendrimer is not cost efficient to mass synthesize for further research purposes, such as the surface modification of a QD.

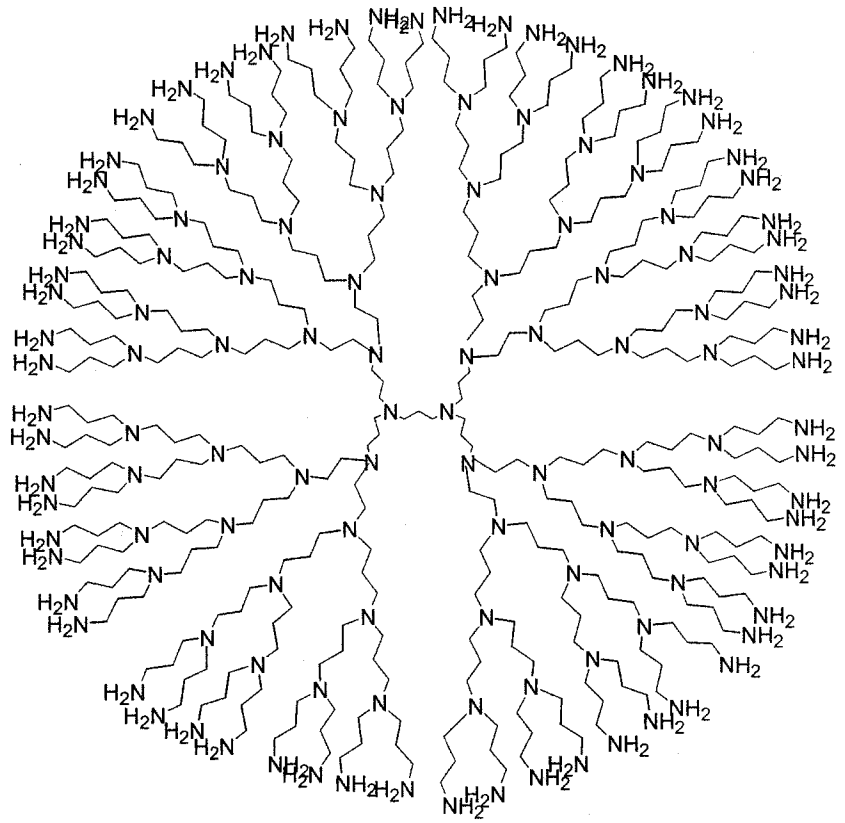

Figure 3.1. Structure of the fifth generation DAB dendrimer interior consists entirely of tertiary amine groups linked by three-carbon chains.[119]

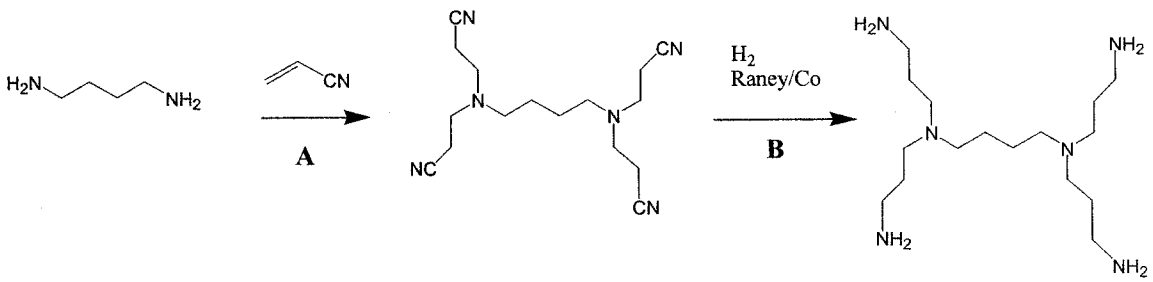

Scheme 3.1. Synthesis of a poly(propylene imine) dendrimer (reaction A and B) employing Michael addition (A) followed by reduction (B).[119]

A more versatile and also commercially available dendrimer is the poly(amidoamine) dendrimer, also known as PAMAM (cf. Figure 3.2). This dendrimer was first synthesized by Tomalia[35] using the reaction scheme shown in Scheme 3.2.

PAMAM is available with terminal amine or carboxylic acid functionalities. Each generation doubles the number of amine functionalities, while each ½ generation doubles the number of carboxylic acid functionalities. At $1193/g the tenth generation PAMAM initially seems more cost efficient than DAB. However, with a calculated molecular weight of 934,698 g/mol, the actual millimolar cost is $ $1.12x10^6$/mmol, which is three orders of magnitude higher than DAB.

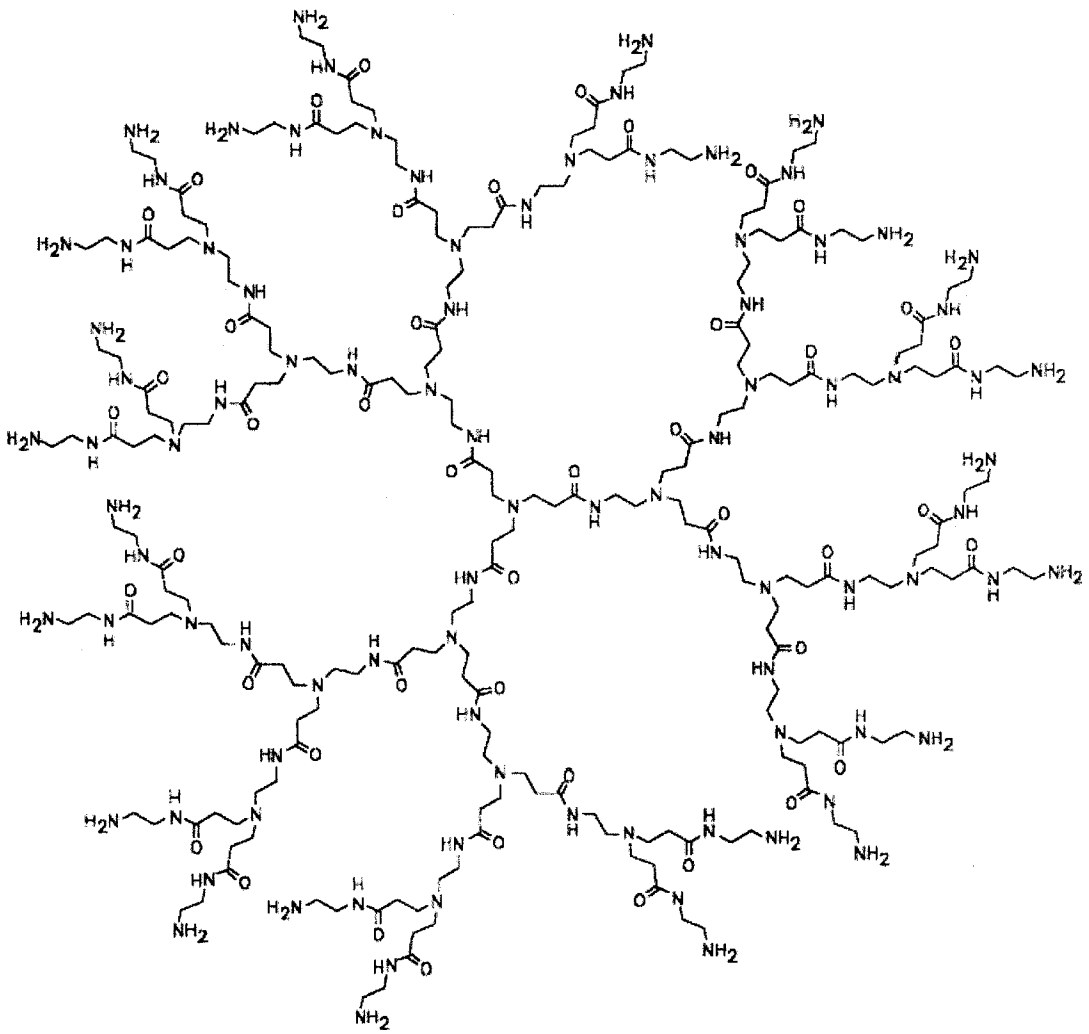

Figure 3.2. Structure of the fourth generation of a poly(amidoamine) (PAMAM) dendrimer.[130]

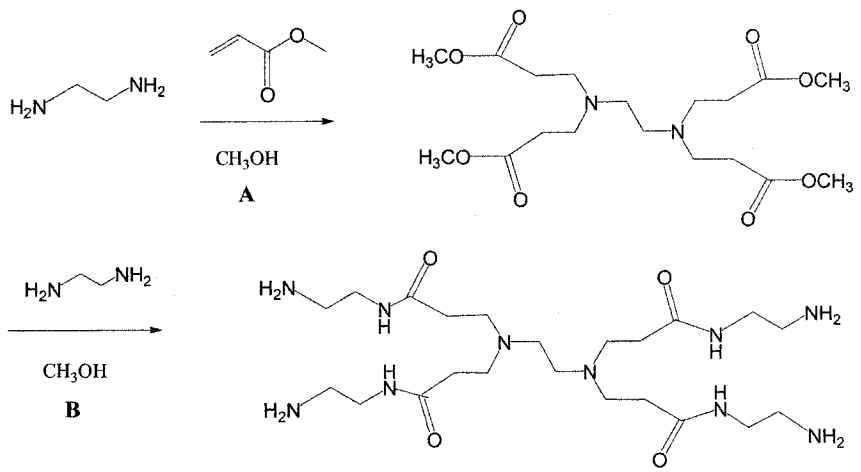

Scheme 3.2. Synthesis of an ethylene diamine (EDA) core PAMAM dendrimer consisting of two consecutive steps: Michael addition of primary amine to methylacrylate (A) followed by amidation of the formed multiester with EDA (B).[34-36]

In addition to DAB and PAMAM, there are three other well-studied classes of higher generation dendrimers. They are Newkome's [27]-arborol system[116] (cf. Figure 3.3.A), Fréchet's aromatic polyether dendrimers[131] (cf. Figure 3.3.B), and Moore's phenylacetylene dendrimer[127] (cf. Figure 3.3.C). The later is most noteworthy and relevant to this dissertation, as it has been used in light-harvesting devices. Moore reported observing an interesting gradient effect. As the generations increase, the number of conjugated bonds decreases from the periphery to the core.[126] As shown in Figure 3.3.C the third generation has one alkyne linking aromatic rings, the second generation has two alkynes with one benzene ring, and generation one has three alkynes alternating with benzene rings. Consequently, a directional energy flow to the core was measured with the help of a chromophore that had been attached to the core.[127] The ability of a dendrimer to direct energy to the core is important to the work presented and will be discussed further in Chapter 6.

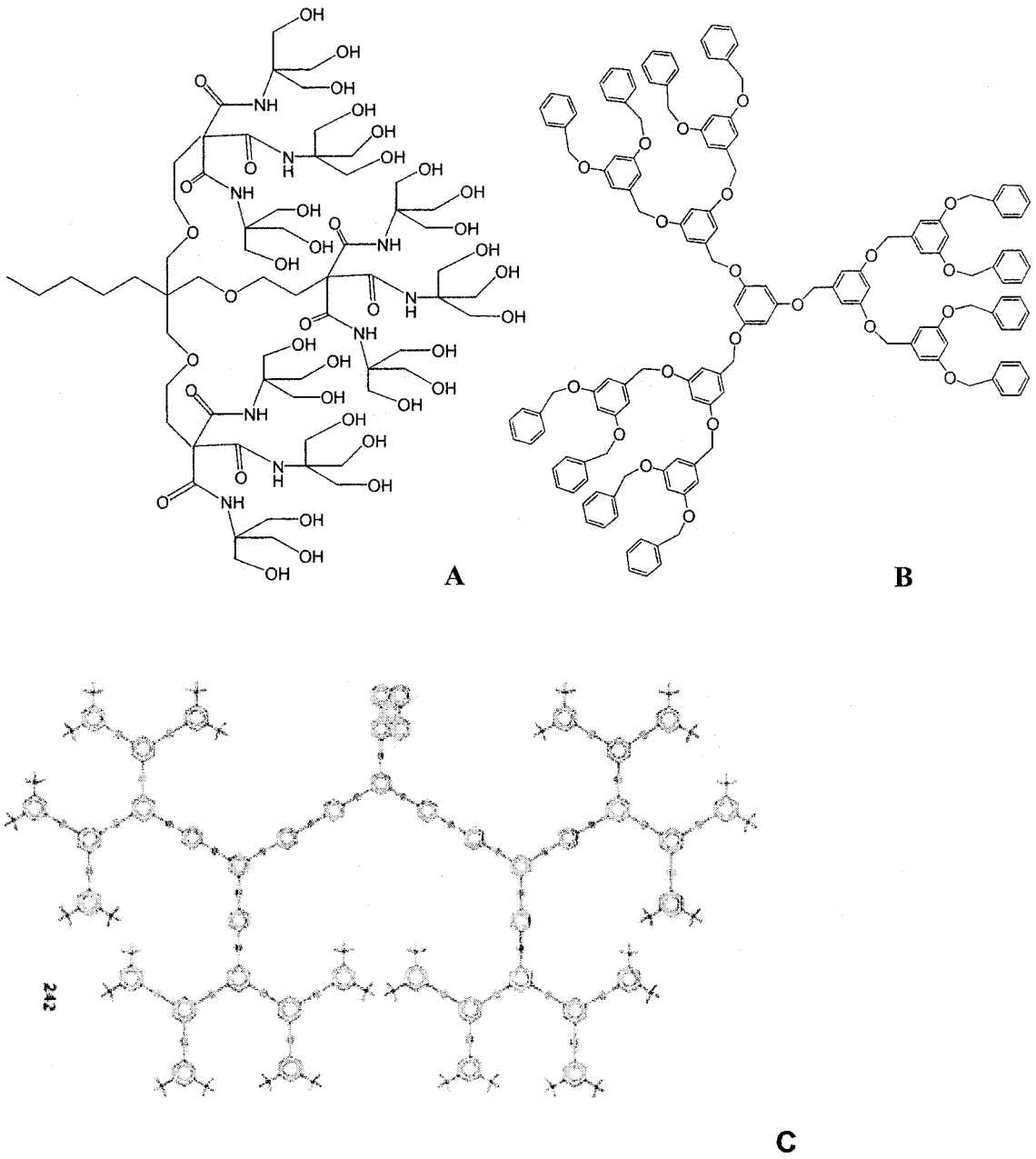

Figure 3.3. Classes of well studied dendrimers are (A) Newkome's [27]-arborol system is an attempt to mimic micelles,[116] (B) Fréchet's aromatic polyether dendrimers,[131] and (C) and Moore's phenylacetylene dendrimer.[127]

Many other interesting dendrimers have been reported and characterized.[130] Zimmerman's review[132] focused on the dendrimer's ability to function in host-guest type interactions, which can be useful in applications such as encapsulating agents,[133] artificial gene-transfer materials,[132,134] and MRI (magnetic resonance imaging) contrast agents.[122] Meijer's review[119] focused on the structural aspects of dendrimers and their physical properties. One of the unexpected findings was that dendrimers are so flexible that back folding of the peripheral branches is possible making the core more accessible than expected. In general, the dendrimer is flexible and adapts its form and shape depending on experimental circumstances. In addition to these findings, Fréchet showed that by taking advantage of the spatial arrangement of functionalities in the dendrimer, the dendritic scaffold could be utilized as unique artificial building blocks to encapsulate, isolate, or shield a guest molecule, catalyst or quantum dot. His review also included an extensive literature survey on dendrimers.[133]

The dominant methods of dendrimer synthesis are Tomalia's divergent approach and Fréchet's convergent method,[135] both of which are schematically shown in Figure 3.4. DAB and PAMAM are both synthesized following Tomalia's divergent approach (Scheme 3.1 and 3.2). The divergent method starts with the core unit and adds generation after generation. The number of coupling reactions increases with each successive generation therefore increasing the risk of structural defects that cannot be repaired easily. As the structural defects increase, the molecular weight distribution for the dendrimer broadens. The convergent method starts at the other end, the periphery of the dendrimer and works its way to the core. The number of synthetic steps per generation

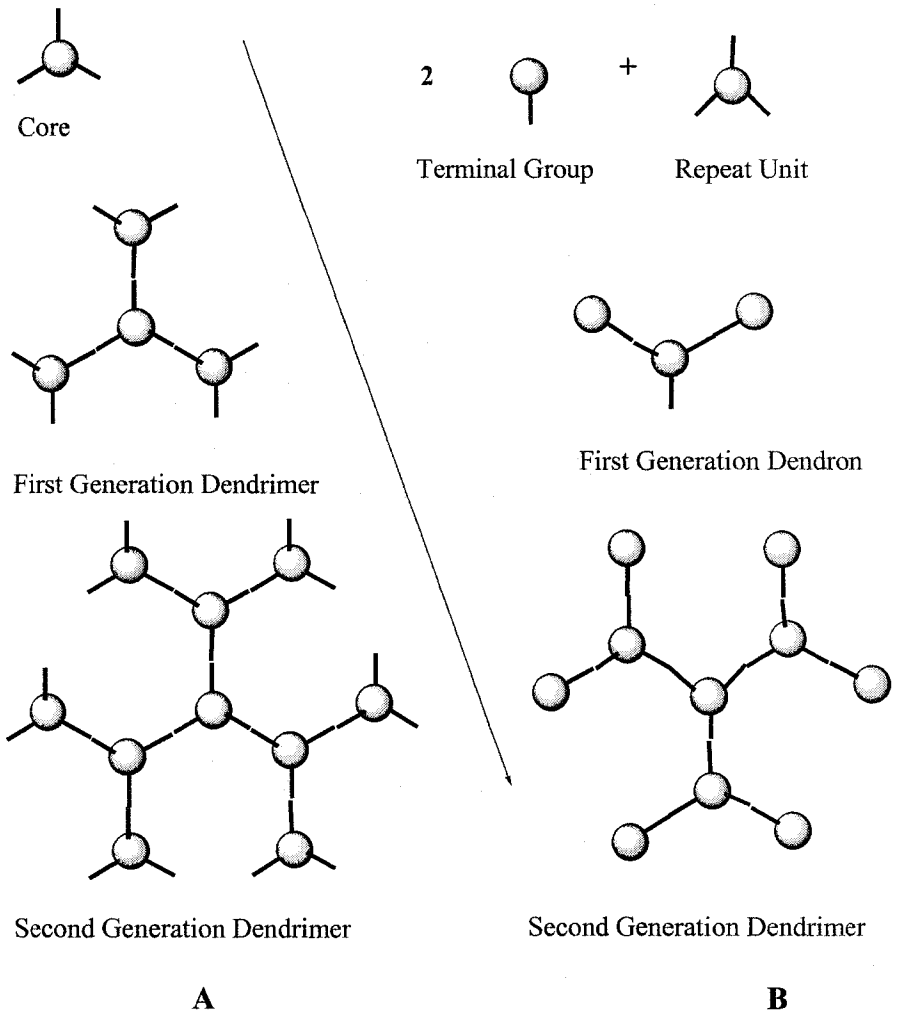

Figure 3.4. Divergent (**A**) and convergent (**B**) approach to synthesizing dendrimers.

stays constant, but the number of functional groups decreases requiring less of each reagent with each additional generation. Defect materials can be eliminated via column chromatography, since the molecular weight for defective dendrimers will be different from the target dendrimer. However, the disadvantage with the convergent synthesis is that it limits the obtainable number of generations to around 5 or 6 generations, depending on the dendrimer. The generation limit is caused by the increase in congestion in the dendrimeric core that drops the reaction yield with each additional generation.

Fréchet discussed these limitations in a review on convergent synthesis of dendrimers published in 2001.[136]

A major difficulty is assessing the purity of dendrimers. Various NMR techniques such as ^{1}H, ^{13}C, and ^{15}N are widely used but are limited in their ability to detect small impurities or irregularities in the dendrimer branch. Also with higher generation numbers, the solubility of the dendrimer in the deuterated solvents becomes an issue. The most recent advances in ESI (electron spray ionization) and MALDI-TOF (matrix assisted laser desorption ionization – time of flight) mass spectroscopy have been useful in analyzing small impurities and finding small imperfections in a dendrimer.[137] However, these techniques are limited to dendrimers that are polar or basic in nature because of incompatibilities within the sample ionization region. For example, compounds such as the Fréchet-type dendrimers that do not sufficiently ionize (ESI), or do not interact with the matrix (MALDI) are more difficult to analyze. Due to the highly symmetric design and the large number of repeating functional groups in a dendrimer, using infrared spectroscopy to characterize dendrimers is impractical. Similarly, elemental analysis is not able to detect subtle changes in the molecular structure.[37] In addition, the well documented ability of dendrimers to encapsulate small molecules becomes a disadvantage when attempting to purify the dendrimer from reagents and solvent molecules.

The same difficulties discussed for dendrimers are also encountered with dendrons. The difference between a dendron and a dendrimer is that the former has a

single focal point instead of a core. Thus, the dendron is shaped like a slice of a pie while the dendrimer is more like the whole pie. Currently, dendrons have not been reviewed separately, although this class of molecules has been mentioned in the reviews on dendrimers. However, dendrons become important when one realizes that Fréchet's convergent method actually synthesizes dendrons first. The dendrimer is complete only when the dendrons are attached to the central core unit. This thesis focuses on attaching various dendrons to CdSe quantum dots. Chapter 4 summarizes the current state of knowledge on the subject of dendronized nanoparticles and their synthesis.

4. Dendronized Nanomaterials

The binding of inorganic nanoparticles to organic molecules has created a rapidly expanding field of research. To prepare such conjugates from nanomaterials, the surface chemistry of the nanoparticles must be designed so that the stabilizing ligands are fixed to the nanoparticle. In the case of gold nanoparticles and cadmium sulfide (CdS) or cadmium selenide (CdSe) quantum dots (QDs), the binding of an organic molecule to the particle surface is frequently accomplished using a thiol functional group. In many instances the organic molecule is a simple alkyl thiol with variable chain length. When these alkyl thiols react with a nanoparticle, the resulting product is a monolayer-protected cluster (MPCs).[104,109,138-140] Table 4.1 lists a variety of dendrons attached to QDs and nanoparticles.

Thiols with terminal functional groups at the end of the chain,[60] such as mercaptoacetic acid,[26] are used to facilitate the coupling of larger molecules, such as fluorescein,[141] ferrocene,[139,142] phorphrin,[103] and even buckminsterfullerene.[133,136,143] DNA and proteins have been coupled to mercaptopropionic acid coated QDs via amide bond formation.[107,144] In addition, biological molecules can be attached to nanoparticles directly via the thiol groups that are already part of the peptide molecule.[24,145]

Table 4.1. List of Dendrons and Dendrimers attached to semiconductor QDs and Metal Nanoparticles and references.

Nanomaterial	Dendrimer, Dendrons	Reference
Ag	PAMAM	150
Au	Thiol functionalized PAMAM	153
Au	Nonaferrocenyl dendron	154
Au	Fréchet-type polyaryl ether	155,156
Au	Attached Biosensors	60
Au8	PAMAM-OH	151
CdS	Functionalized DAB	157
CdSe	Dendrimer stability	148
CdS	PAPAM vs. polymer stability	149
CdS	Blue, Red Respectively	158
CdS	PAPAM arrested precipitation	43
CdSe	N-functionalized PAMAM Dendrons	159
CdSe, TiO_2	Dendrimers	13
CdSe/CdS	Dendron boxes	160
(CdSe)/ZnS	OH-functionalized Dendrons	146
CdSe	PAMAM	161
Cu^{2+}, Pt^{2+}, Pd^{2+}	PAMAM, displace for Au, Ag, Pd, Pt	152
Pd	14 Dendrons attached to 1 QD	162

By far the largest number of publications on dendrimers in conjunction with nanomaterials is concerned with the use of the PAMAM as a nanoreactor and stabilizer of nanomaterials. Dendrimers can control the size of a synthesized semiconductor nanoparticle, in particular CdS. Unlike the previously discussed synthesis of QDs (cf. Chapter 2), this dendrimer is used as a template that controls the growth of the QD, sets the size of the QD and then stabilizes the QD after the synthesis.[146] Murphy was the first to report the fact that the final size of the QD increases with the molecular weight, *i.e.*, higher generation dendrimers.[43] PAMAM stabilized CdS QDs are synthesized via arrested precipitation.[147] In short, addition of Cd^{2+} ions to a dendrimer solution is followed by addition of S^{2-} ions, that produces the CdS nanoparticles.[148] To show the template effect that the PAMAM dendrimer has on the synthesis of CdS QDs, Murphy synthesized CdS QDs using linear polymer analogues.[149] Murphy concluded that the higher concentration of chelating nitrogens in the PAMAM dendrimer provided a key feature for the synthesis of small, defect-free CdS nanoparticles.[149] The results show that QDs can be obtained with a narrow size distribution. However, the quantum yield of emission had dropped significantly. PAMAM dendrimers have also been used to synthesize metal nanoparticle dendrimer composites, such as silver,[150] gold,[151] copper, platinum, palladium, gold and silver.[152]

There are multiple methods described for the exchange of the QD TOPO coating by thiolated organic compounds. Peng[106,112] demonstrated recently the usefulness and workability of using thiol core functionality. This effort shows that the dendron will attach covalently to a nanocrystal, using triethylamine in the case of an aromatic thiol and

a stronger base such as tetramethylammonium hydroxide in the case of an aliphatic thiol dendron.

Nie[26] successfully attached a protein to a CdSe/ZnS QD. He uses mercaptoacetic acid to functionalize the QD surface. By replacing the datively bound TOPO coating with a covalently attached mercaptoacetic acid coating he achieves a change in solubility from chloroform to water or methanol. The later solvents are better suited for an amide coupling reaction.

This thesis, however, probes the influence dendrimers, or more specifically dendrons, have on the photoluminescence properties of semiconductor QDs. Energy transfer in dendritic macromolecules has been demonstrated with the energy transfer occurring through space instead of through bonds. Increasing dendron generations led to a steady increase in photoluminescence.[126,163] Fréchet created an efficient, almost quantitative, system comprised of a terbium ion core and carboxylic acid functionalized polyaromatic ether dendrons.[164] He demonstrated that the PL intensity can be increased when using dendrons of larger generation.[164] However, several groups have recently obtained results that indicate that attaching organic ligands to QDs quenches the photoluminescence.[46,112,159,160] For instance, Fox demonstrated energy transfer from surface-bound arene to the gold nanoparticle core. However, she still observes emission quenching of the photoluminescence of the gold nanoparticles.[155]

Part II Discussion and Results

5. Synthesis and Characterization of Coated CdSe QDs

Financial as well as safety concerns for the research presented here dictated the necessity of finding alternative sources of CdSe QDs, other than the standard sources of purchasing or synthesizing them via Bawendi's organometallic route. A viable solution was Peng's environmentally friendly alternative.[21] During an investigation of quantum dot formation, Peng discovered that the phosphonic acid impurity in the technical grade *n*-trioctylphosphine oxide used by Bawendi played a crucial role in the synthesis of CdSe QDs. This discovery meant that neither dimethyl cadmium nor dimethyl selenide, which are extremely toxic, are necessary. This discovery, in turn, has led to an expanded range of sources for both cadmium and selenium. Cadmium oxide, cadmium acetate, and cadmium carbonate, amongst other cadmium salts, can be used in place of dimethyl cadmium. Furthermore, the toxic dimethyl selenium solution can be replaced by using selenium powder dissolved in *n*-trioctylphosphine. Fatty acids, amines, and phosphine oxides can serve as ligand/solvents for the synthesis of high quality nanocrystals as long as phosphonic acid is present in the final solution. In addition, the Peng synthesis can be executed at a temperature that is below the flashpoint of TOPO, reducing the risk of explosions during synthesis. In the Peng synthesis, size is controlled by monomer concentration and temperature with the total synthesis leading to small nanoparticles with a narrow size distribution. In fact, the size distribution of the obtained CdSe QDs is

reportedly so narrow (5-10% relative standard deviation) that lengthy, size-selective precipitation is no longer necessary.

The final size and size distribution of the CdSe QDs synthesized herein are determined by UV/Visible (UV/Vis) absorption spectroscopy and photoluminescence (PL) measurements. UV/Vis spectroscopy is a common technique for determining size, since published absorbance/size correlation charts are available which, in turn, have been verified using transmission electron microscopy.[165] The PL emission peak gives information on particle size distribution (not particle size) and is expressed as units of full width at half maximum (FWHM). The bandwidth of the emission spectra, denoted as the Full Width at Half Maximum (FWHM) stems from the temperature, natural spectral line width of the dots, and the size distribution of the population of dots within a solution or matrix material. Spectral emission broadening due to size distribution is known as inhomogeneous broadening and is the largest contributor to the FWHM. Narrower size distributions yield smaller FWHM. For CdSe a 5% size distribution corresponds to ~ 30nm FWHM while in PbSe a 5% size distribution corresponds to ~ 100nm FWHM. An acceptable industrial standard for size distribution is a PL FWHM of $\leq$ 40 nm (source: Evident Technologies Product Catalog). Here, FWHM data are recorded to characterize PL emission peaks only. Theoretically, UV/Vis absorption peaks also have a FWHM. However, absorption peaks of small QDs in the size range of 2.0 nm to 2.5 nm are so broad that measuring FWHM is meaningless.

In the next several sections, the synthesis and characterization of quantum dots used during this project are discussed.

5.1 Synthesis and Characterization of TOPO coated CdSe QDs

Initially, CdSe QDs were synthesized with a TOPO coating using the Peng synthesis in order to produce a standard for comparison during the characterization of various QD containing synthetic products. The experimental details for this synthesis are described in Chapter 9. A typical UV/Vis spectrum and PL spectrum for TOPO coated CdSe QDs (*i.e.*, CdSe/TOPO (**I**)) are shown in Figure 5.1. The absorption maximum of 476 nm indicates a QD of 2.2 nm in diameter using an absorbance/size correlation chart (cf. Figure 5.2). Unfortunately, a rising baseline characteristic of CdSe nanoparticles obscures spectral data at wavelengths significantly lower than the observed maximum. [146] The PL has a maximum at 498 nm and a FWHM of 32 nm. Lifetime measurements yield an emission lifetime of τ = 14 ns, which agrees with reported values.[66]

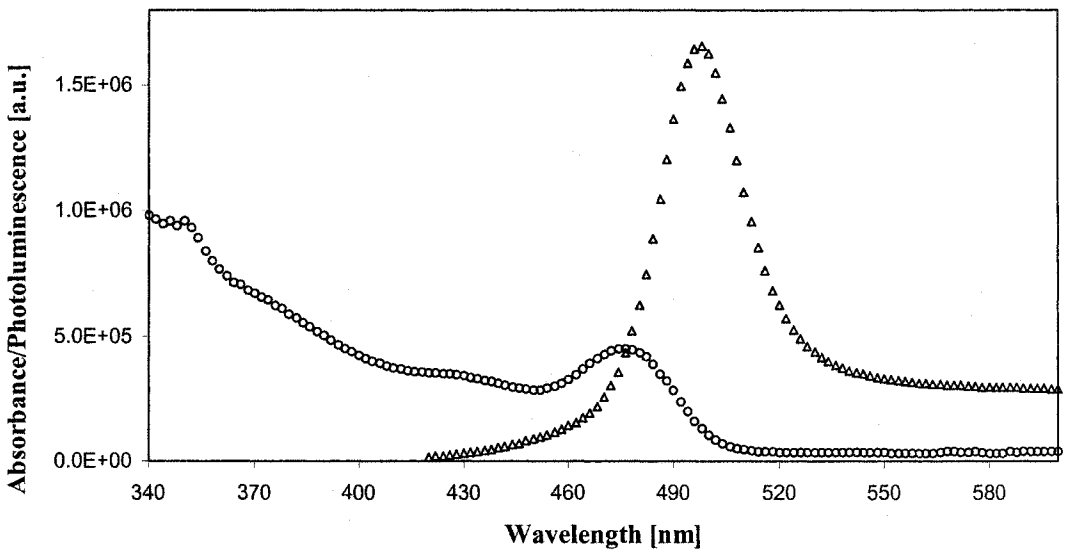

Figure 5.1. UV/Vis absorption (ooooooo) and PL (ΔΔΔΔΔΔ) spectra of CdSe/TOPO (**I**). UV/Vis maximum lies at 476 nm (expanded 400 000 times). PL emission maximum at 498 nm (excitation set at 400 nm) and FWHM is 32 nm.

5.2 Synthesis and Characterization of ODE coated CdSe QDs

The synthesis of CdSe QDs in octadecene (ODE) solution instead of a TOPO solution does not alter the particle size, the size distribution, or the absorption and emission properties of the final product. UV/Vis absorption maxima of different batches (*i.e.*, synthesis performed on different days) ranged from 450 to 510 nm, which indicates a difference in particle size from 1.5 to 2.5 nm.

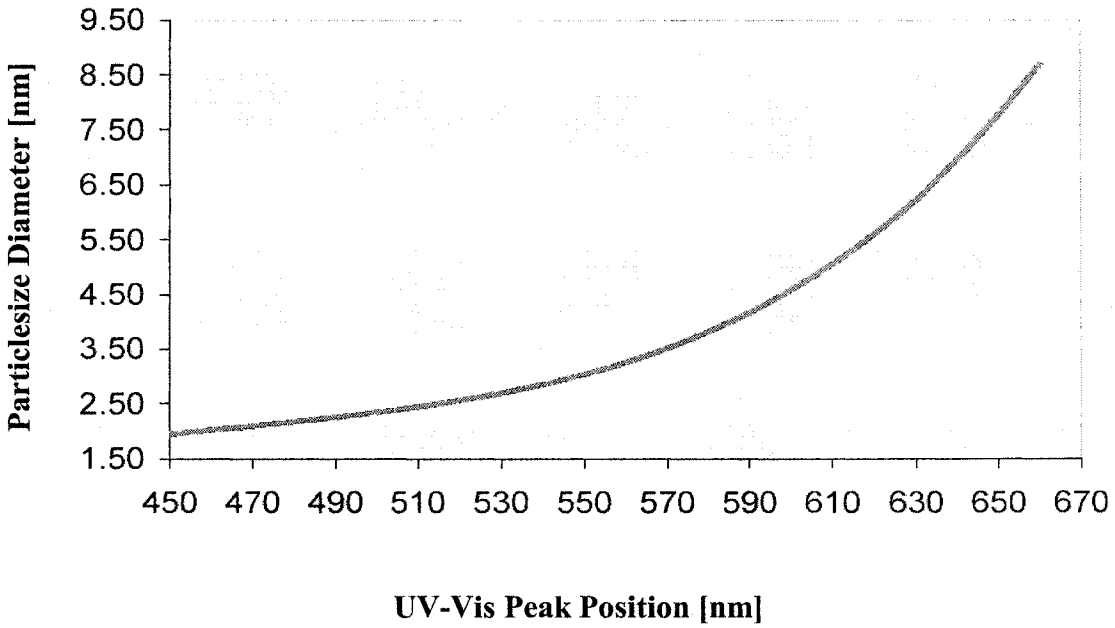

Figure 5.2. Size versus UV/Vis absorption peak position of CdSe/TOPO QDs. Adapted from www.evidenttech.com.

Figure 5.3 shows the UV/Vis absorption and PL spectrum of the ODE coated CdSe QDs. From the UV/Vis absorption, we determined that the diameter of the CdSe QDs is 2.4 nm. The PL spectrum is used to verify the narrow size distribution (*i.e.*, a FWHM of 36 nm). Thus, the ODE coated CdSe QDs have the same size and size distribution as the TOPO coated QDs (cf. Figure 5.1). Moreover, identical photoluminescence emission spectra, obtained at two different excitation wavelengths, namely excitation at 470 nm and at 400 nm, establish the homogeneity of the sample. The lifetimes for these two batches are 14 ns for CdSe/TOPO and 15 ns for CdSe/ODE. Lifetimes for a total of eight batches of CdSe/ODE are discussed in the next section.

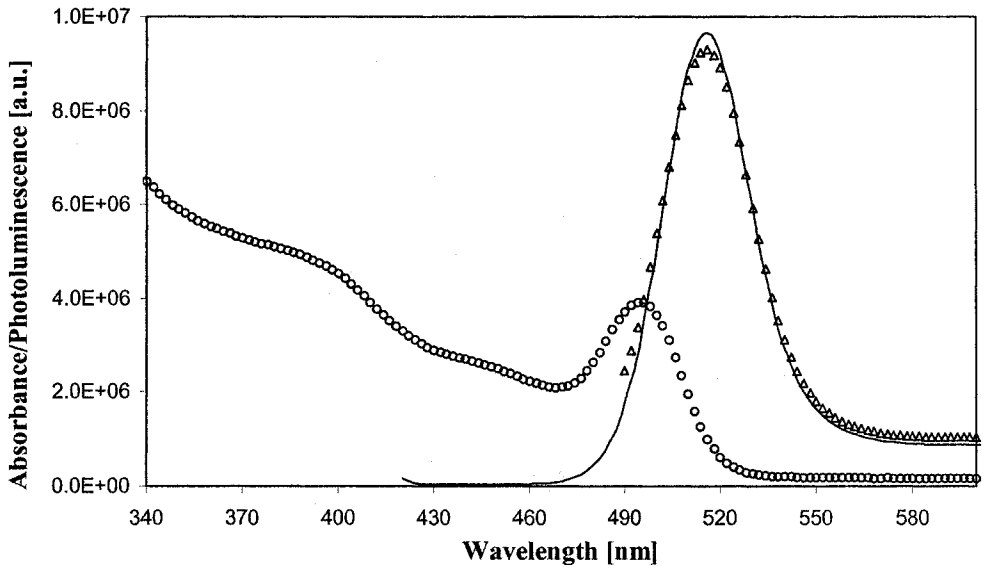

Figure 5.3. UV/Vis absorption (ooooooo) and PL (ΔΔΔΔΔΔ) and (——) of CdSe/ODE (**II**). UV/Vis maximum at 496 nm (expanded 3,000,000 times). PL emission maximum at 518 nm, both times when excitation wavelength is set at 470 nm (ΔΔΔΔΔΔ), and at 400 nm (——), Full width at half max (FWHM) is 36 nm.

A TEM (cf. Figure 5.4) was measured for a sample of the CdSe/ODE QDs. One can clearly see from that figure that the size distribution in this particular sample appears larger than FWMH measurements suggest. However, problems with equipment delayed the TEM measurements and the sample was not measured directly after sample preparation. During the delay, the sample was improperly stored and handled. Thus, the change in size distribution can be attributed to agglomeration. A follow-up UV/Visible spectrum was not measured due to the low concentration of the TEM sample. Similarly, an attempt to obtain information on the crystallinity by x-ray diffraction failed due to insufficient sample thickness.

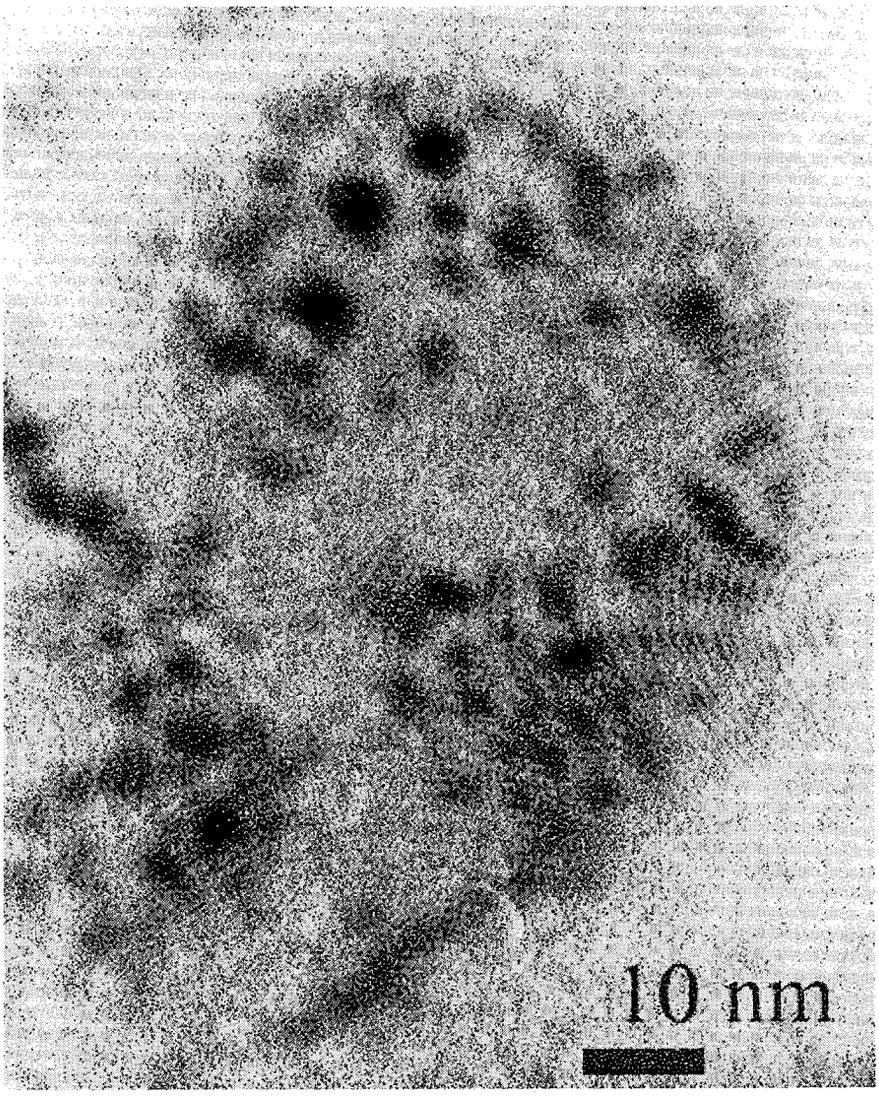

Figure 5.4. TEM for a sample of CdSe/ODE (**II**). Fringes are due to the scanner.

A second attempt to obtain a TEM with a freshly prepared sample, this time of dendronized QDs revealed round particles with narrow size distribution. From experience it was ascertained that the particles are certainly smaller than 5 nm in diameter. Due to problems with the development of the film taken of that sample a TEM picture is not available.

Thermogravimetric analysis (TGA) has shown that progressive heating of QDs leads to volatilization of the organic fraction. A residue of CdSe presumably remains in the sample pan. TGA experiments (cf. Figure 5.5) result in an estimated total organic content of 75%. The first weight loss, labeled A in Figure 5.5, corresponds to ~15% of the weight of the total product, and is assigned to the removal of trapped solvent (*i.e.*, hexane). The second step (cf. B in Figure 5.5) starts at temperatures above 200°C. This is a higher temperature than the temperature that free ODE volatilizes (cf. dashed line in Figure 5.5), but is assigned to volatilization of bound ODE. However, the total removal of ODE from the QD surface is not complete until ~350°C has been reached. This fraction accounts for 60% of the total product weight. Another decrease of 5% weight occurs up to 550°C, but the cause of this weight loss is not presently known. It could be due either to the loss of organic material, or to volatilization of low melting small QDs. The later explanation is rather unlikely, however, since the removal of ODE should lead to agglomeration and formation of bulk CdSe at that point in the thermogravimetric process. Values of the weight fractions for CdSe/ODE are, therefore, 15% of the total weight loss is due to solvent, 60% is from the ODE coating and 5% from possible decomposition products of ODE. This gives a total organic weight loss of 80%, which implies that the remaining 20% of the total weight is inorganic CdSe. Normalizing the TGA to 100% by removing the 15% due to solvent volatilization gives a final composition of approximately 25% inorganics and 75% organics for CdSe/ODE (**II**).

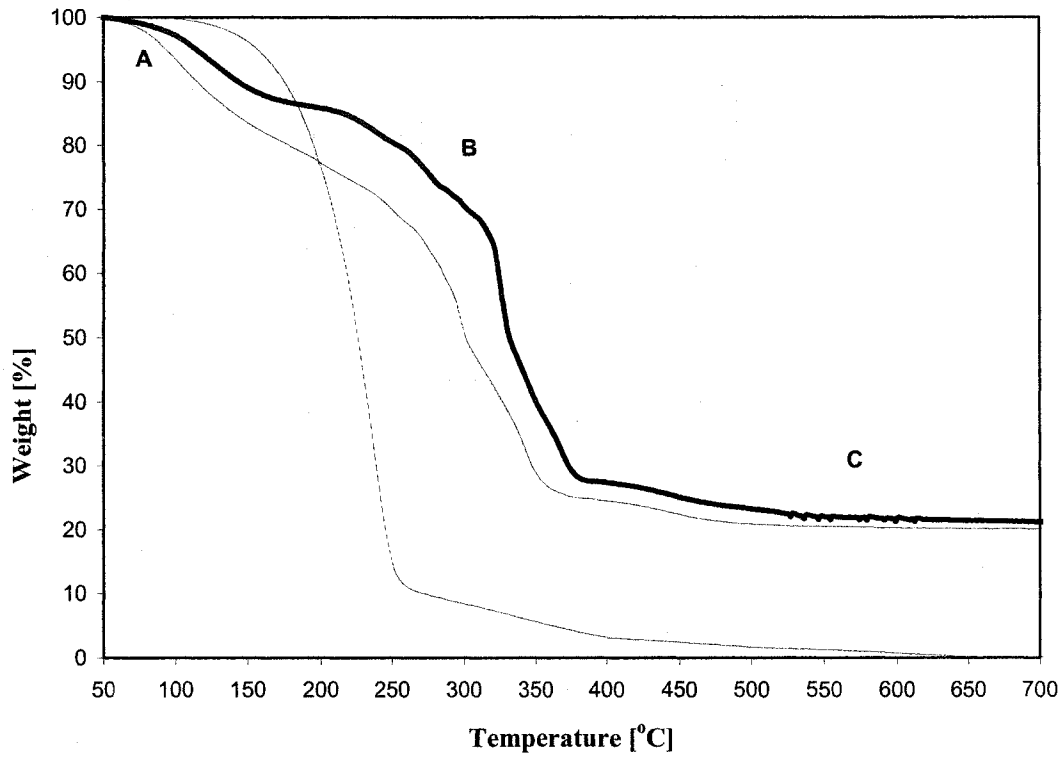

Figure 5.5. Thermograms for ODE (dashed line) and two samples of CdSe/ODE (**II**) (thin and thick solid line). Temperature increment was 20°C/min.

Elemental analysis of CdSe/ODE is not consistent with the inorganic content found by TGA. Elemental analysis yields C, 83.60%; H, 15.51%; Cd, 0.92%; and Se, 0.85% (cf. Chpter 9). Values found for carbon and hydrogen agreed with the mole ratio calculated for ODE within error limits. Assuming that the Cd and Se percentages found in elemental analysis are correct then the QD composition is 50 ODE molecules to 1 Cd to 1.3 Se with an overall inorganic content of only 1.77%. It seems unlikely that this many ODE molecules could be coordinated to each cadmium ion. However, when one assumes that the C percentage is applicable, then the elemental ratio changes to 8 ODE molecules to 1 Cd to 1 Se with an overall inorganic content of 9.26%, which is closer to the fraction of inorganics obtained from TGA, *i.e.*, 25% inorganic. Moreover, this is not

the first time that discrepancies between TGA and elemental analysis have been observed. Working with gold QDs coated with alkylthiols of different chain length, Murray finds that elemental analysis seemed to under-report the gold content. However, the C, H, O, S ratio of the different coatings are in agreement with the atom ratio as expected from the molecular composition.[138] Furthermore, he found TGA to under-report by 5% the organic content in palladium dodecanethiol QDs.[109] Fox reports a 7% disagreement between TGA and elemental analysis for the organic portion of thiolated gold QDs.[155] Vossmeyer, on the other hand, can achieve agreement only when comparing TGA results of 44% organics with the C, H, O portions in the elemental analysis, but disregarding sulfur completely. In his case, working with thiolated CdS QDs, the source of sulfur is two-fold. He raises the interesting question whether the mass loss in TGA could be mainly due to decomposition of the organic ligand in course of which the Cd-SR and/or CdS-R bonds are cleaved. Only the latter would be in agreement with TGA data.[51]

Initially, the lifetime measurements for CdSe/ODE were analyzed assuming a single lifetime, as expected from literature data (cf. Table 5.1. entry 3 and 4). However, a much better fit to the experimental data was obtained when two lifetimes were assumed (entry 5-10). Batches 3 and 4 were retro fitted with two lifetimes (values in parentheses). Batches 5 to 10 gave lifetimes ranging from 6.5 to 35.7 ns for the fast component (*i.e.*, τ 1 in Table 5.1) and from 101.9 to 162.5 for the slower component (*i.e.*, τ 2 in Table 5.1) depending upon the batch. Understanding the variation in the lifetime measurements for what is otherwise the same material lead to repeating the measurements with sample #10. Table 5.2 lists the lifetimes obtained for that sample at different times and the time (t)

elapsed. From these data, it is obvious that the lifetime does not change significantly over time with a single exception. Both the slow and fast component lifetimes are faster when the QD is repeatedly excited with a laser within a close time interval (*i.e.*, 3 minutes). The research done thus far does not provide a possible explanation for the mechanism leading to two separate lifetimes for this system. Normally, the existence of two separate lifetimes implies the existence of an inhomogeneous mixture of two species. Investigating cadmium tellurium (CdTe) QDs, Eychmueller[166] finds that the mean luminescence lifetime depend on the emission wavelength, with the mean lifetime decreasing from ~ 120 ns at 1.94 eV to ~20 ns at 2.43 eV. However, he finds only one lifetime, as does everyone else. Another possible explanation is the difference in the size distribution from batch to batch as indicated by the value of the FWHM. Mostly, the lifetimes seem slower when the size distribution increases. Currently, a full explanation for the mechanism leading to two separate lifetimes for this system is not available.

Table 5.1. CdSe/ODE QD batches 1 to 10, FWHM [nm], lifetime τ [ns] and UV/Vis absorption maxima. For comparison, a sample of CdSe/TOPO acquired from Evident Technologies, measured τ = 14 ns.

CdSe/ODE Batch #	FWHM [nm]	τ1 [ns]	τ2 [ns]	UV/Vis [nm]
1	30			492
2	30			468
3	30	15 (4.35)	(31.06)	450
4	29	22 (6.99)	(34.02)	510
5	36	19.4	125.6	474
6	34	21.5	103.8	496
7	32	19.1	101.9	498
8	32	6.5	107.9	484
9	38	8.5	162.5	474
10	42	35.7	159.6	470

Table 5.2. Repeat lifetime measurements for CdSe/ODE QD batch #10.

Time elapsed [hrs]	τ1 [ns]	τ2 [ns]
t = 0	35.7	159.6
t = 17	29.6	158.1
t = 17:03	21.3	148.9
t = 19	28.8	155.7
t = 21	28.2	155.2

5.3 Synthesis and Characterization of MAA coated CdSe QDs

NMR evidence indicates that mercaptoacetic acid (MAA) replaces the ODE coating completely. After washing CdSe/MAA with copious amounts of hexane ODE peaks are no longer visible in the NMR (see Chpter 9 for peak positions of CdSe/ODE). The NMR shows only the one resonance at 3.1 ppm (3.27 ppm for free MAA) that is expected from MAA in D_2O. Figure 5.6 shows both the UV/Vis absorption and the photoluminescence spectrum of a typical sample of CdSe/MAA (**III**). Comparison of the UV/Visible absorption spectra of CdSe/ODE and CdSe/MAA (cf. Figure 5.7) shows a 12 nm red shift in the QD peak for the CdSe/MAA. This shift indicates a small size increase from 2.2 nm to 2.3 nm in diameter and, therefore, implies that only minor crystal growth occurs when exchanging the coordinating ODE coating for the covalently bound mercaptoacetic acid coating. Additionally, the FWHM of the PL spectra (cf. Figure 5.8) indicates that the size distribution does not change during the replacement of ODE with MAA.

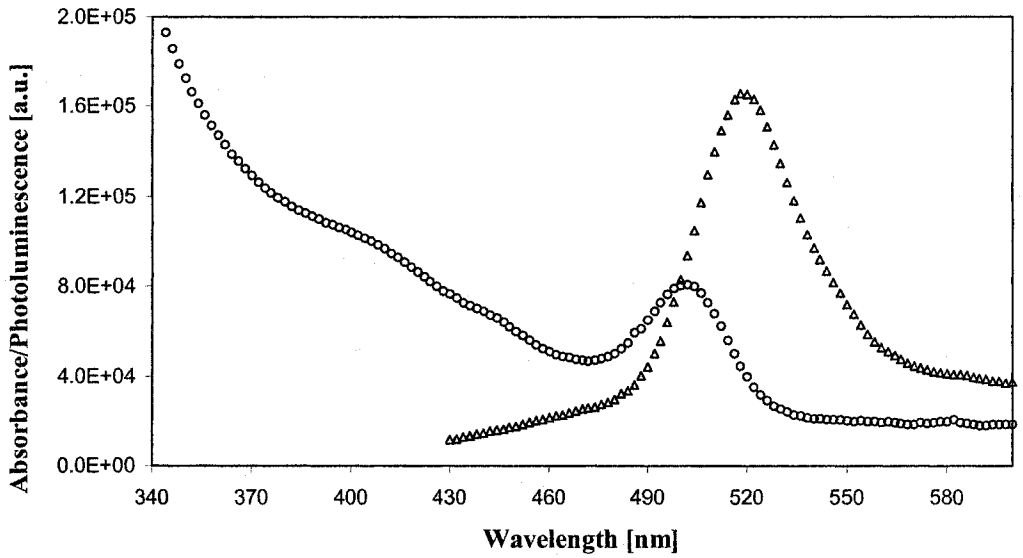

Figure 5.6. UV/Vis absorption (ooooooo) and PL (ΔΔΔΔΔΔ) of CdSe/MAA (**III**). UV/Vis maximum at 506 nm (expanded 400 000 times). PL emission maximum at 520 nm (excitation set at 400 nm), FWHM 40 nm.

A more dramatic change is the drop in PL emission intensity. As can be clearly seen in Figure 5.8, the relative emission intensity drops fifty fold when comparing the CdSe/MAA (solid line) with CdSe/ODE (dotted line). The broad peak ranging from 550 nm to 700 nm with a maximum at approximately 614 nm (cf. solid line in Figure 5.8) is not noticeable, since the dominant peak at 520 nm is very strong. However, in the CdSe/MAA, the muted dominant transition makes the broad emission peak more noticeable. The possible explanations for the differences in the overall shape of the PL spectrum are either (i) the broad peak in CdSe/MAA is due to the CdSe/ODE (*i.e.*, the starting material) and adding MAA only decreases the intensity of the main emission peak or (ii) the peaks at 520 nm and 614 nm are solely due to CdSe/MAA. The sharpening of the broad emission peak between 550 nm and 700 nm and the slight shift from 604 nm to 626 nm in maximum of this peak could be due to the change from a physisorbed coating (*i.e.*, the ODE) to a covalently bonded coating (*i.e.*, the MAA). In the

next chapter, we will discuss the synthesis and characterization of the dendrons that will later be attached to the CdSe QDs using a similar technique to the attachment of MAA to CdSe present here.

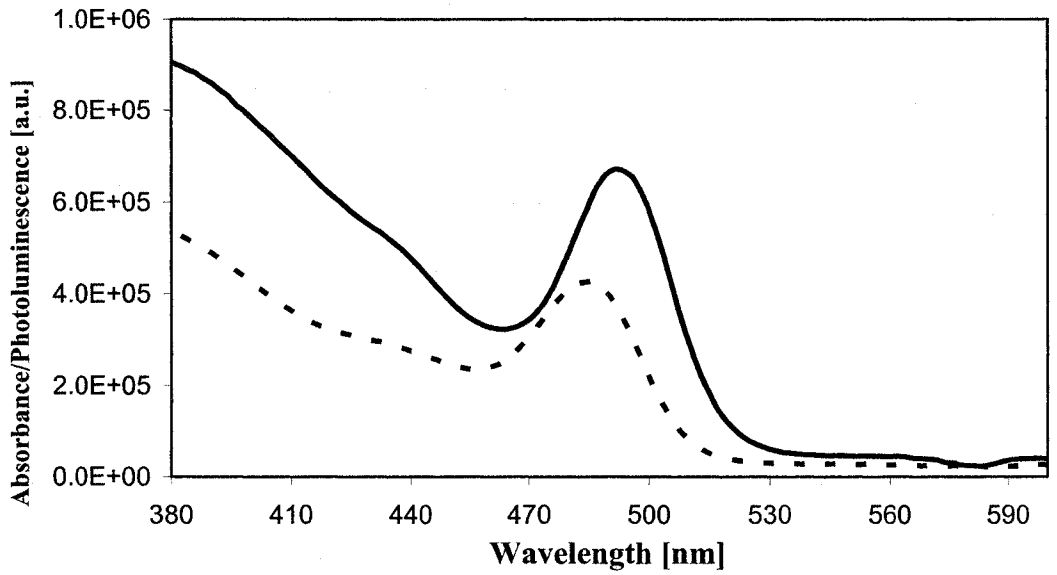

Figure 5.7. Comparison of UV/Vis absorption spectrum of product CdSe/MAA (**III**) (solid line) and starting material CdSe/ODE (**II**) (dotted line).

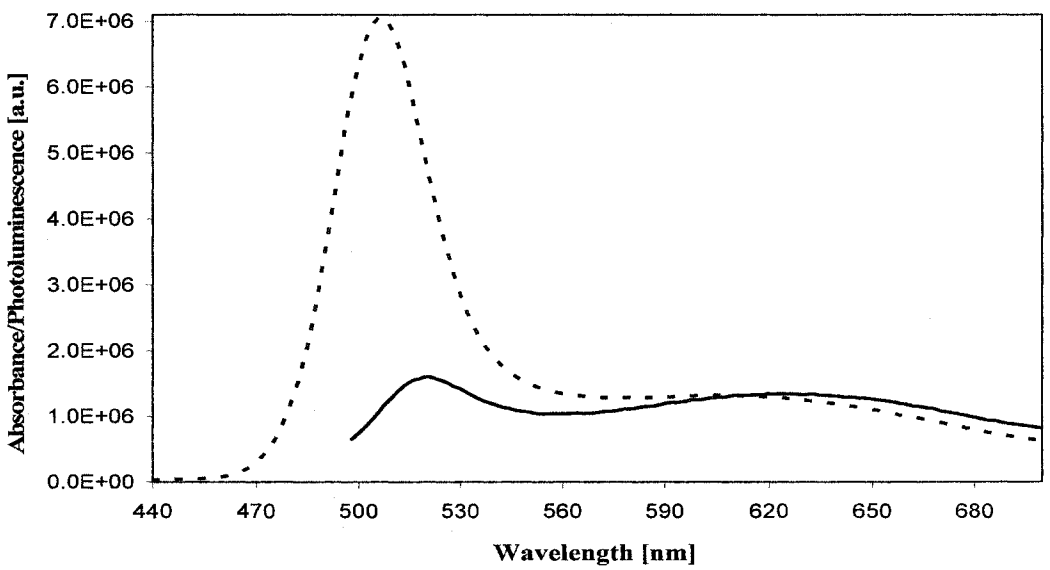

Figure 5.8. Comparison of PL spectrum of the product CdSe/MAA (**III**) (solid line) and the starting material CdSe/ODE (**II**) (dotted line).

6. Synthesis and Characterization of Dendrons

In the previous chapter, the synthesis and characterization of CdSe QDs with various types of organic coatings was presented. Birman[167] suggested embedding a semiconductor quantum dot array into an organic medium because the interaction of the Frenkel excitons in the organic molecules with Wannier excitons in the QD would allow one to control the optical non-linearity of the quantum dot/organic matrix system. Frenkel excitons are excitons arising from dipole-dipole interactions with strong electron/hole correlation and with the exciton being fixed in location within the crystal. Wannier excitons, on the other hand, are excitons that have a weaker electron/hole correlation and are free to move about the crystalline/molecular system. The existence of the organic matrix also allows the system parameters such as QD radius and QD spacing within the organic matrix to be well defined and controlled. Although Birman does not identify dendrons as a possible source of organic coatings, from his cited references,[168] one can conclude that thiolated CdSe and CdS QDs may be worth investigating.

From the suggestions presented by Birman and from the consideration of synthetic accessibility, the synthesis of focally substituted organothiol dendrons with different functionalized cores is pursued in this work. Dendrons are characterized by the core functionality, *i.e.*, amine, thiol, alcohol, and the number of repetitions of the structure, *i.e.*, the number of generations.

However, as explained in more detail below, the alcohol functionality had to be converted to a thiol, thus creating two sets of dendrons. The first set has an aromatic thiol as the core functionality, whereas, the second set has a thiol group attached to the one end of a three-carbon alkyl chain, making it an aliphatic thiol dendron. Figure 6.1 shows the structures of all three sets of dendrons with R = OH being the alcoholic dendrons, R = $NCH_3C{=}OC_6H_4SH$ being the aromatic thiols, and R = SH representing the aliphatic thiols for the three generations (cf. Figure 6.1A for generation one, Figure 6.1B for generation two and Figure 6.1C for generation three).

The alcoholic and aromatic thiol dendrons are synthesized according to previously published procedures.[169] The Fréchet-type synthesis used by Gorman to create the basic dendron allows for the scale-up of the reaction, since the total number of reaction steps decreased from three synthetic steps/generation in the original Fréchet synthesis to two synthetic steps/generation.[37] In particular, the activation of the *n*th generation alcoholic dendrons by mesylation (cf. Scheme 6.1) and then the reaction of the mesylated dendron with the repeat unit alcohol to give the next higher generation [G-(*n* + 1)]-OH (cf. Scheme 6.1) improves the overall reaction yield of the basic dendron. The terminal substituent on the dendron is added to the basic dendron in a similar manner as a standard repeating unit (cf. Scheme 6.2). However, instead of making the methyl ester, benzyl chloride is used to make the benzyl ester, which is then reduced to the alcohol with benzyl oxide groups on the benzene rings in the para positions. Before the thiol functionality can be added to the dendron, it must first be synthesized. This synthesis is shown in Scheme 6.3. The addition of the thiol functionality to the dendron begins by

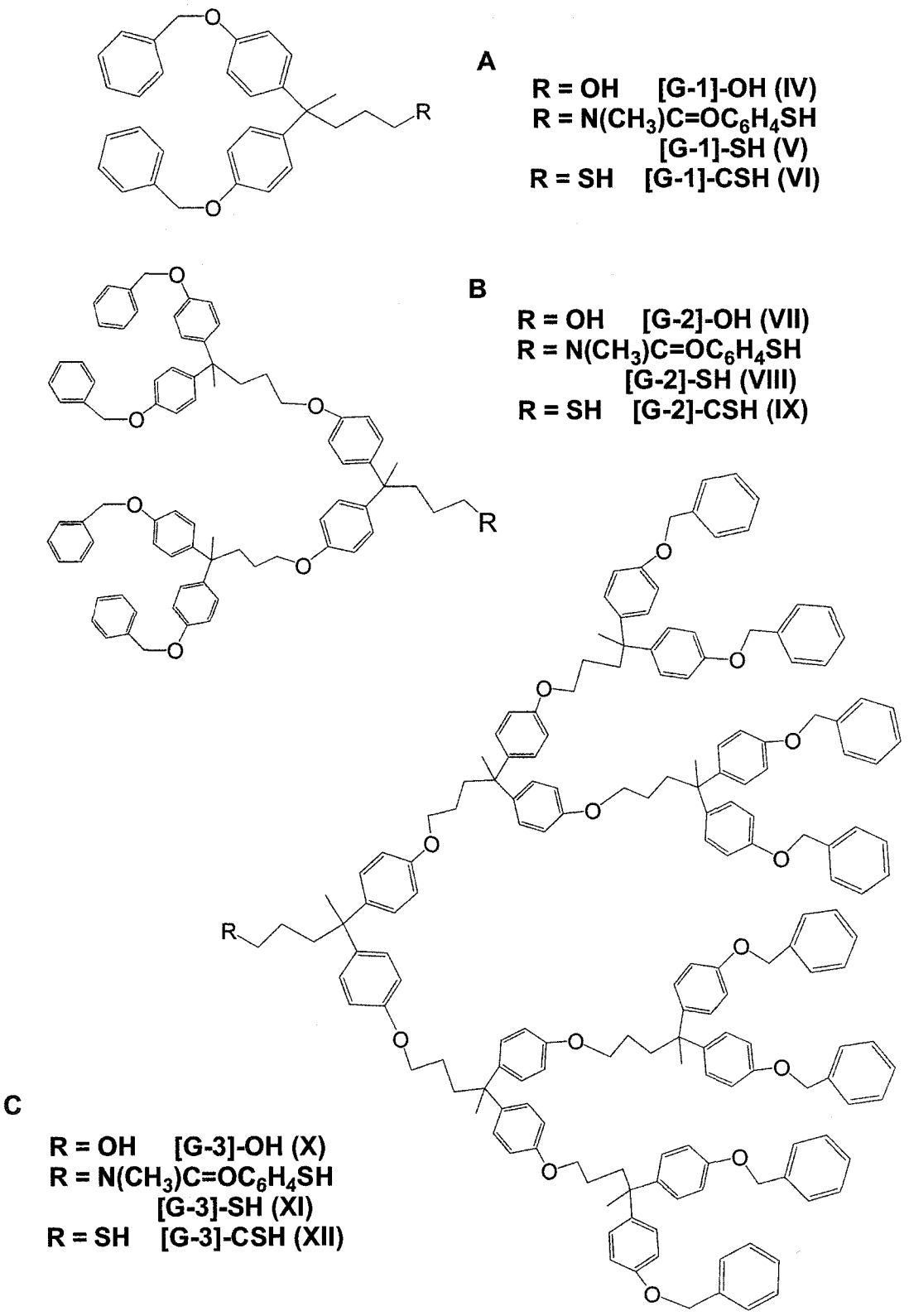

Figure 6.1. Structures of dendrons (**IV**) to (**XII**).

converting the alcohol in the dendron to a secondary amine. (cf. Scheme 6.1) The acyl chloride core structure with its protected aromatic thiol group (synthesized as in Scheme 6.3) is then covalently attached to the secondary amine forming an amide link (cf. Scheme 6.1) to create a functionalized dendron intermediate. The final step in the creation of the functionalized dendron is to deprotect the aromatic thiol. The yield of the deprotection step varies from 73% to 86 %, depending on the generation. The overall yield of the 17-step synthesis that gives the third generation deprotected aromatic thiol is less than 20%. Syntheses of the lower generation dendrons have higher percent yields.

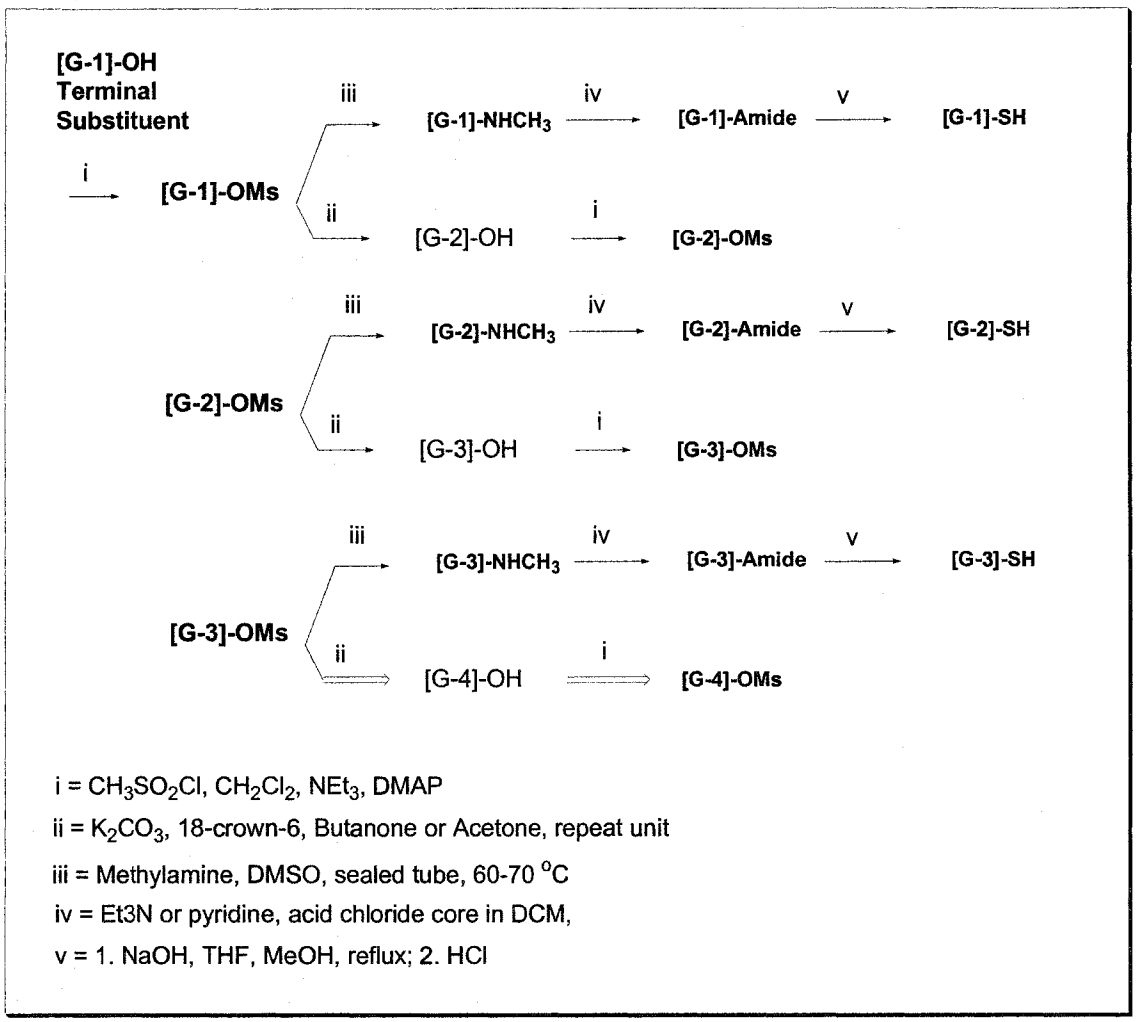

Scheme 6.1. Synthesis of generation n=1, 2, and 3 aromatic thiol dendrons (**V, VIII,** and **XI**) and alcohol dendrons (**IV, VII,** and **X**), adapted from[169].

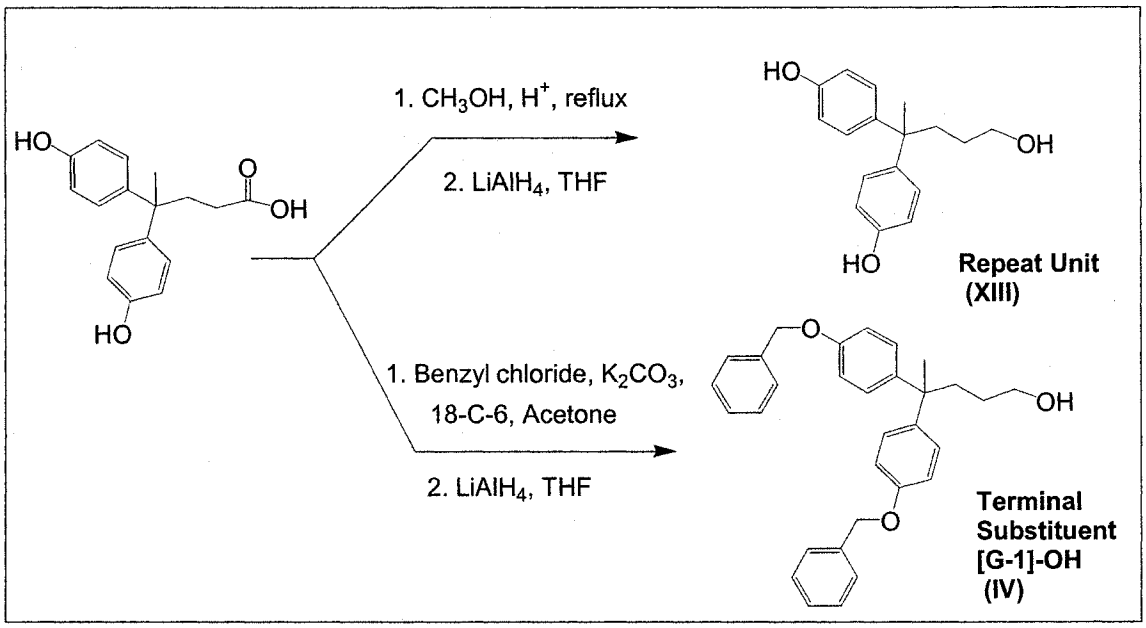

Scheme 6.2: Synthesis of repeat unit (**XIII**) and terminal substituent (**IV**) that is also the first generation alcohol, adapted from[169].

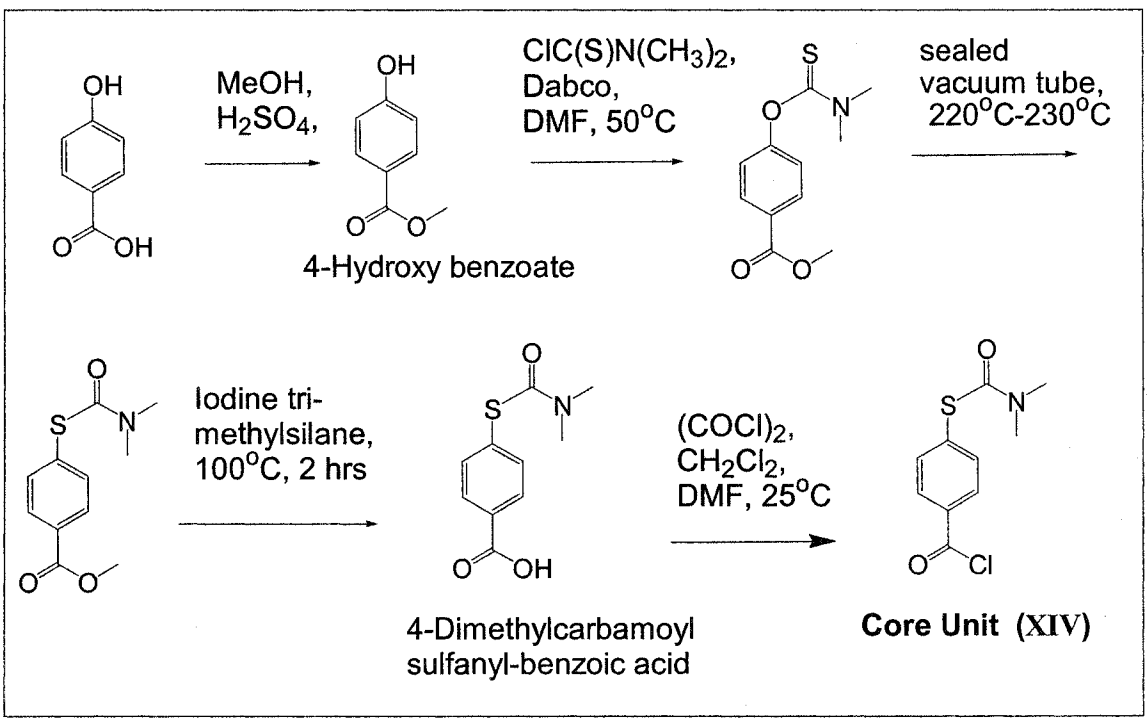

Scheme 6.3. Synthesis of protected thiol acyl chloride core unit (**XIV**). This is the core functionality for the aromatic dendron, adapted from.[169]

However, during the purification of the functionalized dendrons, we discovered that the thiol dendrons dimerize by the time these dendrons are eluted from the silica gel column, because oxidation of the SH group results in a sulfur-sulfur bridged dimer. Reduction of this bridged dimer with dithiothreitol (DTT), as shown in reaction Scheme 6.4, did not succeed in separating the dimers. Previous successful studies into the reduction of sulfur-sulfur bridged dimer systems used a 20 to 1000 fold excess of DTT and degassing of the solvents from 2 to 10 hours.[170,171] However, these methods did not work with the dendronic systems. Furthermore, the cyclic DTT reaction byproduct is not UV active and, therefore, does not show in thin layer chromatography (TLC). Since the byproduct of the reaction cannot be monitored, verifying the removal of this byproduct during the purification of the reaction mixture is difficult. Peng[106] has used DTT successfully to reduce sulfur-sulfur bridged dendrons. Since his dendrons were soluble in a water/methanol mixture, Peng was able separate the DTT by-product from the reaction mixture allowing for purification of the dendrons. However, Simanek has shown the insufficiency of the DTT reduction in larger dendronic systems.[172] Since the standard DTT reduction technique does not work for the dendrons synthesized herein, new methods for sulfur-sulfur reduction was needed. Both Gunsalus[173] and Fox[156] successfully used $NaBH_4$ in THF to reduce sulfur-sulfur bridged dimers. In the Gunsalus experiments, small bridge dimers were reduced. However, in the Fox experiments the dimerized thiolated dendrons were reduced and attached to gold nanoparticles in one step. With small modifications, we were able to reduce the dimerized functionalized dendrons using the Gunsalus procedure of $NaBH_4$ in THF.

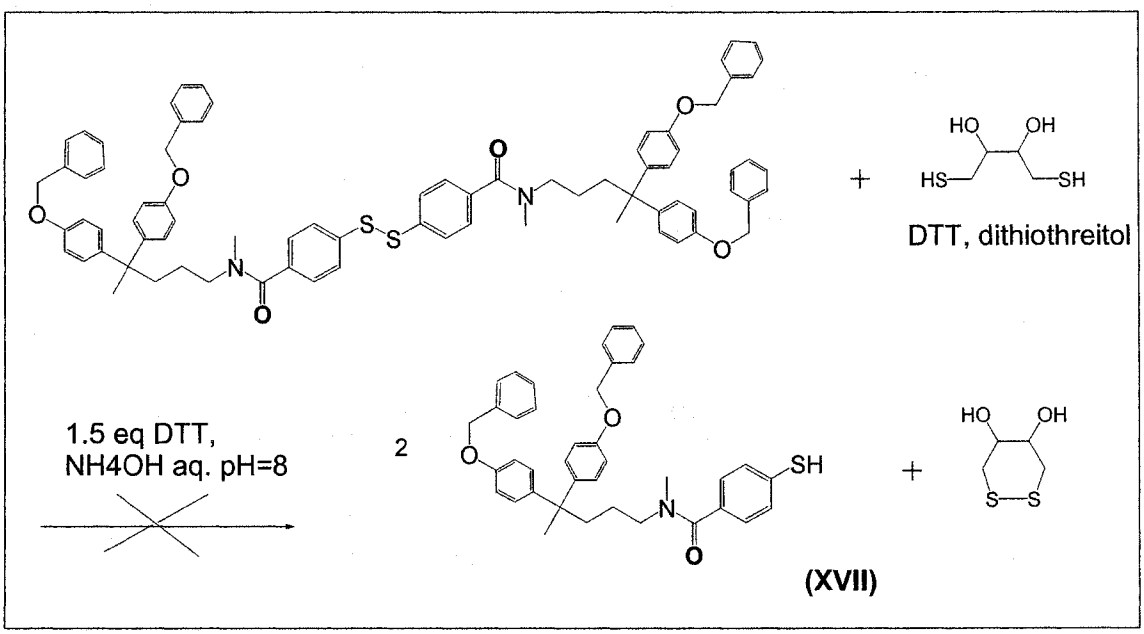

Scheme 6.4. Using DTT the reduction of the first generation aromatic thiol dimer (**XVII**) is unsuccessful. It should be noted that sodium boron hydride is successful in reducing the sulfur-sulfur bridge. However, for brevity, this mechanism is not shown.

Once the problems with the purification of the aromatic thiols were solved, we were then able to begin the synthesis and purification of the aliphatic thiols. Generation one and two alcoholic dendrons are converted to the respective generation aliphatic thiol dendrons by a two step modified procedure[174] (cf. Scheme 6.5 for details).

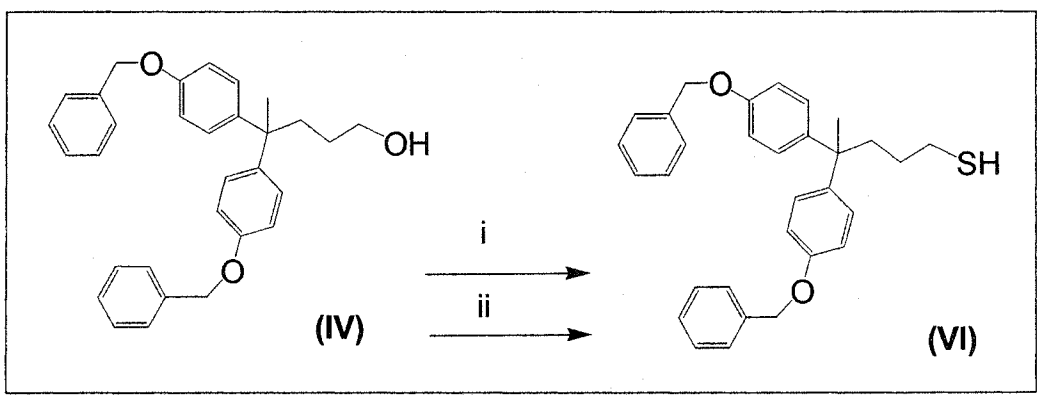

Scheme 6.5. Synthesis of the first (**VI**) generation aliphatic thiol dendron. i = triphenylphosphine, THF, diisopropyl azodicarboxylate, thioacetic acid, ii = reduction to remove protecting group using lithium aluminum hydride and hydrochloric acid work-up.

Unfortunately, the third generation alcoholic dendron did not react under the reaction conditions shown in Scheme 6.5. However, during the synthesis of the third generation aromatic thiol, the third generation mesylate (**XV**) was made. Since this material was available, we were able to use the third generation mesylate with sodium hydrogensulfide (*i.e.*, NaSH) to make the third generation aliphatic thiol dendron (cf. Scheme 6.6). To prevent the problems encountered during the purification of the aromatic thiol dendrons, the aliphatic thiol dendrons were not purified using a silica gel column. Instead, an extraction with methylene chloride was sufficient.

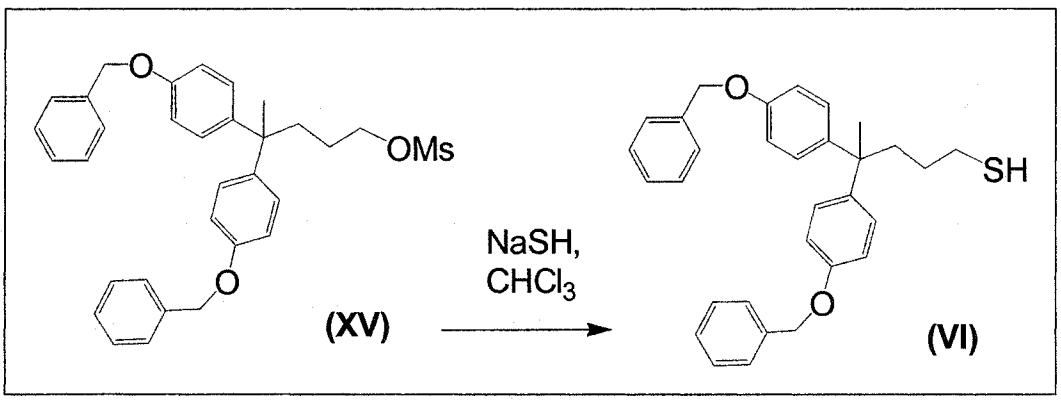

Scheme 6.6. Synthesis of the third generation aliphatic thiol dendron (**XII**). For clarity a first generation dendron is shown instead of a third generation dendron.

The alcohol functionalized dendrons of generation n =1, 2 and 3 (**IV, VII, X**) are characterized by ^{1}H and ^{13}C NMR. Generation 1 and 2 are also confirmed by mass spectroscopy. The third generation could not be characterized by mass spectroscopy because the molecular mass is too large for the available instrumentation. The details of these characterizations can be found in Chpter 9.

The first- and second-generation aromatic thiol dendrons (**V, VIII**) are also characterized by ^{1}H and ^{13}C NMR. The ^{1}H NMR confirms the SH proton of the second-generation dendron but not of the first generation. The inability to detect the first generation SH is thought to be due to rapid S-H proton exchange. The first and second generation thiol dimer has also been confirmed by mass spectroscopy. Again, the third generation thiol has too great a molecular mass for mass spectroscopy. Both generations one and two of aliphatic thiol dendrons (**VI, IX**) are characterized and confirmed by ^{1}H, ^{13}C NMR, mass spectroscopy, and elemental analysis. The details of these characterizations can be found in Chpter 9. In the next Chapter, we will present the synthesis and characterization of dendronized CdSe QDs.

7. Synthesis and Characterization of Dendronized CdSe QDs

One novel aspect of this work is the use of ODE as a photoactive coating of the QD instead of the TOPO/TOP and an examination of the reactivity of ODE coated QDs. The reason for our choice of ODE as a coating is the fact that TOPO/TOP coated QDs present synthetic constraints when attempting to replace the datively bound TOPO/TOP with the desired dendron. For example, Lajos Balogh[159] was able to displace the standard TOPO/TOP coating of a QD (generally a CdSe/ZnS QD, or a similar core/shell quantum dot) with pyridine to be able to attach amine functionalized dendrons. However, during the replacement of TOPO with pyridine, the QD surface was exposed, which allows for crystal growth. Peng succeeded in synthesizing a thiolated QD by adjusting the pH to 10.3 using tetramethylammonium hydroxide.[160] The disadvantage to this synthetic approach is that it requires a high-quality dry box. Furthermore, contradicting reports exist in the determination of the exact amount of TOPO remaining attached on the QD surface after ligand exchange. Bawendi determines that up to 15% of TOPO remains firmly bound on the QD surface.[30] Alivisatos concurs after first claiming not to find any phosphorus using XPS, and thus no TOPO, then adding to have found 12% P by integrating a small P peak.[29] Contradicting these findings Peng publishes ^{1}H NMR results of CdSe/TOPO QDs before and after the replacement of TOPO by aromatic hydrophilic thiols. The peaks in the aliphatic proton region of TOPO were completely replaced and two new broad peaks in the aromatic region appeared, belonging to the thiol.[112] ODE, on the other hand, can be displaced readily from the surface of the QD because of the weaker bond. This factor facilitates the covalent attachment of the incoming dendron. An

illustration of this is the fact that ODE can be readily replaced by TOPO when CdSe/ODE (**II**) is stirred in the presence of TOPO. The successful exchange between ODE and TOPO is accompanied by a change in solubility from non-polar to polar solvents and based on the lack of change in the absorption spectrum, without a significant change in QD diameter (*i.e.*, a change < 0.2 nm). The PL spectrum of CdSe/ODE QDs indicates that emission intensity and particle size distribution is unaffected as well. In the remaining sections of this Chapter, we will discuss the attachment of the dendrons synthesized in Chapter 6 to the QDs discussed in Chapter 5.

7.1 Synthesis and Characterization of Alcohol Dendronized CdSe QDs

In Chapter 5, we discussed the synthesis of mercaptoacetic acid coated CdSe QDs. Nie[26] has successfully attached proteins to a mercaptoacetic acid coated core/shell QD (abbreviated CdSe/ZnS/MAA). Due to the protein size (*i.e.*, 100 KDa), only 2-5 proteins can be attached to a QD with a 5 nm diameter. Thus, the binding of a large protein directly to the surface of a QD, instead of to the QD coating, would not be practical, since most of the QDs surface would be left unprotected. Dendrons, although their molecular weight is much smaller than that of a protein, are not expected to completely cover the QDs surface because of steric hindrance due to the branching in the dendron. Since we expected similar behavior in comparison to the protein experiments, we planned to use the surface modification of MAA coated QDs to synthesize the dendron coated QDs. However, the surface modification for these experiments will be achieved via esterfication using the alcohol dendrons (**IV, VII, X**) instead of amidation.

Various attempts to couple alcohol functionalized dendrons to the carboxylic acid of the CdSe/MAA (**III**), which would result in an ester link between the mercaptoacetic acid coated QDs and the alcohol dendrons, failed. The first attempt involved the commonly used coupling reaction for esterfication which applies dicyclohexylcarbodiimide (DCC) and dimethylaminopyridine (DMAP).[62,175,176] This attempt was probably unsuccessful due to steric hindrance, since the DCC has to couple to the carboxylic acid hydroxide oxygen, and the dendron alcohol functionality to the carbonyl carbon of the carboxylic acid in MAA. Fischer esterfication was dismissed as a possible route due to the lack of stability of CdSe QDs in hydrochloric acid, which was determined by the addition of a small amount of hydrochloric acid to the CdSe QDs. Addition instantly decolorized the yellow QD solution, indicating the destruction of the CdSe QDs. From this colorless solution, an unknown black precipitate forms. Attempts to proceed via a mixed anhydride intermediate[175,177,178] failed most likely due to the presence of traces amounts of acid in the acetic anhydride. Thus, the only remaining choice for an esterfication reaction was the use of coupling reagent BF_3•etherate.[179-181] Unfortunately, this reagent is too weak an electrophile to cause the desired coupling reaction.

7.2 Synthesis and Characterization of Model Ligand Coated CdSe QDs

The experience of coupling alcohols to MAA coated QDs showed that sometimes the standard organic synthetic pathways may not be applied to reactions involving QDs. Since the syntheses of the thiol dendrons used in this project are not high-yield syntheses

(cf. Chapter 6), very little of the dendron is available for testing different reaction mechanisms. Therefore, a model compound with the same basic functionality as the dendrons needed to be found in order to test new synthetic pathways. For this purpose, 6-mercaptopurine riboside (MPR), a commercially available thiol (cf. Figure 7.1). MPR was chosen because of its aromatic thiol and due to the lack of any interfering functional groups that might also react with the QDs such as additional thiols or primary and secondary amines. MPR has a molecular weight of only half the mass of the first generation dendron, but it is a large, commercially available thiol and, therefore, chosen as an acceptable model ligand for the aromatic thiol dendrons.

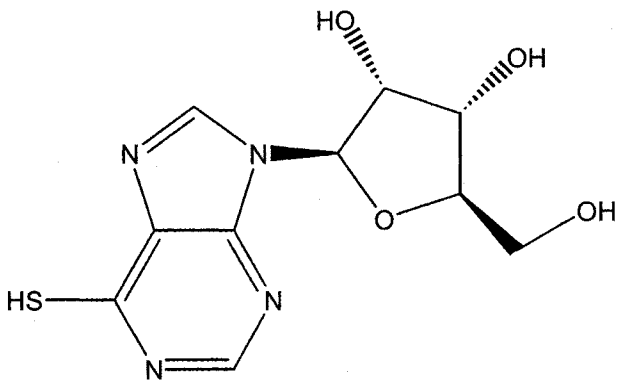

Figure 7.1. The molecular structure of 6-mercaptopurineriboside was chosen to serve as a model ligand to explore possible routes to attach thiol dendrons to CdSe QDs.

With the model compound chosen, the first obvious challenge was to find the appropriate solvent mixture to allow both main components, the MPR and the CdSe/ODE QD, to interact without either component precipitating out of the mixture. ODE coated QDs dissolved readily in hexane and benzene, but not in polar solvents. The model ligand does not dissolve in non-polar solvents, but is slightly soluble in methanol and very

soluble in DMSO. The initially attempted synthesis of CdSe/MPR involved using a methanol/ODE mixture. However, when the QD/ODE solution was added to the MPR/methanol mixture, the MPR precipitates. The solution to the overall problem of a suitable solvent system was found by carefully balancing the ratio of methanol and DMSO with the QD/ODE mixture. This ratio was experimentally determined by adding a methanol solution to an existing QS/ODE solution without stirring. The addition generates two layers in the round bottom flask. A saturated MPR solution in DMSO was added dropwise with stirring. The concentration of MPR initially added to the methanol/QD/ODE solution was based on experience from synthesizing MAA coated QDs. The base, tetradecylammonium hydroxide, was then added dropwise and the reaction was refluxed overnight at 59°C. When the reflux was completed and stirring was discontinued, the methanol and ODE phases separated again. Both phases were cloudy and colorless. However, a yellow solid was stuck to the wall of the flask. Attempts to dissolve this yellow precipitate with a plethora of organic solvents were unsuccessful. The appropriate solvent was found by accident, when a small amount of the yellow solid was left in a centrifuge tube needing to be washed. During cleaning of this tube with water, a bright yellow, clear solution was formed. CdSe/MPR (**XVI**) dissolves in both water and D_2O. Thus, with these adaptations, namely using chloroform and DMSO in addition to methanol and changing the ratio of that solvent mixture, the two-phase system that is used to make MAA coated QDs (cf. Chapter 5) works very well with this model ligand.

Figure 7.2 shows the UV/Vis spectra of the free MPR and the CdSe/MPR QD (**XVI**). The PL spectrum of the CdSe/MPR QD is also shown. As was seen with the MAA coated QDs (cf. Figure 5.8), the photoluminescence intensity drops. However, for this system, the drop in photoluminescence intensity is accompanied by a size distribution increase. In fact, the FWHM for CdSe/MPR is 50 nm instead of the 30 nm seen in CdSe/MAA QDs (cf. Figure 5.8). The change in the FWHM of this broad peak is probably due to an increase in particle size distribution, comparable to the one observed when coating CdSe/ODE ODs with MAA.

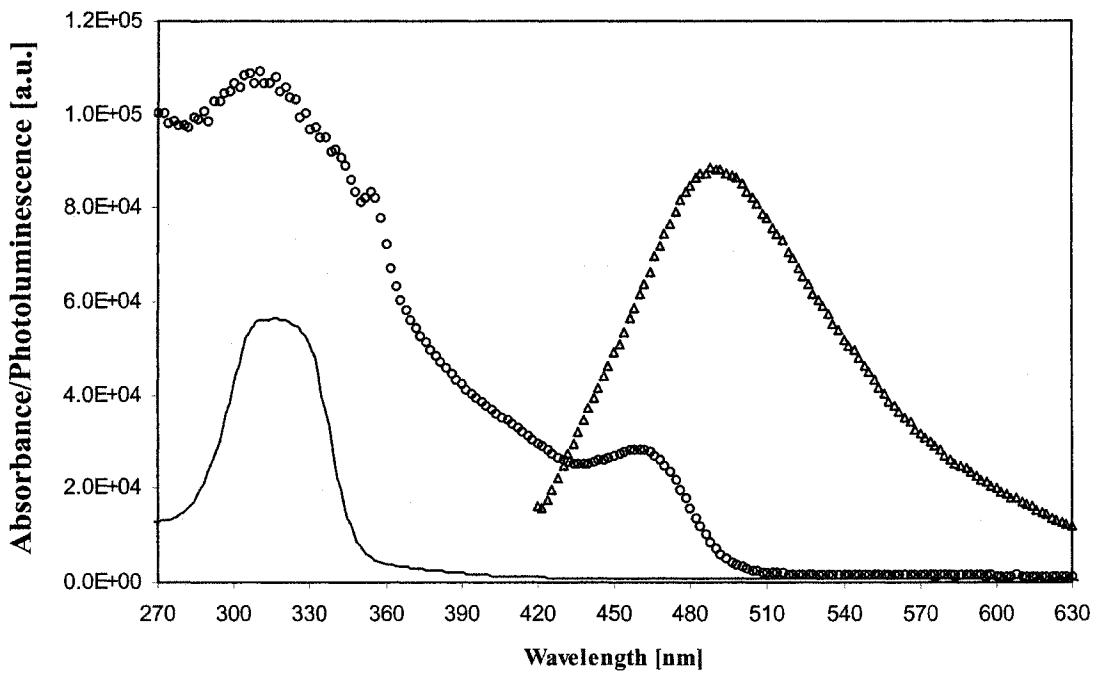

Figure 7.2. UV/Vis absorption (ooooooo) and PL (ΔΔΔΔΔΔ) of CdSe/MPR (**XVI**) in water. UV/Vis absorption of MPR ligand in DMSO (——). UV/Vis maximum of CdSe/MPR (**XVI**) is 460 nm (ooooooo) and 316 nm for the MPR ligand (——). Both expanded 30,000 times. PL emission maximum lies at 488 nm. Full width at half max (FWHM) is 50 nm.

Thermogravimetric analysis (TGA) experiments for CdSe/MPR (**XVI**) (cf. Figure 7.3) result again in three distinguishable temperature Zones, designated A, B, and C. Zone A, which is from 0°C to 200°C, shows a 5% weight loss. This weight loss is attributed to the loss of trapped solvent (H_2O, bp = 100°C). The fact that the pure MPR ligand has zero weight loss for the first 200°C seems to confirm this assumption. Zone B from 200°C to 600°C shows a 75% and 65% weight loss (from two different samples) represents the loss of the organic coating. Zone C (all temperatures > 600°C) gives the estimate of total inorganic content at 20% and 30%, depending upon QD sample. The difference between the two TGAs can be explained by considering the difference in QD size for the two QD samples. The batch represented by the thin line in Figure 7.3 was synthesized with bigger QDs, in order to obtain x-ray diffraction measurements. These measurements will be discussed later. The large QDs have an UV/Vis absorption maximum at 510 nm, implying a 2.5 nm diameter size (cf. Fig. 5.2). The QDs represented by the thick solid line were only 2.1 nm in diameter (*i.e.*, have a UV-Vis max at 470 nm). The noise that is apparent in the small diameter sample is due to very small amount, *i.e.*, 1.5 mg, of CdSe/MPR QDs used. Ideally, the sample size should be 8-10 mg. One can clearly see that the onset of the final Zone (*i.e.*, Zone C) is different for both samples, namely 750°C for the smaller QDs versus 650°C for the larger QDs. As discussed before in Chapter 5, the reasons for the onset variation due to QD size are not well understood. However, possible mechanisms for the difference in the onsets will be discussed in Chapter 8.

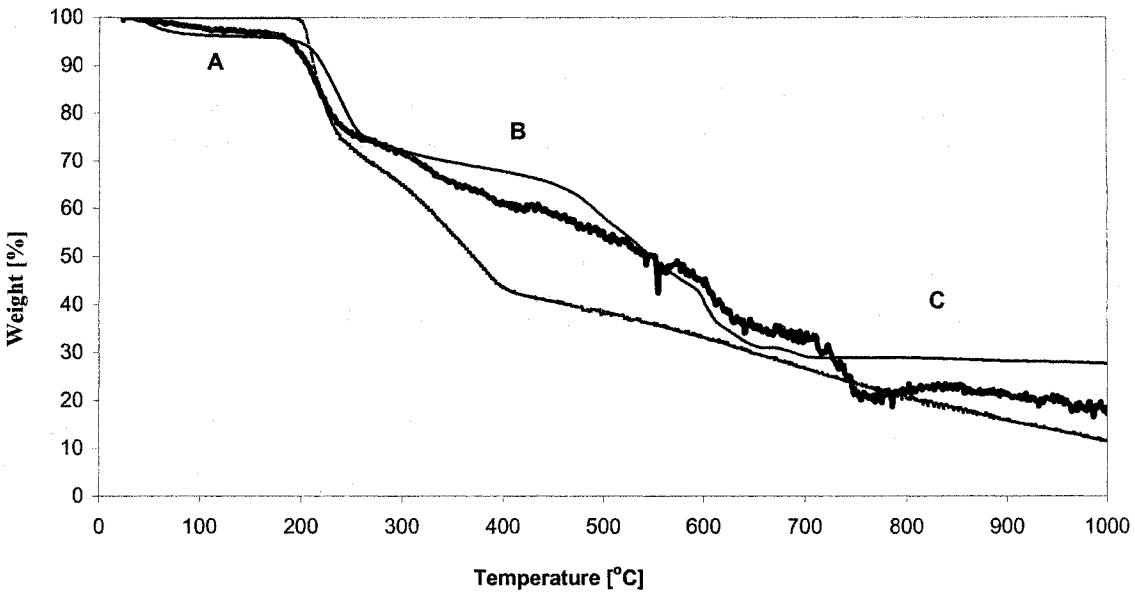

Figure 7.3. Thermograms for MPR ligand (dashed line) and two samples of CdSe/MPR (**XVI**) (thin and thick solid line). Temperature increment was 20°C/min.

In summary, the experience with the MPR model ligand gave the following results. The solubility of the different components has to be considered carefully when preparing the reaction mixture. The solubility of the final product may differ significantly and in unexpected ways from the solubility of all of the starting materials. The yield of any given reaction batch may be as low as 14 mg (see Chpter 9 for further details) and, therefore, not always suited for the characterization measurements that were originally planned.

7.3 Synthesis and Characterization of Aliphatic Thiol Dendronized QDs

After working with the model ligand, the first endeavor in attaching a dendron to the CdSe/ODE QDs was made using the first generation aliphatic thiol dendron (**VI**) instead of an aromatic dendron. The reason for this choice was the amount of available dendron in case problems arose during the synthesis. The aliphatic thiol dendron like all the others synthesized (cf. Figure 6.1), is insoluble in methanol. However, methanol is an integral component of the reaction scheme for attaching the thiol model compound (cf. Section 7.2). Therefore, a new solvent mixture was required which would dissolve the dendron but still have the bilayered system necessary to perform the thiol attachment. The solution becomes a mixture of ODE: methanol: chloroform in a 2:1:1 ratio. With this new solvent mixture, the reaction proceeded as planned. However, the product, CdSe/SC-G1 (**XIX**) fell out of solution and no solvent, as of yet, has been discovered to redissolve this product. Consequently no solution measurement data, such as UV/Vis, PL, or NMR are available for this compound. Furthermore, prolonged attempts to get this material into solution led to premature decomposition.

After this experience, dendronized QD solutions were always degassed with copious amounts of argon during washing, precipitation and dissolution. The purified samples are stored in the freezer (-5°C) under an argon blanket. This rigorous treatment has led to a significant increase in shelf life. In fact one of the dendronized QD samples has yet to decompose (e.g., the second generation aliphatic thiol dendronized CdSe QD).

Since all remaining aromatic and aliphatic thiol dendrons are soluble in chloroform, but not in methanol, the solvent ratio of 2:1:1 ODE: methanol: chloroform previously determined was used for all remaining samples. The reaction of the second-generation aliphatic thiol dendron, G2-CSH (**IX**) proceeded as planned. This time, however, the product of CdSe/SC-G2 (**XX**) was soluble in chloroform. Figure 7.4 shows the UV/Vis spectrum (open circles) and the PL spectrum (open triangles) of the dendronized QDs. Lifetime measurements yield a two component decay with the fast component having a lifetime of 5.2 ns and with the lifetime of the slower component being 132.6 ns. ^{1}H NMR shows broadened peaks (cf. Chpter 9) as is expected from published literature[109,182].

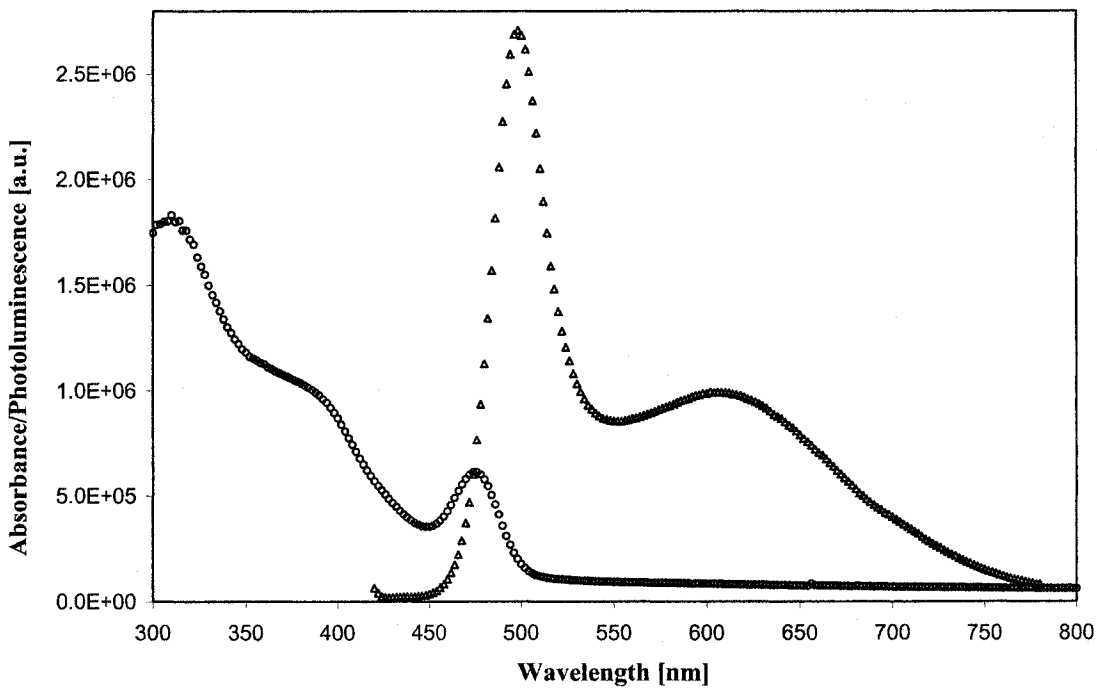

Figure 7.4. UV/Vis absorption (○○○○○○○) and PL (△△△△△△△) of CdSe/SC-G2 (**XX**) in chloroform. UV/vis maximum of CdSe/SC-G2 (**XX**) (○○○○○○○) is 476 nm, luminescence maximum is 498 nm and the FWHM is 34 nm.

TGA data (cf. Figure 7.5) for QDs functionalized with the second generation aliphatic thiol dendron show that Zone A gives a 5% weight loss due to trapped solvents and reagent impurities. The free dendron sample loses only less than 2% at that stage. Up to 600°C (cf. Zone B in Figure 7.5) 65% and 75% organic matter is lost. Further, 20% and 30% of presumably inorganic mater is lost in Zone C (cf. Figure 7.5). However, the graphs in Zone C first level off, but above 900°C more weight loss is registered. At 1200°C only 5% and 15% of the original mass remains. As will be discussed in Chapter 8 elemental analysis of this sample does not agree with these percentages; instead elemental analysis finds lower than expected percentages for Cd and Se.

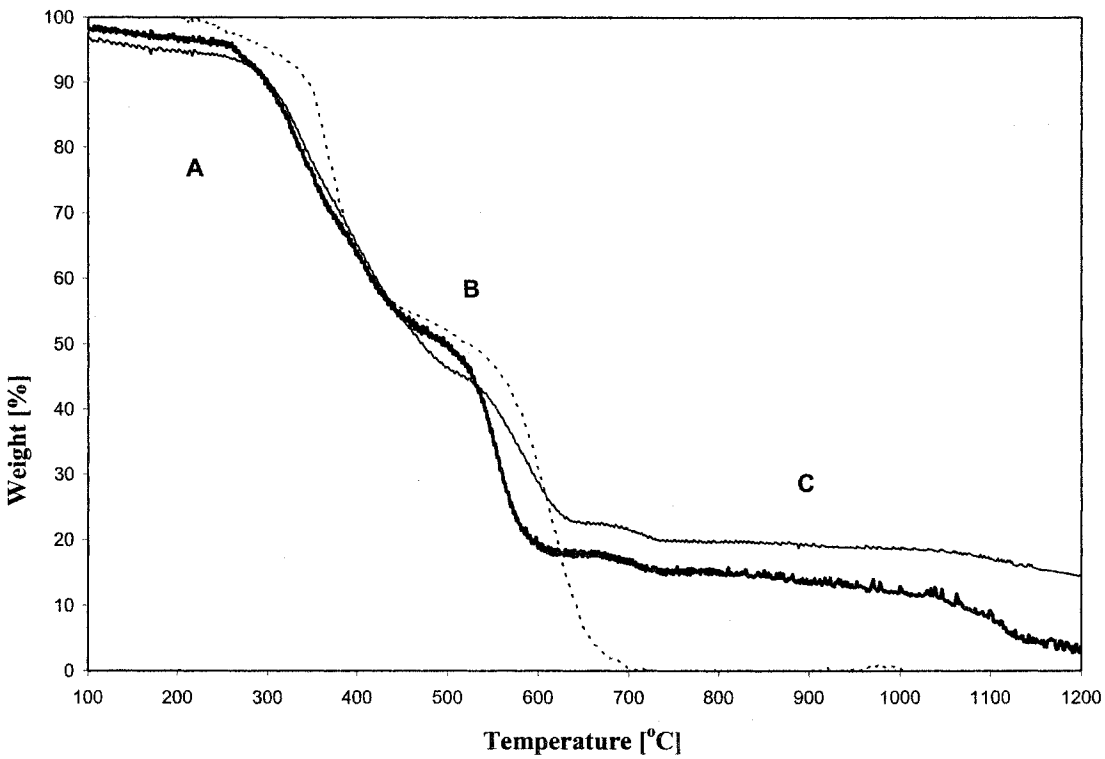

Figure 7.5. Thermograms for the second-generation aliphatic thiol dendron G2-CSH (**IX**)(dashed line) and two thermograms from one batch of CdSe/SC-G2 (**XX**) (thin and thick solid line). Temperature increment was 20°C/min.

Although the third generation aliphatic thiol dendron G3-CSH (**XII**) was synthesized, the dendronized QD, CdSe/SC-G3 (**XXI**) was not. The reason for not pursuing the synthesis of the third generation dendronized QD was that the photoluminescence intensity was not improving as the dendron increased in generation (as observed in the data for all of the first and second generations aliphatic and aromatic dendrons). In fact, rather the opposite happens and will be discussed in more detail later in this Chapter. Thus, the focus shifted to the question of how many dendrons actually bind covalently to the QD surface and how to measure experimentally this number of attachment. While TGA seems to provide some answers, TGA in conjunction with elemental analysis may give the best explanation and will be discussed in Chapter 8.

7.4 Synthesis and Characterization of Aromatic Thiol Dendronized QDs

The first generation aromatic thiol dendronized QD using dendron G1-SH (**V**), (cf. Figure 6.1) was synthesized according to procedures and methods established in Section 7.3. As with the first generation aliphatic thiol dendron the reaction product CdSe/S-G1 (**XVII**) precipitates to yield an insoluble solid. TGA data for these materials, however, were obtained (cf. Figure 7.6). They establish for them the highest inorganic relative content (*i.e.*, 55%) for any of the dendronized QD samples. This rather low content of organics may be responsible for the low solubility in organic solvents. However, the low organic content does not necessarily mean a smaller number of dendrons are attached to the QD as compared to the second generation coated QDs. The

smaller molecular weight of the first generation dendrons is less than half of the molecular weight of the second generation.

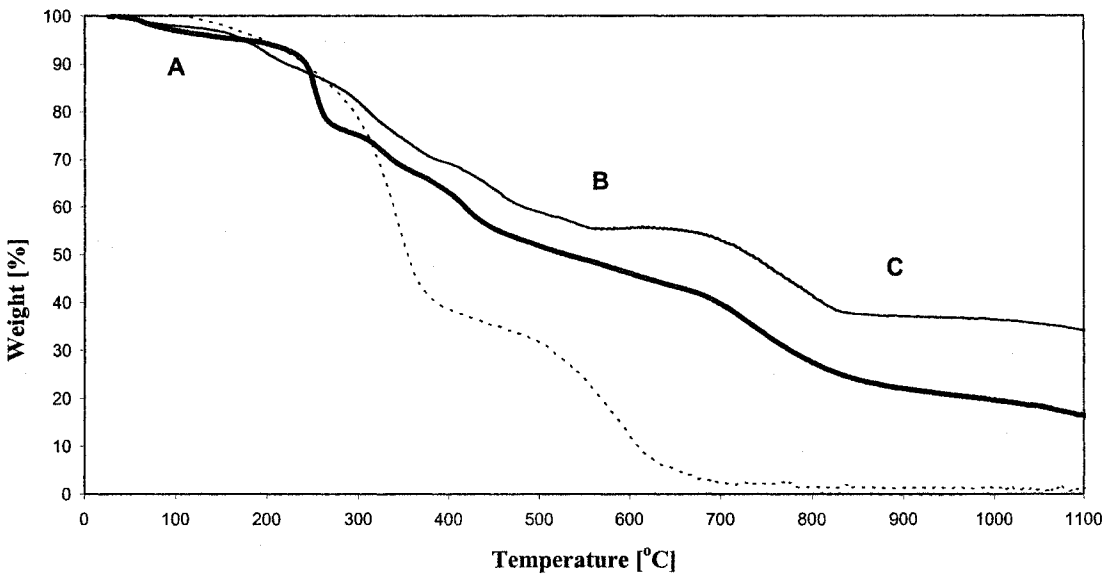

Figure 7.6. Thermograms of CdSe/S-G1 (**XVII**) are each (thin and thick solid line) from two different preparations and are compared with the TGA of free dendron G1-SH (**V**) (dashed line). Temperature increment was 20°C/min.

All three samples, QDs and free dendron show a loss in Zone A of 5% of the total weight (cf. Figure 7.6). Zone B, assigned to the loss of the bound dendron, is 40% and 50% of the total weight for two separate samples. Since the lack of solubility prevents determining particle size using UV/Vis, the particle size of these samples could not be established and, therefore, the change in the bound dendron weight between samples cannot be quantitated. From the experience with the MPR model ligand coated QDs (cf. Section 7.2), the variation in relative weight loss for the organic coating can be attributed to a variation in QD size. In Zone C a total of 45% and 55% of the weight is lost. The TGA registers weight loss above 900°C, with a final percentage of 10% and 25% remaining at 1200°C. As mentioned previously, the nature of the material lost was

assumed to be inorganics but is actually still unknown. Interestingly, the sample represented by the thick line continues losing weight until the end of the run at 1100°C, while the other sample levels off as expected. TGA data reported on CdSe/TOPO by Bawendi does not explain any of the observations here. First, he focuses on determining the relative amounts of surface pyridine, TOPO and the percent removal of TOPO.[30] He does not mention the temperature range he employs. However, other TGA studies found in the literature for other types of QDs, mainly CdS,[183,184] CdTe,[185] gold[50,162] or palladium,[109] show thermographs of a temperature range between 50°C and 600°C. A systematic study on weight loss and particle size of QDs with the same dendron coating is needed to resolve these uncertainties.

The reaction of the second generation aromatic thiol dendron, G2-SH (**VIII**) yielded the product, CdSe/S-G2 (**XVIII**), which is soluble in chloroform. Therefore, Figure 7.7 shows the UV/Vis spectrum (open circles) of the dendronized QD as well as the PL spectrum (open triangles). The truncated PL spectrum of the starting material (cf. Fig. 7.7, solid line) clearly illustrates that the emission intensity decreases with the attachment of the dendron. On the other hand, the constant FWHM of 40 nm in the PL spectrum indicates that the QD size distribution does not increase.

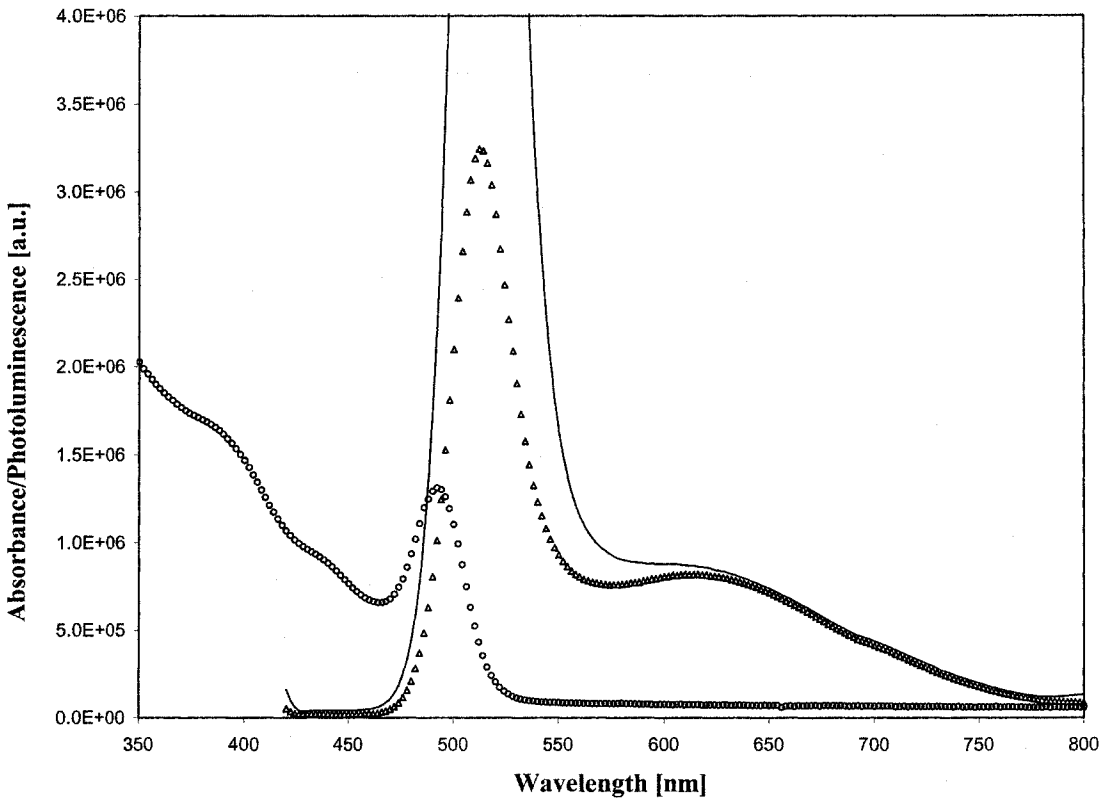

Figure 7.7. UV/Vis absorption (ooooooo) and PL (ΔΔΔΔΔΔ) of CdSe/S-G2 (**XVIII**) in chloroform. PL of CdSe/ODE (**II**) starting material in hexane (——). UV/Vis maximum of CdSe/S-G2 (**XVIII**) is 492 nm (expanded 1,000,000 times), and is unchanged from the starting material (not shown). PL emission maximum is positioned at 512 nm (ΔΔΔΔΔΔ). Peak position of truncated starting material is unchanged, but relative intensity is 3 times higher. Full width at half max (FWHM) is 40 nm for both product and starting material.

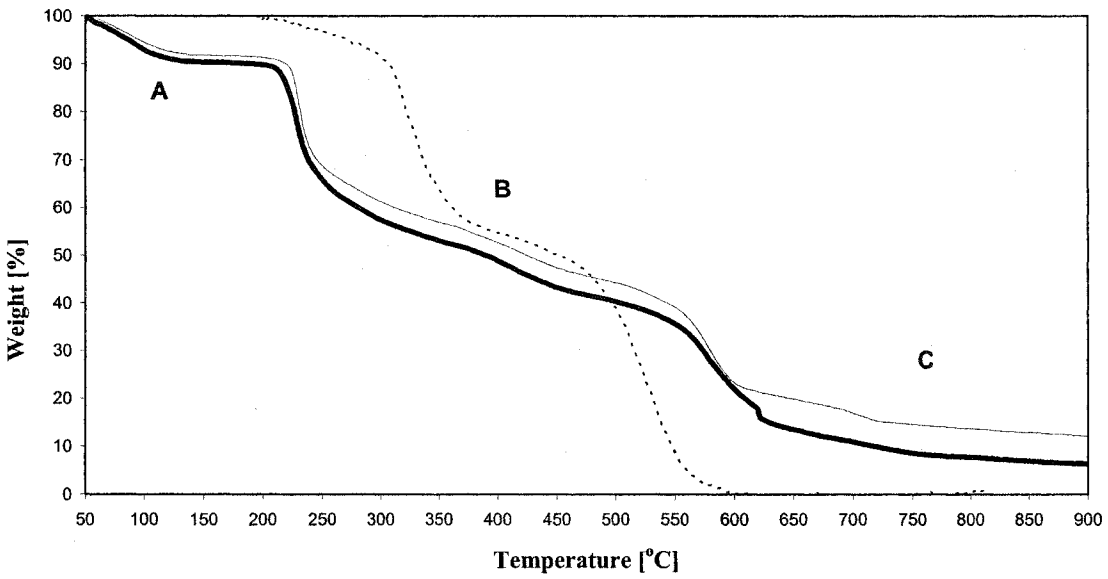

Figure 7.8. TGA of CdSe/S-G2 (**XVIII**) repeated twice (thin and thick solid line) and compared with TGA of free G2-SH (**VIII**) dendron (dashed line). Temperature increment was 20°C/min.

TGA data (cf. Figure 7.8) for QDs functionalized with the second generation aromatic thiol dendrons show that Zone A gives a 10% weight loss. Up to 600°C (cf. Zone B in Figure 7.8) 70% organic matter is lost and the entire 90% remaining of the free dendron. In Zone C 10% to 15% is lost and the graphs level off this time just past 900°C. At that point only 5% and 10% remain. A summary of the TGA data for all compounds can be found in Table 7.1.

Table 7.1. Summary of TGA results. Temperature Zones A, B, and C correspond to the labels in the TGA figures of respective compounds.

Dendronized QDs, Coating or Dendrons	**Zone A** 50°C-200°C Trapped Solvent	**Zone B** 200°C-600°C Organic Material	**Zone C** 600°C-1200°C Inorganic Material
CdSe/ODE	15%	65%	20%
ODE	20% (ODE)	80%	
CdSe/MPR	5%	70%, +/-5%	35%, +/-5%
MPR	0%	70%	30% (organics)
CdSe/S-G1	5%	45%, +/-5%	50%, +/-5%
G1-SH	5%	85%	10% (organics)
CdSe/S-G2	10%	70%	20%, +/-2%
G2-SH	<2%	98%, +/-2%	
CdSe/SC-G2	5%	70%, +/-5%	25%, +/-5%
G2-CSH	<2%	70%	30% (organics)

Unfortunately, it was apparent from the previous experience with the other systems in this study that attaching the third generation aromatic thiol dendron to the CdSe QDs would fail.

The question that automatically arises from the data presented in Chapter 7 is how many dendrons actually bind to the QD surface? Elemental analysis, providing an empirical ratio of all elements involved, TGA data and empirical calculations will be discussed in Chapter 8.

8. Dendron binding to QDs surfaces

As detailed in Chapter 7, dendronized QDs have been made by covalently attaching a variety of synthesized thiol dendrons (cf. Chapter 6) to previously prepared CdSe/ODE QDs (cf. Chapter 5). CdSe/ODE (**II**) proved to be rather stable when kept under argon even at room temperature. Figure 8.1 shows the slow decay of the QD surface as determined from a blue shift in the UV/Vis absorption. This blue shift is due to the decrease in particle size during the initial decay. Peng investigated this blue shift in more detail and found that upon controlled etching with hydrochloric acid the CdSe QDs decreased in size from about 3.3 nm to about 2.5 nm prior to precipitation[160]. The blueshift in Table 8.1 is small compared to Peng's findings. On further aging the particles agglomerate to yield bigger particles as evidence by an absorption red shift. Over a 10-month period, the particle size increase for the CdSe/ODE (**II**) was less than 0.2 nm in diameter. One also begins to notice a visible fine precipitate in the sample solution, possibly being agglomerated particles too large to stay in solution. Dendronized QDs are similarly stable when kept under argon in the dark at - 5°C, although the overall stability was not studied systematically.

With the realization that dendronizing QDs does not lead to improved emission intensity (cf. Chapter 7), the focus of this work shifted to examining the nature of the material obtained. TGA was used extensively during this examination (cf. Table 7.1). It was reassuring to find that repeated TGA measurements on dendronized QDs from the same batch or measurements from different batches of the same dendronized QDs were

consistent with the small differences between batches being easily explained by small changes in particle size. It is intuitively believable that larger dendrons attached to QDs would have a larger weight loss in a region where organic materials are known to decompose compared to QDs coated with small dendrons, such as generation one thiol. Zone A, B, and C are somewhat arbitrary and were chosen because of precedent in the literature,[156,186,187] and the experience with thermograms of ODE (cf. Figure 5.5), that completely vanishes below 600°C. Contrary to these assumptions, entries in Table 8.1 (which presents the data in Table 7.1 with expansion of Zone C) show that at 600°C, 30% of the model ligand (MPR), 10% of the first generation and 30% of the second-generation

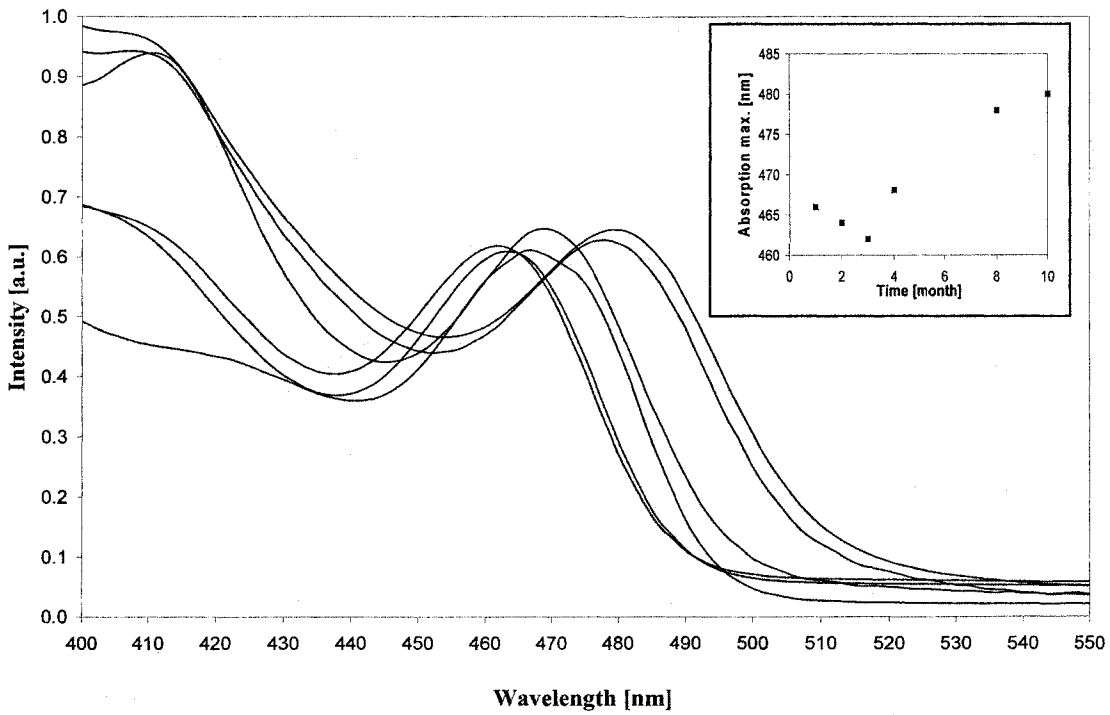

Figure 8.1. Measuring decomposition in CdSe/ODE QDs by UV/Vis absorption over a period of 10 month. The sample was degassed with argon and kept at room temperature in a sealed quartz cell. The inset shows the change in absorption maximum over ten month time period.

dendrons still remain. This lack of complete organic consumption before 600°C may be due to the fact that the TGA is purged with nitrogen, thus preventing the complete combustion reaction. Since CdSe melts above 1300°C, it was assumed that CdSe would be left in the platinum sample pan once all organics are removed. The CdSe/ODE is the only QD for which the TGA reaches a constant weight loss at 600°C and does not lose any additional material upon further heating. At 600°C, 900°C as well as 1200°C the curve remains constant. Thus, it was first assumed that the leftover material, 20% of the total sample weight, was indeed all CdSe. However, this assumption would later lead to contradictory data when compared to the elemental analysis data described below. All the thiolated QDs steadily lose weight, although the first generation thiolated dendronized QDs decrease in weight at a faster rate than either the aliphatic and aromatic, second-generation thiolated dendronized QDs. For the second generation QDs, the weight is approximately level between 600°C and 900°C, but drops again after 900°C. This latter observation will be explained in more detail shortly.

QDs submitted for elemental analysis in addition to CdSe/ODE (**II**), were the model ligand coated QD CdSe/MPR (**III**) and the second-generation aliphatic thiol dendron CdSe/SC-G2 (**XX**). The first generation aliphatic thiol dendron, CdSe-SC-G1 (**XIX**), was not submitted for elemental analysis due to loss of sample caused by premature decomposition (cf. Chapter 7.3). The first and second generation aromatic thiol dendrons were not analyzed.

The TGA data of CdSe/MPR and CdSe/SC-G2 QDs are supported by elemental analysis data recorded at 900°C. At that temperature the remaining weight for the CdSe/MPR sample and CdSe/SC-G2 sample in TGA are 28% and 17.5% +/- 2.5%, respectively. Elemental analysis of CdSe/MPR found 27.90% of cadmium and selenium combined. CdSe/SC-G2 was analyzed twice by elemental analysis and resulted in 16.76% and 15.75% of inorganics. As mentioned above, TGA data for CdSe/ODE are not supported by elemental analysis. Repeated TGA experiments result in a residual inorganics of 20% (by weight), which are presumably CdSe in a 1:1 ratio; whereas, elemental analysis finds less than 2% Cd and Se combined with a Cd:Se ratio of 1:1.3. The 1:1.3 ratio of Cd to Se might be caused by the inclusion of uncharged Se, since the reaction is run in a 3-fold excess of Se. However, this excess would need to be investigated further, since it leads one to conclude that the base CdSe/ODE QD has an overall net charge. Reported elemental analysis results concerning the ratio of Cd and Se agree on a close to 1:1 ratio, 1.02 +/- 0.14.[29] A 1.05 ratio found by elemental analysis was also confirmed by x-ray photoelectron spectroscopy (XPS) that resulted in a ratio of 1.03.[188] However, these analyses were performed on CdSe QDs that were synthesized with Bawendi's traditional organometallic reaction that uses dimethyl cadmium and dimethylselenium in a 1:1 ratio. However, it is worth pointing out that Peng uses Cd and Se in ratios up to 1:10 excess of Se, in order to boost PL quantum efficiency.[189] As detailed in Chpter 9, CdSe/ODE QDs are synthesized employing a 1:3 ratio. Elemental analysis data for the Peng-type CdSe QDs are not available.

However, the elemental analysis led to the discovery that attaching a thiol containing compound (either the model ligand MPR or the G2-CSH) replaces portions of the Se in a QD with sulfur. For example, the elemental analysis results of CdSe/SC-G2, third entry in Table 8.2, finds weight percentages that calculate to a ratio of 10 dendrons, 8 non-dendron sulfur, 15 cadmium and 7 selenium. Recalculating these ratios this time keeping C, H, O, S elements in ratios allowed for by the dendron, namely 79 C, 79 H, 6 O, and 1 S, and assuming a Cd to Se ratio of 1:1 the analysis would result in C, 64.59%; H, 5.42%; S, 2.18%; Cd, 11.48%; Se, 8.06%. The largest deviation is found for sulfur, 3.18% representing a 45% excess, and selenium, and 3.94% representing a 49% loss. This is a most unexpected finding and, to the best of our knowledge, has never before been reported. This replacement of Se by S may explain both the difficulty in removing all of the organics before 600°C (since the organic S is firmly entrenched in the QD) as well as the continuous decrease in weight in the TGA at 900°C. CdS sublimes around 980°C, which leads one to assume that the change between 600°C and 900°C is due to further loss of organics and the weight loss between 900°C and 1200°C may be due to the sublimation of CdS with the remaining weight being CdSe. These unexpected results were confirmed by repeated elemental analysis of the second generational aliphatic dendronized QD and the model ligand coated QDs, CdSe/MPR. The obvious next step in such an exciting find would be to determine a method for removing the organic dendron/ligand while maintaining the entrenched sulfur. If such a process could be discovered, this new synthetic approach leads to mixed core/shell QDs without an overall increase in QD diameter. Since the decrease in photoluminescence is due to the attachment of thiolated organic coatings, removal of the organics would most likely yield

a significant increase in emission photoluminescence comparable to the increase observed in other core/shell QD systems. Peng found 20-40% photoluminescence quantum yield increase and Alivisatos reports up to 50% increase, both for CdSe/CdS core/shell QDs.[93,94] In fact Peng[190] just published research on determining the dissociation pH for thiol ligands from CdSe, CdS, and CdTe QDs. Contrary to findings reported in Chapter 7.1, namely that CdSe QDs are not stable in hydrochloric acid, Peng finds that titration with HCl, H_2SO_4, or trifluoroacetic acid does not decompose the QDs. As long as the pH is adjusted to the pKa of the thiol ligand, the QDs are recoverable without any noticeable change in their absorption spectra. However, attempts to remove the organic coating via dissociation of the thiol ligand will not result in photoluminescence enhancement since the cleaving occurs between the Cd and S bond. Preferential would be a method that cleaves the sulfur-carbon bond thus leaving the sulfur to coat the QD surface to create a core/shell QD. In fact, Gao[185] recently published the photodegradation of thiol ligands on CdTe QDs. As a result he finds strong photoluminescence enhancement. The fluorescence quantum yield can reach up to 85%. In addition these QDs were found to be very stable and water soluble, which makes them a candidate for biolabeling.[185] However, the same enhancement of photoluminescence quantum yield may not be achieved with CdSe. The standard potential of expected for a thiol is too low to quench CdTe emission. In contrast, CdSe bandgap is lower than the standard potential of a thiol, thus hole trapping can occur.[191]

Table 8.1. TGA results at three different temperatures previously summarized as Zone C.

Zone C	At 600°C	At 900°C	At 1200°C
CdSe/ODE	20%	20%	20%
ODE	0%		
CdSe/MPR	35%, +/-5%	20%, 28%	N/A, 10%
MPR	30%	15%	
CdSe/S-G1	50%, +/-5%	22%, 37%	10%, 25%
G1-SH	10%		
CdSe/S-G2	20%, +/-2%	7%, 12%	6%, 10%
G2-SH	0%		
CdSe/SC-G2	25%, +/-5%	15%, 20%	3%, 17%
G2-CSH	30%		

The elemental analysis data in Table 8.2 give a ratio of 1:1.3:50 for the Cd:Se:ODE quantum dots. Such a result dispels the notion that ODE is similar to TOPO in the sense that one ODE binds to the Cd atom on the QD surface[29]. TOPO binds so strongly to the CdS surface that even the bidentate 2,2-bipyrimidine $(C_4N_2H_3)_2$ replaces TOPO only partially.[192] This work shows that ODE is easily and completely replaced by a thiol ligand. An attempt to verify the 1:50 ratio of Cd to ODE, by measuring the ^1H NMR failed, however, because the ^1H NMR is not able to distinguish between free and coordinated ODE.

In calculating the empirical formula for the dendronized QDs, one the other hand, one has to take into consideration the portion of material that is not accounted for, *i.e.*, the

analysis rarely adds to 100% total weight. Since TOP, containing both oxygen and phosphorus, neither of which is measured in the elemental analysis, it is difficult to remove them from the prepared CdSe quantum dots. The removal of TOP in the CdSe/ODE system was verified by ^{31}P NMR. The ^{31}P NMR showed no trace of phosphorus. The lack of an NMR peak indicates that TOP is most likely not attached to the surface of the QD. Both, ^{1}H and ^{31}P have 100% abundance. The γ values representing the spin state are only half for ^{31}P as compared to ^{1}H. That means that a ^{31}P NMR spectrum with twice the number of scans is as sensitive as a ^{1}H NMR. Thus, ruling out a major weight contribution from phosphorus, most of the missing weight can be attributed to the amount of oxygen present in the dendrons. Since oxygen was not part of the elemental analysis, this amount has to be assumed and added to the total. The calculated values for oxygen, indicated with an asterisk in Table 8.2, are added and then the total results were normalized to 100%. This normalization is required because the oxygen in the dendrons does not completely account for the missing weight. The remaining weight is probably due to solvent trapped within the dendrons (as evidenced by the TGA results). Only after these adjustments does the ratio of the elements present calculate to integers. Moreover, only with the addition of the calculated oxygen values and normalization of the total weight is the integrity of the atom ratio within a dendron or the model ligand preserved. For example, the deprotonated model ligand has 10 carbons, 11 hydrogens, 4 nitrogens, 4 oxygens and 1 sulfur as determined from the molecular structure. From Table 8.2, it can be ascertained from the ratio of C:H:N:O:S that 5 model ligands are present in a sample with 5 Cd and 1 Se. Thus, the overall composition of the QD (ignoring the organic ligand) is 5 Cd:1 Se:5 S.

Table 8.2. Elemental analysis and calculated atom ratios of QDs starting material CdSe/ODE (**II**), one of the dendronized QDs CdSe/SC-G2 (**XVIII**), and the model ligand coated QDs, CdSe/MPR (**XVI**). Numbers with an asterisk * are calculated oxygen values based on carbon found by elemental analysis.

	C %	H %	N %	O %	S %	Cd %	Se %
Atomic weight	12.011	1.0079	14.0067	15.9994	32.06	112.41	78.96
CdSe/ODE	**46 ODE, 1 Cd, and 1.3 Se.**						
Found	83.60	15.51				0.92	0.85
Calculated	84.07	14.11				0.95	0.87
# Atoms	828	1656				1	1.3
CdSe/MPR	**5 MPR, 5 Cd, and 1 Se.**						
Found	26.09	3.13	12.03	*14.33	8.10	25.11	2.79
Calculated	26.73	2.47	12.47	*14.24	7.14	25.02	3.51
# Atoms	50	55	20	*20	5	5	1
CdSe/SC-G2	**10 Dendrons, 8 non-dendron S, 15 Cd, and 7 Se.**						
Found	66.23	6.17		*6.70	3.18	11.81	3.94
Calculated	66.92	5.62		*6.77	3.17	11.89	3.90
# Atoms	790	790		*60	18	15	8
CdSe/SC-G2	**10 Dendrons, 8 non-dendron S, 17 Cd, and 8 Se.**						
Found	62.55	5.82		*6.33	3.84	12.68	4.08
Calculated	62.96	5.28		*6.37	3.83	12.68	4.19
# Atoms	790	790		*60	18	17	8

As mentioned previously, the aliphatic thiol dendronized QDs CdSe/SC-G2 were analyzed twice. The resulting ratios after all the adjustments were performed show that there is a higher S content in the Cd:Se:S base QD than the amount of S provided by the covalently attached dendrons. In other words, if the C and H ratio (cf. Table 8.2) gives a total of 10 dendrons present, then only 10 S atoms should be present in the base QD. The elemental analysis, however, indicates a total of 18 S which implies that 67% of the Se in the CdSe QD was replaced with S. As discussed in Chapter 6, the aliphatic dendrons

were synthesized from an alcohol functionalized dendron using thioacetic acid (TAA). Purification of these dendrons was difficult and NMR confirms the presence of residual TAA. Since TAA would also add to the C and H percentages in the elemental analysis, the amount of TAA must be considered when calculating atom ratios. Recalculating the data with TAA taken into consideration does not cause a significant change in the final C or H ratio, since the TAA has significantly fewer C and H atoms in comparison to the large second generation dendron. Thus, one can conclude that the excess S originates from TAA impurity.

To further prove the replacement of Se by S and thus the presences of core/shell CdSe/CdS QDs instead of pure CdSe QDs, x-ray powder diffraction was attempted. However, before attempting to measure the dendronized QDs, x-ray powder diffraction of the CdSe/ODE system was attempted, but was unsuccessful due to the low inorganic content of the sample (cf. Table 8.2). With this background in mind, the CdSe/MPR system was chosen because it has a larger inorganic portion than the second-generation aliphatic dendronized QDs. Wurtzite CdS nanoparticles usually show two sets of three peaks, the first set in the two theta (2θ) range between 20 and 35 degrees and the second set in the 2θ range of 40 to 60 degrees. The peaks in the first range represent the (002), (100), and (101) planes which, in the smallest particles, will fuse into a single broad peak. Similarly, the three peaks in the second range, which represent the (110), (103), and (112) planes, will also appear as a single broad peak in small QDs.[51,193] Unfortunately, the x-ray diffraction patterns for CdSe nanoparticles are reported to be almost identical to the CdS nanoparticles. In the x-ray diffraction spectrum depicted in Figure 8.2, one can

barely distinguish the fused peaks in the 20 to 35 degree 2θ region. Furthermore, the second region of peaks is even less clear. Thus, for the CdSe/MPR system the x-ray powder diffraction spectrum can be attributed to either the CdS or CdSe.

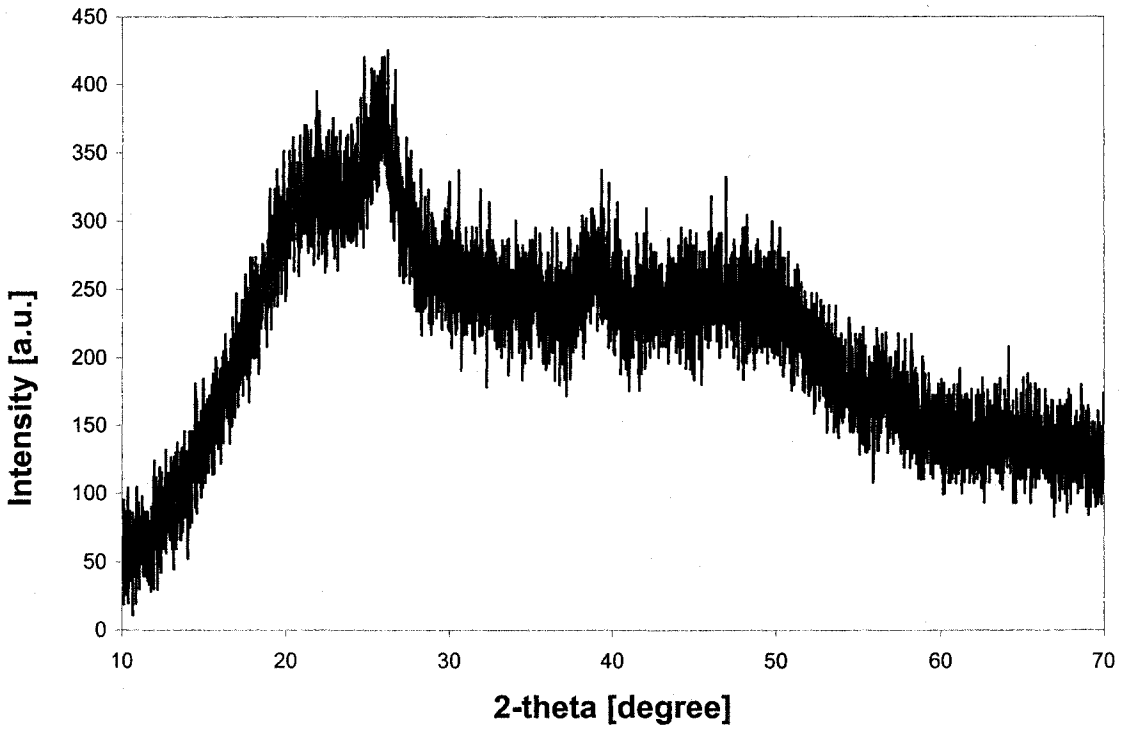

Figure 8.2. X-ray diffraction of CdSe/MPR (**XVI**).

Since x-ray powder diffraction did not definitively determine the presence of core/shell CdSe/CdS quantum dots, the characterization of this new core shell system was also attempted using ^{1}H and ^{13}C NMR of the organic ligand covalent bond to the S. The CdSe/CdS/MPR QD system is the ideal system for such a study since it has only a single H attached to the aromatic ring that carries the thiol sulfur making the NMR less difficult to interpret. However, the proton of interest is 3 bonds removed from the cadmium, C*H*-N-C-S-Cd, thus lowering any effect the QD core may have on the chemical shift. In fact,

the proton of interest shifted upfield by 0.1 ppm, from 8.5 to 8.4. At this point, however, it is not possible to verify if this small shift is caused by the surface attachment of the sulfur to a CdSe quantum dot or the incorporation of the S into the CdSe quantum dot to make a core/shell CdSe/CdS quantum dot. While it is true that ^{13}C NMR might lead to a definite answer of the ligand binding in these unique QD systems, unfortunately the lack of solubility of the CdSe/CdS/MPR QD system prevents the attainment of a ^{13}C NMR (*i.e.*, the ^{1}H NMR took 24 hours to acquire).

9. Conclusions

CdSe QDs with a diameter of 2.0-2.5 nm have been synthesized in a solution of 1-octadecene (ODE). The QDs were monodisperse, highly luminescent, and were soluble in nonpolar solvents such as hexane. The surface of the QDs was then modified with thiol functionalized dendrons and thiol functionalized ligands. This passivates the QD surface and affects the overall photophysical properties of the CdSe QD. The expected enhancement of the luminescence emission quantum yield was not realized. However, TGA in combination with elemental analysis uncovered a previously unreported phenomenon, namely that the sulfur of the dendron does not bind covalently to the Cd atoms on the QD surface, but rather displaces the Se in the QD to make a core/shell CdSe/CdS/dendron QD system. An independent confirmation of this finding could be obtained using energy dispersive X-ray (EDAX)[80] or extended x-ray absorption fine structure (EXAFS) measurements.[194-196]

Since one of the most important aspects in QD synthesis is the production of highly luminescent materials and it has been shown that core/shell quantum dots show significant increase in photoluminescence, an obvious next step in this research is to develop synthetic techniques that would detach the organic materials from the S in the these new CdSe/CdS/dendron systems.

Such a technique would yield 2 nm CdSe/CdS core/shell QDs, which represents a 2-fold decrease in diameter from the currently available core/shell systems. CdSe/CdS core/shell QDs are reported with CdSe core of 2.3 to 3.9 nm.[93] A shell of three monolayers of CdS ads 1 nm thickness. The total core/shell QD diameter for a 2.3 nm core adds up to a particle size of 4.3 nm in diameter. Similarly, one might also want to focus on semiconductor materials other than CdSe, which has been widely studied. ZnSe emits brightly in the blue region and is tunable from 2.8 to 3.4 eV with quantum yields of 20% to 50%.[33]

Part III Experimental

10. Reagents and Instrumentation

Chemicals bought from Aldrich were of commercial reagent quality and used as received. Solvents for reactions were purchased from Aldrich in the anhydrous form. They were all degassed with high purity argon and used without further purification or drying. Bulk solvents for column chromatography are from Fischer and are of reagent grade purity. Octadecene (ODE) and tetradecylphosphonic acid (TDPA) are from Alfa Aesar. All reactions are performed under high purity argon from Air gas, Inc., PA.

Flash column chromatography was performed using Silica gel 230-400 mesh 60Å and 150Å from Fisher Scientific. Flexible TLC plates for thin layer chromatography came from Fisher Scientific, silica gel 60Å, F-254, and 200 micron. Spots were visualized using a black light at 254 nm. ODE was visualized by developing plates in an aqueous solution consisting of a mixture of sodium carbonate and potassium permanganate.

UV-Visible spectra were obtained using a Hewlett Packard 8452A Diode Array Spectrophotometer. NMR spectra were measured using a Bruker 400 MHz FT-NMR equipped with a QNP probe. Photoluminescence (PL) spectra were recorded on a SPEX Industries Inc., SPEX 1681, 0.22 m Version 3.30 c spectrometer with DM3000 software. Lifetime measurements were performed with a Quanta-Ray DCR Nd:YAG Laser

instrument. TGA determinations were made on a Perkin Elmer 7 Series/ UNIX TGA 7 fitted with a high temperature furnace. X-ray powder diffraction was taken with a Phillips APD 3720, with a PW 1729 x-ray generator. Transmission electron microscopy (TEM) was performed with a JEOL 4000-EX electron microscope (Japanese Electron Optics Ltd., Japan) at a resolution of 1.7 Å.

Schwarzkopf Microanalytical Laboratories of Woodside, New York performed elemental analyses. Mass spectral data were acquired on an Agilent Technologies 1100 Series LC/MSD model G1946D using atmospheric pressure photo ionization (APPI). Ionization was carried out with a drying gas flow of 6 liters/min., a nebulizer pressure of 60psi, drying gas temperature of 300°C, vaporizer temperature of 450°C and a capillary voltage of 4000 volts. The mass range scanned was between 140 and 1500 amu with fragmentor values ranging from 60 volts at 50amu to 125 volts at 1800 amu. Both positive and negative ion data was collected. Samples were prepared by dissolving in a mixture of chloroform and toluene (dopant) and were introduced into the mass spectrometer with methanol containing 0.1% formic acid, 50uM ammonium acetate and 0.1% chloroform. The flow rate of the solvent was 500ul/min. Data was processed using Agilent's Chemstation software.

10.1 Preparation of CdSe QDs

Synthesis of n-trioctylphosphine oxide (TOPO) coated QDs, CdSe/TOPO (**I**). Cadmium oxide (CdO) (52.0 mg, 0.4 mmol) and tetradecylphosphonic acid (TDPA) (223.0 mg, 0.8 mmol) are placed in a round bottom flask, evacuated and backfilled with

argon. A reflux condenser is attached to the round bottom flask. A magnetic stirrer and a high temperature thermocouple are inserted. The flask is immersed in a sand bath, 2 mL TOPO is added, and the mixture is heated to 310°C. After 45 minutes at that temperature, the red emulsion turns to a clear colorless liquid. Selenium powder (94.75 mg, 1.2 mmol) is placed in a small vial, evacuated and backfilled with argon. Two mL of *n*-trioctylphosphine (TOP) is added to the selenium powder, and the mixture is sonicated until the black powder is dissolved and a clear colorless liquid is obtained. In the mean time the temperature in the round bottom flask has been lowered to 270°C. At that temperature the selenium solution is injected rapidly, causing the temperature to drop below 250°C and the solution to turn clear yellow. After five additional seconds the heat is removed completely, the solution is cooled to room temperature and n-butanol is added to precipitate the CdSe/TOPO QDs as a yellow powder. The QDS are soluble in chloroform or toluene. Several wash cycles are performed by first dissolving the QDs in toluene, then centrifuging any insoluble impurities, followed by precipitating the supernatant containing the QDs with butanol. This precipitate is centrifuged and the colorless solution is decanted. The yellow precipitate is dissolved in toluene and centrifuged again, repeating the cycle. The material, dissolved in toluene is stable for at least half a year when kept under argon.

Synthesis of Octadecene (ODE) coated CdSe QDs, CdSe/ODE (**II**). Cadmium oxide (CdO) (52.0 mg, 0.4 mmol) and tetradecylphosphonic acid (TDPA) (223.0 mg, 0.8 mmol) are placed in a round bottom flask under argon. Five mL ODE is added and the mixture is heated to 310°C. After 45 minutes at that temperature the red emulsion turns

into a clear colorless liquid. Selenium powder (94.75 mg, 1.2 mmol) dissolved in 2 mL *n*-trioctylphosphine (TOP) is prepared in a small vial and is injected rapidly to the round bottom flask at 270°C. Again a drop in temperature below 250°C occurs. When the solution has turned pale yellow, after about five seconds, the heat is removed completely. Upon cooling to room temperature a white precipitate forms and is removed via centrifugation. The CdSe/ODE QDs are soluble in hexane and ODE. Stored in ODE solution and under argon atmosphere, the CdSe/ODE QDs are stable. Excess ODE can be removed by extraction with a methanol/chloroform 1:1 solution[20] to obtain a yellow powder, yield: 245mg. ^{1}H NMR (C_6D_6), δ 0.88 (t, 3 H, C*H*$_3$), 1.26 (s, 24 H, C*H*$_2$), 1.37 (m, 4 H, C*H*$_2$), 2.02 (q, 2 H, C*H*$_2$), 4.93 (d, 1 H, =C*H*$_2$), 5.01 (d, 1 H, =C*H*$_2$), 5.8 (m, 1 H, =C*H*). Anal. Calcd for $(C_{18}H_{36})_{46}Cd_1Se_{1.3}$: C, 84.07; H, 14.11; Cd, 0.95; Se, 0.87. Found: C, 83.60; H, 15.51; Cd, 0.92; Se, 0.85.

Synthesis of Mercaptoacetic acid (MAA) coated CdSe QDs, CdSe/MAA (**III**). Fourteen mL of CdSe/ODE (**II**) was placed in a round bottom flask under flowing argon. 14 mL methanol containing MAA (200 µl, 3 mmol) was added, and tetramethylammonium hydroxide (6 mmol, 25w% in methanol) added dropwise. The mixture was heated under reflux at 59°C overnight. The reaction was then stopped and allowed to cool to 28°C. Stirring is discontinued and the two layers are allowed to separate. The ODE layer on top is now colorless and is removed. The yellow methanol layer on the bottom, which contains the CdSe/MAA QDs (**III**) was washed with hexane causing the QDs to precipitate. The QDs are dissolved in water and are precipitated with ethyl acetate. The precipitate was washed with hexane until a TLC spotting test for

alkenes is negative. The final purified precipitate was dried for 1 hr in vacuum at ambient temperature. The compound is sufficiently soluble in water or deuterium oxide for NMR studies. Yield: 14 mg. ^{1}H NMR (D_2O), δ 3.1 (s, 2 H), 4.7 (D_2O) solvent peak). Free MAA: 3.26 (s, 1 H).

10.2 Preparation of Fréchet-type Dendrons

General procedure for the synthesis of protected aliphatic thiol dendrons (**XXII, XXIII**). Triphenylphosphine (2 equiv) was placed in a flask under argon and dissolved in 2 mL of anhydrous THF. The solution was cooled to 0°C and diisopropyl azodicarboxylate (2 equiv) was added dropwise with stirring, forming a thick, white precipitate in a yellow solution. After the reaction mixture was stirred for 30 minutes, thioacetic acid (2 equiv) and dendritic alcohol (**IV** or **VII**) (1 equiv) were dissolved in 1 mL THF and added to the reaction mixture dropwise. After stirring for 5 hours at 0°C, the reaction mixture was stirred overnight at room temperature and then quenched by the addition of 1 mL of ethanol. The solution was concentrated under a stream of argon, and the resulting thick oil dissolved in dichloromethane (DCM). Silica gel (230-400 mesh) was added to the oil DCM mixture forming a slurry that was dried on a rotary evaporator. The residue was suspended in hexane and loaded onto a column of silica gel (230-400 mesh) prepared in hexane and first eluted with hexane (500 mL) and then with hexane/ethyl acetate (99:1). Only after the TLC shows no sign of triphenylphosphine oxide (approximately after 1 L of eluent), is the eluent strength increased gradually to 3%

ethyl acetate. After this chromatographic purification the yield of protected dendritic thiols ranges between 50-60%.

G1-SC(=O)CH3 (**XXII**): ^{1}H NMR ($CDCl_3$) δ 1.30-1.40 (m, 2 H), 1.57 (s, 3 H), 2.05-2.11 (m, 2 H), 2.25 (s, 3 H), 2.81 (t, 2 H), 5.01 (s, 4 H), 6.87 (d, 4 H, J = 9 Hz), 7.11 (d, 4 H, J = 9 Hz), 7.26-7.45 (m, 10 H); ^{13}C NMR ($CDCl_3$) 24.98, 27.90, 29.65, 30.54, 41.08, 69.91, 114.16, 127.45, 127.84, 128.16, 128.49, 137.15, 141.84, 156.70, 195.60; Mol. Wt.: 510.69; $(M + NH_4^+)^+$: 528.2, API-ES pos. scan; Anal. Calcd for $C_{33}H_{34}O_3S$: C, 77.61; H, 6.71; O, 9.40; S, 6.28. Found: C, 75.87; H, 7.42; S, 8.52.

G2-SC(=O)CH3 (**XXIII**): ^{1}H NMR ($CDCl_3$) δ 1.30-1.40 (m, 2 H), 1.50-1.68 (m, 13 H), 2.02-2.10 (m, 2 H), 2.16-2.20 (m, 4 H), 2.22 (s, 3 H), 3.67 (t, 2 H), 3.80 (t, 4 H), 5.00 (s, 8 H), 6.71 (d, 4 H, J = 9 Hz), 6.85 (d, 8 H, J = 8 Hz), 7.04 (d, 4 H, J = 8 Hz), 7.10 (d, 8 H, J = 9 Hz), 7.28-7.43 (m, 20 H); ^{13}C NMR ($CDCl_3$) 25.50, 27.86, 28.18, 30.50, 37.93, 38.29, 41.59, 44.68, 63.17, 68.12, 69.80, 113.67, 114.06, 127.47, 127.86, 128.15, 128.25, 128.51, 137.10, 141.69, 141.98, 156.65, 156.78, 195.58; Mol. Wt.: 1199.58; $(M + Cl^-)^-$: 1234.2, APPI neg. scan; Anal. Calcd for $C_{81}H_{82}O_7S$: C, 81.10; H, 6.89; O, 9.34; S, 2.67. Found: C, 74.6; H, 7.32; S, 2.73.

General procedure for the synthesis of deprotected aliphatic thiol dendrons (**VI, IX**). The protected dendritic thiol (1 equiv) was placed in a flask and dissolved in 5 mL of anhydrous THF. The solution was cooled to 0°C and degassed with argon for 15 minutes. A solution of lithium aluminum hydride (1 M in THF 1.1 equiv) was added

dropwise. Upon stirring for 2 hours, the reaction was quenched with a degassed, aqueous solution containing 5% sodium phosphate (Na_2HPO_4), extracted into a DCM layer, and dried over sodium sulfate. The solvent was evaporated. The products yields are 42% for G2-CSH (**IX**) and 55% G1-CSH (**VI**). They were used without further purification.

G1-CSH (**VI**): ^{1}H NMR ($CDCl_3$) δ 1.35-1.45 (m, 2 H), 1.57 (s, 3 H), 1.82 (m, 3 H), 2.05-2.11 (m, 2 H), 2.49 (m, 2 H), 5.01 (s, 4 H), 6.87 (d, 4 H, J = 9 Hz), 7.11 (d, 4 H, J = 9 Hz), 7.26-7.45 (m, 10 H); ^{13}C NMR ($CDCl_3$) 24.60, 27.97, 29.69, 30.54, 40.82, 69.96, 114.13, 127.51, 127.91, 128.22, 128.55, 137.15, 141.84, 156.69; Mol. Wt.: 468.65; $(M + NH_4^+)^+$: 486.1, $(M + Na^+)^+$: 491.0, API-ES pos. scan.

G2-CSH (**IX**): ^{1}H NMR ($CDCl_3$) δ 1.30-1.42 (m, 2 H), 1.50-1.65 (m, 13 H), 2.06-2.12 (m, 2 H), 2.14-2.20 (m, 4 H), 3.55 (m, 2 H), 3.86 (m, 4 H), 5.01 (s, 8 H), 6.71 (d, 4 H, J = 9 Hz), 6.85 (d, 8 H, J = 8 Hz), 7.04 (d, 4 H, J = 8 Hz), 7.10 (d, 8 H, J = 9 Hz), 7.28-7.43 (m, 20 H); ^{13}C NMR ($CDCl_3$) 25.01, 27.96, 28.94, 37.93, 38.37, 44.75, 44.83, 63.43, 68.30, 70.00, 113.76, 114.17, 127.53, 127.91, 128.16, 128.30, 128.56, 137.20, 141.62, 142.05, 156.73, 156.89. Mol. Mol. Wt.: 1157.54; Anal. Calcd for $C_{79}H_{80}O_6S$: C, 81.97; H, 6.97; O, 8.29; S, 2.77. Found: C, 74.60; H, 7.32; S, 2.73.

Preparation of third generation aliphatic dendritic thiol G3-CSH (**XII**) [197,198]. To a stirred solution of third generation dendritic alcohol (**X**) (1 equiv, 0.275 mmol, 690 mg) in 5 mL DCM under argon sodium hydrogen sulfide (3.1 equiv, 0.86 mmol, 48 mg) dissolved in 1 mL DMSO was added dropwise. After stirring overnight at room

temperature, the mixture was cooled to 0°C and acidified adding 0.1 N HCl dropwise (H_2S evolution). The mixture was extracted with chloroform and the organic layer washed with water and brine (saturated aqueous sodium chloride solution). The organic portion was dried over sodium sulfate and evaporated to dryness. The product G3-CSH (**XII**) was used without further purification: yield 36%; ^{1}H NMR ($CDCl_3$) δ 1.2-1.9 (m, 35 H), 2.0-2.3 (m, 14 H), 2.6-2.9 (m, 3 H), 3.1-3.4 (m, 2 H), 3.6-3.9 (m, 12 H), 5.0 (s, 16 H), 6.7 (d, 12 H,), 6.9 (d, 16 H), 7.0-7.2 (m, 30 H), 7.2-7.5 (m, 42 H); ^{13}C NMR ($CDCl_3$) 24.98, 25.59, 27.92, 38.32, 38.61, 44.59, 44.79, 45.04, 60.36, 67.95, 68.24, 69.92, 113.71, 114.13, 127.50, 127.89, 128.05, 128.18, 128.54, 128.73, 137.13, 141.63, 142.01, 156.68, 156.84, 156.91, 171.13, . Mol. Wt.: 2535.33.

10.3 Preparation of Dendronized CdSe QDs

Preparation of CdSe/MPR (**XVI**). To 14 mL of CdSe/ODE QDs (245 mg CdSe/ODE dissolved in 14 mL ODE) under argon, a mixture of chloroform (7 mL), methanol (7 mL) and DMSO (1 mL) containing 6-mercaptopurine riboside (MPR) (200 mg, 0.7 mmol) is added carefully creating a bilayer system. The yellow color of the top layer indicates the presence of the QDs. The bottom layer containing the thiol ligand is clear and colorless. The layers are mixed with vigorous stirring and tetramethylammonium hydroxide (0.5 mL, 1.2 mmol, 25w% in methanol) solution is added via syringe. The reaction is heated to reflux at 57°C and kept overnight. The reaction is cooled to room temperature and stirring is discontinued. The reconstituted layers now show the yellow color of the QDs in the bottom layer, and the top ODE layer

is colorless. The top layer is removed and ethyl acetate is added to the yellow bottom layer. The resulting precipitate is washed with several aliquots of hexane until the wash solution does not give a positive test for alkenes (ODE) in TLC. The precipitate was dried and is sufficiently soluble in deuterated D_2O to record an ^1H NMR: yield 100 mg; Free MPR ligand: ^1H NMR (DMSO) δ 3.58 (d, 2 H), 3.96 (m, 1 H), 4.13 (t, 1 H), 4.46 (t, 1 H), 5.07 (d, 1 H), 5.23 (d, 1 H), 5.54 (d, 1 H), 5.89 (d, 1 H), 8.20 (s, 1 H), 8.5 (s, 1 H), 13.85 (s, 1H); ^{13}C NMR (DMSO) 61.06, 70.11, 74.19, 85.60, 87.52, 135.36, 141.16, 143.87, 145.22, 176.00. MPR bound to CdSe QD: ^1H NMR (D_2O) δ 3.75 (d, br, 2 H), 4.2 (br, 1 H), 4.35 (br, 1 H), 4.45 (br, 1 H), 4.5-4.7 (solvent H_20), 6.0 (br, 1 H), 8.2 (s, br, 1 H), 8.4 (s, br, 1 H); Anal. Calcd for $(C_{10}H_{12}N_4O_4S)_5Cd_5Se$: C, 26.73; H, 2.47; N, 12.47; O, 14.24; S, 7.14; Cd, 25,02; Se, 3.51. Found: C, 26.09; H, 3.13; N, 12.03; S, 8.10; Cd, 25.11; Se, 2.79.

General procedure for the synthesis of dendronized CdSe QDs (**XVII, XVIII, XIX,** and **XX**) was adapted from the preparation of CdSe/MPR, since the mercaptopurine riboside is used as a model ligand. The exception being that the use of DMSO was not necessary since the thiol dendrons dissolve in chloroform. On the other hand, care must be taken not to precipitate the dendrons when adding methanol, which that is needed to create the bilayer, which in turn is needed to gauge the completion of the reaction. All dendronized QDs are washed with hexane to remove ODE, dissolved in chloroform and precipitated with methanol.

CdSe/S-G1 (**XVII**): CdSe/ODE (**II**) (245 mg in 14 ml ODE), G1-SH (**V**) (137 mg, 0.228 mmol) dissolved in 7 mL chloroform, 7 mL methanol, and tetramethylammonium hydroxide (0.1 mL, 0.24 mmol, 25w% in methanol) are added under argon. The mixture was refluxed overnight at 59°C. After purification 9.2 mg of a yellow powder is obtained that is insoluble.

CdSe/S-G2 (**XVIII**). CdSe/ODE (490 mg in 20 mL ODE), G2-SH (**VIII**) (154.88 mg, 0.12 mmol) in 10 mL chloroform, 10 mL methanol, and tetramethylammonium hydroxide (0.1 mL, 0.24 mmol, 25w% in methanol) are added under argon and refluxed overnight. A yellow precipitate is collected and purified. This product dissolves in chloroform. Yield: 105 mg. ^{1}H NMR ($CDCl_3$) δ 1.3-1.6 (br, 15 H), 1.9-2.4 (br, 9 H), 2.7 (br, 1.5 H), 2.9 (br, 1.5 H), 3.1 (br, 1H)] 3.4 (br, 15 H), 3.8 (br, 2 H), 4.4 (br, 15 H), 4.7-4.9 (br, 4 H), 5.0 (s, 8 H), 6.7 (br, 8 H,), 6.9 (br, 4 H), 7.0 (br, 10 H), 7.1 (br, 4 H), 7.2-7.5 (br, 22 H).

CdSe/SC-G1 (**XIX**). CdSe/ODE (245 mg in 14 mL ODE), G1-CSH (**VI**) (100 mg, 0.21 mmol) in 7 mL chloroform, 7 mL methanol, and tetramethylammonium hydroxide (0.1 mL, 0.24 mmol, 25w% in methanol) was added under argon and refluxed overnight. The yellow precipitate was collected and purified. Yield 55 mg.

CdSe/SC-G2 (**XX**). CdSe/ODE (490 mg in 20 mL ODE), G2-CSH (**IX**) (320 mg, 0.28 mmol) in 10 mL chloroform, 10 mL of methanol, and tetramethylammonium hydroxide (0.5 mL, 1.2 mmol, 25w% in methanol) was added under argon and refluxed

overnight. The precipitate was purified and dissolves in chloroform. Yield: 180 mg; ^{1}H NMR ($CDCl_3$) δ 1.30-1.65 (br, 15 H), 1.9-2.2 (br, 6 H), 2.5-2.8 (br, 7 H), 3.5-3.7 (br, 4 H), 4.8 (br, 8 H), 6.5 (br, 4 H,), 6.7 (br, 8 H,), 6.9-7.1 (br, 12 H,), 7.1-7.4 (br, 20 H); ^{13}C NMR ($CDCl_3$) 22.66, 25.07, 27.94, 29.70, 31.59, 38.26, 44.71, 55.88, 68.20, 69.86, 113.76, 114.15, 127.50, 127.83, 128.24, 128.49, 137.14, 142.0, 156.63. Anal. Calcd for $(C_{79}H_{79}O_6S)_{10}S_8Cd_{15}Se_7$: C, 66.92; H, 5.62; S, 3.17; Cd, 11.89; Se, 3.90. Found: C, 66,23; H, 6.17; S, 3.18; Cd, 11.81; Se, 3.94. Anal. Calcd for $(C_{79}H_{79}O_6S)_{10}S_8Cd_{17}Se_8$: C, 62.96; H, 5.28; S, 3.83; Cd, 12.68; Se, 4.19. Found (repeat sample): C, 62.55; H, 5.82; S, 3.84; Cd, 12.68; Se, 4.08.

References

(1) Franke, M. E. There is Plenty of Room at the Bottom *Engineering and Science* **1959**.

(2) Andersen, H. Characteristics of scientific revolutions. *Endeavour* **1998**, *22*, 3-6.

(3) Paigen, K. Perspectives: One hundred years of mouse genetics: an intellectual history. II. The molecular revolution (1981-2002). *Genetics* **2003**, *163*, 1227-1235.

(4) Singh, R. S. Darwin to DNA, molecules to morphology: the end of classical population genetics and the road ahead. *Genome* **2003**, *46*, 938-942.

(5) Davis, B. D. Frontiers of the biological sciences. *Science* **1980**, *209*, 78-89.

(6) Anton Simeonov; Masayuki Matsushita; Eric A. Juban; Elizabeth H. Z. Thompson; Timothy Z. Hoffman; Albert E. Beuscher, I.; Matthew J. Taylor; Peter Wirsching; Wolfgang Rettig; James K. McCusker; Raymond C. Stevens; David P. Millar; Peter G. Schultz; Richard A. Lerner; Janda, K. D. Blue-Fluorescent Antibodies *Science* **2000**, *290*, 307-313.

(7) Bruchez, J., Marcel; ; Moronne, M.; Gin, P.; Weiss, S.; Alivisatos, A. P. Semiconductor Nanocrystals as Fluorescent Biological Labels *Science* **1998**, *281*, 2013-2016.

(8) Baratoff, A. The 1986 Nobel Prizes. Development of scanning tunneling microscopy. *Europhysics News* **1986**, *17*, 141-144.

(9) Viernow, J.; Petrovykh, D. Y.; Kirakosian, A.; Lin, J.-L.; Men, F. K.; Henzler, M.; Himpsel, F. J. Chemical imaging of insulators by STM. *Phys. Rev. B* **1999**, *59*, 10356-10361.

(10) Himpsel, F. J.; Kirakosian, A.; Crain, J. N.; Lin, J.-L.; Petrovykh, D. Y. Self-assembly of one-dimensional nanostructures at silicon surfaces. *Solid State Communications* **2001**, *117*, 149-157.

(11) Bennewitz, R.; Crain, J. N.; Kirakosian, A.; Lin, J.-L.; McChesney, J. L.; Petrovykh, D. Y.; Himpsel, F. J. Atomic scale memory at a silicon surface *Nanotechnology* **2002**, *13*, 499-502.

(12) Drexler, K. E. Nanotechnology: From Feynman to Funding *Bulletin of Science, Technology & Society* **2004**, *24*, 21-27.

(13) Rajeshwar, K.; de Tacconi, N. R.; Chenthamarakshan, C. R. Semiconductor-Based Composite Materials: Preparation, Properties, and Performance *Chem. Mater.* **2001**, *13*, 2765-2782.

(14) Brus, L. E. Electron-electron and electron-hole interactions in small semiconductor crystallites: the size dependence of the lowest excited electronic state. *J. Chem. Phys.* **1984**, *80*, 4403-4409.

(15) Rossetti, R.; Brus, L. E. Electron-Hole Recombination Emission as a Probe of Surface Chemistry in Aqueous CdS Colloids *J. Phys. Chem.* **1982**, *86*, 4470.

(16) Hagfeldt, A.; Graetzel, M. Light-Induced Redox Reactions in Nanocrystalline Systems *Chem. Rev.* **1995**, *95*, 49-68.

(17) Murray, C. B.; Norris, D. J.; Bawendi, M. G. Synthesis and characterization of nearly monodisperse CdE (E = sulfur, selenium, tellurium) semiconductor nanocrystallites *J. Am. Chem. Soc.* **1993**, *115*, 8706-8715.

(18) Qu, L.; Peng, Z. A.; Peng, X. Alternative Routes toward High Quality CdSe Nanocrystals *Nano Letters* **2001**, *1*, 333-337.

(19) Peng, Z. A.; Peng, X. Formation of High-Quality CdTe, CdSe, and CdS Nanocrystals Using CdO as Precursor *J. Am. Chem. Soc.* **2001**, *123*, 183-184.

(20) Peng, X.; Yu, W. W. Formation of High-Quality CdS and Other II-VI Semiconductor Nanocrystals in noncoordinating Solvents: Tunable Reactivity of Monomers *Angew. Chem., Int. Ed. Engl.* **2002**, *41*, 2368.

(21) Peng, X. Green Chemical Approaches toward High-Quality Semiconductor Nanocrystals *Chem. Eur. J.* **2002**, *8*, 334-339.

(22) Eychmüller, A. Structure and Photophysics of Semiconductor Nanocrystals *J. Phys. Chem. B* **2000**, *104*, 6514-6528.

(23) Talapin, D. V.; Rogach, A. L.; Kornowski, A.; Haase, M.; Weller, H. Highly Luminescent Monodisperse CdSe and CdSe/ZnS Nanocrystals Synthesized in a Hexadecylamine-Trioctylphosphine Oxide-Trioctylphospine Mixture *Nano Letters* **2001**, *1*, 207-211.

(24) Gerion, D.; Parak, W. J.; Williams, S. C.; Zanchet, D.; Micheel, C. M.; Alivisatos, A. P. Sorting Fluorescent Nanocrystals with DNA *J. Am. Chem. Soc.* **2002**, *124*, 7070 -7074.

(25) Li, Z. F.; Ruckenstein, E. Water-Soluble Poly(acrylic acid) Grafted Luminescent Silicon Nanoparticles and Their Use as Fluorescent Biological Staining Labels *Nano Letters* **2004**, *4*, 1463-1467.

(26) Chan, W. C. W.; Nie, S. Quantum Dot Bioconjugates for Ultrasensitive Nonisotopic Detection *Science* **1998**, *281*, 2016-2018.

(27) Hines, M. A.; Guyot-Sionnest, P. Synthesis and Characterization of Strongly Luminescing ZnS-Capped CdSe Nanocrystals *J. Phys. Chem.* **1996**, *100*, 468-471.

(28) Mokari, T.; Banin, U. Synthesis and Properties of CdSe/ZnS Core/Shell Nanorods *Chem. Mater.* **2003**, *15*, 3955-3960.

(29) Bowen, K. J. E.; Colvin, V. L.; Alivisatos, A. P. X-ray Photoelectron Spectroscopy of CdSe Nanocrystals with Applications to Studies of the Nanocrystal Surface *J. Phys. Chem.* **1994**, *98*, 4109-4117.

(30) Lee, J.-K.; Kuno, M.; Bawendi, M. G. Surface derivatization of nanocrystalline CdSe semiconductors. *Mat. Res. Soc. Symp. Proc.* **1997**, *452*, 323-328.

(31) Rafeletos, G.; Norager, S.; O'Brien, P. Evidence for the chemical nature of capping in CdSe nanoparticles prepared by thermolysis in tri-n-octylphosphine oxide from P-edge EXAFS spectroscopy *J. Mater. Chem.* **2001**, *11*, 2542-2544.

(32) Nazzal, A. Y.; Qu, L.; Peng, X.; Xiao, M. Photoactivated CdSe Nanocrystals as Nanosensors for Gases *Nano Letters* **2003**, *3*, 819-822.

(33) Hines, M. A.; Guyot-Sionnest, P. Bright UV-Blue Luminescent Colloidal ZnSe Nanocrystals *J. Phys. Chem. B* **1998**, *102*, 3655-3657.

(34) Tomalia, D. A.; Baker, H.; Dewald, J.; Hall, M.; Kallos, G.; Martin, S.; Roeck, J.; Ryder, J.; Smith, P. A new class of polymers: starburst-dendritic macromolecules. *Polym. J.* **1985**, *17*, 117.

(35) Tomalia, D. A.; Baker, H.; Dewald, J.; Hall, M.; Kallos, G.; Martin, S.; Roeck, J.; Ryder, J.; Smith, P. Dendritic Macromolecules: Synthesis of Starbust Dendrimer *Macromolecules* **1986**, *19*, 2466.

(36) Tomalia, D. A.; Naylor, A. M.; Goddard III, W. A. Starburst Dendrimers: Molecular-Level Control of Size, Shape, Surface Chemistry, Topology, and Flexibility from Atoms to Macroscopic Matter *Angew. Chem., Int. Ed. Engl.* **1990**, *29*, 138-175.

(37) Hawker, C. J.; Fréchet, J. M. J. Preparation of polymers with controlled molecular architecture. A new convergent approach to dendritic macromolecules *J. Am. Chem. Soc.* **1990**, *112*, 7638-7647.

(38) Trindade, T.; O'Brien, P.; Pickett, N. L. Nanocrystalline Semiconductors: Synthesis, Properties, and Perspectives *Chem. Mater.* **2001**, *13*, 3843-3858.

(39) Greenham, N. C.; Peng, X.; Alivisatos, A. P. Charge separation and transport of conjungated-polymer/semiconductor-nanocrystal composites studied by

photoluminescence quenching and photoconductivity *Phys. Rev. B* **1996**, *54*, 17628-17637.

(40) Alivisatos, A. P. Perspectives on the Physical Chemistry of Semiconductor Nanocrystals *J. Phys. Chem.* **1996**, *100*, 13226-12239.

(41) Nirmal, M.; Brus, L. E. Luminescence Photophysics in Semiconductor Nanocrystals *Acc. Chem. Res.* **1999**, *32*, 407-414.

(42) Wise, F. W. Lead Salt Quantum Dots: the Limit of Strong Quantum Confinement *Acc. Chem. Res.* **2000**, *33*, 773-780.

(43) Sooklal, K.; Hanus, L. H.; Ploehn, H. J.; Murphy, C. J. A blue-emitting CdS/dendrimer nanocomposite *Adv. Mater.* **1998**, *10*, 1083-1087.

(44) Herron, N.; Wang, Y.; Eddy, M. M.; Stucky, G. D.; Cox, D. E.; Moller, K.; Bein, T. Structure and optical properties of cadmium sulfide superclusters in zeolite hosts *J. Am. Chem. Soc.* **1989**, *111*, 530-540.

(45) Wang, Y.; Herron, N. Optical properties of cadmium sulfide and lead(II) sulfide clusters encapsulated in zeolites *J. Phys. Chem.* **1987**, *91*, 257-260.

(46) Bekiari, V.; Lianos, P. High-Yield Luminescence from Cadmium Sulfide Nanoclusters Supported in a Poly(ethylene glycol) Oligomer *Langmuir* **2000**, *16*, 3561-3563.

(47) Woggon, U. Recombination dynamics and nonlinear spectroscopy of quantum dots. *NATO ASI Series, Series B: Physics* **1994**, *339*, 425-450.

(48) Su, W.; Huang, X.; Li, J.; Fu, H. Crystal of Semiconducting Quantum Dots Built on Covalently Bonded T5 [In28Cd6S54]-12: The Largest Supertetrahedral Cluster in Solid State *J. Am. Chem. Soc.* **2002**, *124*, 12944-12945.

(49) Nickel, A.-M. L.; Seker, F.; Ziemer, B. P.; Ellis, A. B. Imprinted Poly(acrylic acid) Films on Cadmium Selenide. A Composite Sensor Structure that Couples Selective Amine Binding with Semiconductor Substrate Photoluminescence *Chem. Mater.* **2001**, *13*, 1391-1397.

(50) Shenhar, R.; Rotello, V. M. Nanoparticles: Scaffolds and Building Blocks *Acc. Chem. Res.* **2003**, *36*, 549-561.

(51) Vossmeyer, T.; Katsikas, L.; Giersig, M.; Popovic, I. G.; Diesner, K.; Chemseddine, A.; Eychmueller, A.; Weller, H. CdS Nanoclusters: Synthesis, Characterization, Size Dependent Oscillator Strength, Temperature Shift of the Excitonic Transition Energy, and Reversible Absorbance Shift *J. Phys. Chem.* **1994**, *98*, 7665-7673.

(52) Goldstein, A. N.; Echer, C. M.; Alivisatos, A. P. Melting in semiconductor nanocrystals. *Science* **1992**, *256*, 1425-1427.

(53) Goldstein, A. N.; Colvin, V. L.; Alivisatos, A. P. Observation of melting in 30-.ANG. diameter cadmium sulfide nanocrystals. *Materials Research Society Symposium Proceedings* **1991**, *206*, 271-274.

(54) Mavoori, H.; Jin, S. Dispersion strengthening for dimensional stability in low-melting-point solders. *JOM* **2000**, *52*, 30-32.

(55) Gao, M.; Lesser, C.; Kirstein, S.; Moehwald, H.; Rogach, A. L.; Weller, H. Electroluminescence of different colors from polycation/CdTe nanocrystal self-assembled films *J. Appl. Phys.* **2000**, *87*, 2297-2302.

(56) Mattoussi, H.; Radzilowski, L. H.; Dabbousi, B. O.; Thomas, E. L.; Rubner, M. F.; Bawendi, M. G. Electroluminescence from heterostructures of poly(phenylene vinylene) and inorganic CdSe nanocrystals. *J. Appl. Phys.* **1998**, *83*, 7965-7974.

(57) Schlamp, M. C.; Peng, X.; Alivisatos, A. P. Improved efficiencies in light emitting diodes made with CdSe(CdS) core/shell type nanocrystals and a semiconducting polymer *J. Appl. Phys.* **1997**, *82*, 5837-5842.

(58) Barnham, K.; Marques, J. L.; Hassard, J.; O'Brien, P. Quantum-dot concentrator and thermodynamic model for the global redshift. *Appl. Phys. Lett.* **2000**, *76*, 1197-1199.

(59) Mattoussi, H.; Mauro, J. M.; Goldman, E. R.; Anderson, G. P.; Sundar, V. C.; Mikulec, F. V.; Bawendi, M. G. Self-Assembly of CdSe-ZnS Quantum Dot Bioconjugates Using an Engineered Recombinant Protein *J. Am. Chem. Soc.* **2000**, *122*, 12142-12150.

(60) Schroedter, A.; Weller, H. Ligand Design and Bioconjugation of Colloidal Gold Nanoparticles *Angew. Chem., Int. Ed.* **2002**, *41*, 3218-3221.

(61) Xiao, Y.; Patolsky, F.; Katz, E.; Hainfeld, J. F.; Willner, I. "Plugging into Enzymes": Nanowiring of Redox Enzymes by a Gold Nanoparticle *Science* **2003**, *299*, 1877-1881.

(62) Gillies, E. R.; Fréchet, J. M. J. Designing Macromolecules for Therapeutic Applications: Polyester Dendrimer-Poly(ethylene oxide) "Bow-Tie" Hybrids with Tunable Molecular Weight and Architecture *J. Am. Chem. Soc.* **2002**, *124*, 14137-14146.

(63) Gilat, S. L.; Adronov, A.; Fréchet, J. M. J. Modular Approach to the Accelerated Convergent Growth of Laser Dye-Labeled Poly(aryl ether) Dendrimers Using a Novel Hypermonomer *J. Org. Chem.* **1999**, *64*, 7474-7484.

(64) Mattoussi, H.; Mauro, J. M.; Goldman, E. R.; Anderson, G. P.; Sundar, V. C.; Mikulec, F. V.; Bawendi, M. G. Self-Assembly of CdSe-ZnS Quantum Dot Bioconjugates Using an Engineered Recombinant Protein. *J. Am. Chem. Soc.* **2000**, *122*, 12142-12150.

(65) Mitch, J. Quantum Dot Lasers Coming Soon *C&EN* **2000**, *23*, 78-79.

(66) Klimov, V. I.; Mikhailovsky, A. A.; S.;, X.; Malko, A.; Hollingsworth, J. A.; Leatherdale, C. A.; Eisler, H.; Bawendi, M. G. Optical gain and stimulated emission in nanocrystal quantum dots. *Science* **2000**, *290*, 314-317.

(67) Rogach, A.; Kershaw, S.; Burt, M.; Harrison, M.; Kornowski, A.; Eychmuller, A.; Weller, H. Colloidally prepared HgTe nanocrystals with strong room-temperature infrared luminescence *Adv. Mater.* **1999**, *11*, 552-555.

(68) Kan, S.; Mokari, T.; Rothenberg, E.; Banin, U. Synthesis and size-dependent properties of zinc-blende semiconductor quantum rods *Nature Materials* **2003**, *2*, 155-158.

(69) Constantine, C. A.; Gattas-Asfura, K. M.; Mello, S. V.; Crespo, G.; Rastogi, V.; Cheng, T.-C.; DeFrank, J. J.; Leblanc, R. M. Layer-by-layer biosensor assembly incorporating functionalized quantum dots. *Langmuir* **2003**, *19*, 9863-9867.

(70) Weller, H.; Fojtik, A.; Henglein, A. Photochemistry of semiconductor colloids: properties of extremely small particles of cadmium phosphide (Cd3P2) and zinc phosphide (Zn3P2). *Chem. Phys. Lett.* **1985**, *117*, 485-488.

(71) Rossetti, R.; Beck, S. M.; Brus, L. E. Direct observation of charge-transfer reactions across semiconductor: aqueous solution interfaces using transient Raman spectroscopy *J. Am. Chem. Soc.* **1984**, *106*, 980-984.

(72) Gaponik, N.; Talapin, D. V.; Rogach, A. L.; Hoppe, K.; Shevchenko, E. V.; Kornowski, A.; Eychmueller, A.; Weller, H. Thiol-Capping of CdTe Nanocrystals: An Alternative to Organometallic Synthetic Routes. *J. Phys. Chem. B* **2002**, *106*, 7177-7185.

(73) Boal, A. K.; Das, K.; Gray, M.; Rotello, V. M. Monolayer Exchange Chemistry of gama-Fe2O3 Nanoparticles. *Chem. Mater.* **2002**, *14*, 2628-2636.

(74) Olshavsky, M. A.; Goldstein, A. N.; Alivisatos, A. P. Organometallic synthesis of gallium-arsenide crystallites, exhibiting quantum confinement *J. Am. Chem. Soc.* **1990**, *112*, 9438.

(75) Kher, S. S.; Wells, R. L. A Straightforward, New Method for the Synthesis of Nanocrystalline GaAs and GaP *Chem. Mater* **1994**, *6*, 2056-2062.

(76) Carpenter, J. P.; Lukehart, C. M.; Henderson, D. O.; Mu, R.; Jones, B. D.; Glosser, R.; Stock, S. R.; Wittig, J. E.; Zhu, J. G. Formation of Crystalline Germanium Nanoclusters in a Silica Xerogel Matrix from an Organogermanium Precursor *Chem. Mater* **1996**, *8*, 1268-1274.

(77) Yang, C.-S.; Kauzlarich, S. M.; Wang, Y. C. Synthesis and Characterization of Germanium/Si-Alkyl and Germanium/Silica Core-Shell Quantum Dots *Chem. Mater.* **1999**, *11*, 3666-3670.

(78) Micic, O. I.; Nenadovic, M. T.; Peterson, M. W.; Nozik, A. J. Size quantization in layered semiconductor colloids with tetrahedral bonding: mercury diiodide *J. Phys. Chem.* **1987**, *91*, 1295-1297.

(79) Wells, R. L.; Aubuchon, S. R.; Kher, S. S.; Lube, M. S.; White, P. S. Synthesis of Nanocrystalline Indium Arsenide and Indium Phosphide from Indium(III) Halides and Tris(trimethylsilyl)pnicogens. Synthesis, Characterization, and Decomposition Behavior of I3In.cntdot.P(SiMe3)3 *Chem. Mater* **1995**, *7*, 793-800.

(80) Peterson, M. W.; Nenadovic, M. T.; Rajh, T.; Herak, R.; Micic, O. I.; Goral, J. P.; Nozik, A. J. Quantized colloids produced by dissolution of layered semiconductors in acetonitrile. *J. Phys. Chem.* **1988**, *92*, 1400-1402.

(81) Chen, S.; Truax, L. A.; Sommers, J. M. Alkanethiolate-Protected PbS Nanoclusters: Synthesis, Spectroscopic and Electrochemical Studies *Chem. Mater.* **2000**, *12*, 3864-3870.

(82) Yu, W. W.; Falkner, J. C.; Shih, B. S.; Colvin, V. L. Preparation and Characterization of Monodisperse PbSe Semiconductor Nanocrystals in a Noncoordinating Solvent *Chem. Mater.* **2004**, *16*, 3318-3322.

(83) English, D. S.; Pell, L. E.; Yu, Z.; Barbara, P. F.; Korgel, B. A. Size Tunable Visible Luminescence from Individual Organic Monolayer Stabilized Silicon Nanocrystal Quantum Dots *Nano Letters* **2002**, *2*, 681-685.

(84) Brus, L. E.; Szajowski, P. F.; Wilson, W. L.; Harris, T. D.; Schuppler, S.; Citrin, P. H. Electronic Spectroscopy and Photophysics of Si Nanocrystals: Relationship to Bulk c-Si and Porous Si *J. Am. Chem. Soc.* **1995**, *117*, 2915-2922.

(85) Chiodini, N.; Paleari, A.; DiMartino, D.; Spinolo, G. SnO2 nanocrystals in SiO2: a wide-band-gap quantum-dot system. *Appl. Phys. Lett.* **2002**, *18*, 1702-1704.

(86) Wageh, S.; Ling, Z. S.; Xu, X.-R. Growth and optical properties of colloidal ZnS nanoparticles *Journal of Crystal Growth* **2003**, *255*, 332-337.

(87) Steigerwald, M. L.; Brus, L. E. Semiconductor crystallites: a class of large molecules *Acc. Chem. Res.* **1990**, *23*, 183-188.

(88) Peng, Z. A.; Peng, X. Nearly Monodisperse and Shape-Controlled CdSe Nanocrystals via Alternative Routes: Nucleation and Growth *J. Am. Chem. Soc.* **2002**, *124*, 3343-3353.

(89) Manna, L.; Scher, E. C.; Alivisatos, A. P. Synthesis of Soluble and Processable Rod-, Arrow-, Teardrop-, and Tetrapod-Shaped CdSe Nanocrystals *J. Am. Chem. Soc.* **2000**, *122*, 12700-12706.

(90) Reiss, P.; Bleuse, J.; Pron, A. Highly Luminescent CdSe/ZnSe Core/Shell Nanocrystals of Low Size Dispersion *Nano Letters* **2002**, *2*, 781-784.

(91) Myung, N.; Bae, Y.; Bard, A. J. Enhancement of the Photoluminescence of CdSe Nanocrystals Dispersed in CHCl3 by Oxygen Passivation of Surface States *Nano Letters* **2003**, *3*, 747-749.

(92) Myung, N.; Bae, Y.; Bard, A. J. Effect of Surface Passivation on the Electrogenerated Chemiluminescence of CdSe/ZnSe Nanocrystals *Nano Letters* **2003**, *3*, 1053-1055.

(93) Peng, X.; Schlamp, M. C.; Kadavanich, A. V.; Alivisatos, A. P. Epitaxial Growth of Highly Luminescent CdSe/CdS Core/Shell Nanocrystals with Photostability and Electronic Accessibility *J. Am. Chem. Soc.* **1997**, *119*, 7019-7029.

(94) Li, J. J.; Wang, Y. A.; Guo, W.; Keay, J. C.; Mishima, T. D.; Johnson, M. B.; Peng, X. Large-Scale Synthesis of Nearly Monodisperse CdSe/CdS Core/Shell Nanocrystals Using Air-Stable Reagents via Successive Ion Layer Adsorption and Reaction *J. Am. Chem. Soc.* **2003**, *125*, 12567-12575.

(95) Cao, Y.; Banin, U. Growth and Properties of Semiconductor Core/Shell Nanocrystals with InAs Cores *J. Am. Chem. Soc.* **2000**, *122*, 9692-9702.

(96) Talapin, D. V.; Mekis, I.; Gotzinger, S.; Kornowski, A.; Benson, O.; Weller, H. CdSe/CdS/ZnS and CdSe/ZnSe/ZnS Core-Shell-Shell Nanocrystals *J. Phys. Chem. B* **2004**, *108*, 18826-18831.

(97) Mews, A.; Eychmueller, A.; Giersig, M.; Schooss, D.; Weller, H. Preparation, characterization, and photophysics of the quantum dot quantum well system cadmium sulfide/mercury sulfide/cadmium sulfide. *J. Phys. Chem.* **1994**, *98*, 934-941.

(98) Mews, A.; Kadavanich, A. V.; Banin, U.; Alivisatos, A. P. Structural and spectroscopic investigations of CdS/HgS/CdS quantum-dot quantum wells. *Phys. Rev. B* **1996**, *53*, R13242-R13245.

(99) Qu, L.; Peng, X. Control of Photoluminescence Properties of CdSe Nanocrystals in Growth *J. Am. Chem. Soc.* **2002**, *124*, 2049-2055.

(100) Veinot, J. G. C.; Galloro, J.; Pugliese, L.; Pestrin, R.; Pietro, W. J. Surface Functionalization of Cadmium Sulfide Quantum-Confined Nanoclusters. 5. Evidence of Facile Surface-Core Electronic Communication in the Photodecomposition Mechanism of Functionalized Quantum Dots *Chem. Mater.* **1999**, *11*, 642-648.

(101) Chen, C.-C.; Yet, C.-P.; Wang, H.-N.; Chao, C.-Y. Self-Assembly of Monolayers of Cadmium Selenide Nanocrystals with Dual Color Emission *Langmuir* **1999**, *15*, 6845-6850.

(102) Brust, M.; Walker, M.; Bethell, D.; Schiffrin, D. J.; Whyman, R. Synthesis of thiol-derivatized gold nanoparticles in a two-phase liquid-liquid system. *J. Chem. Soc., Chem. Commun.* **1994**, *7*, 801-802.

(103) Imahori, H.; Arimura, M.; Hanada, T.; Nishimura, Y.; Yamazaki, I.; Sakata, Y.; Fukuzumi, S. Photoactive Three-Dimensional Monolayers: Porphyrin-Alkanethiolate-Stabilized Gold Clusters *J. Am. Chem. Soc.* **2001**, *123*, 335-336.

(104) Wuelfing, W. P.; Gross, S. M.; Miles, D. T.; Murray, R. W. Nanometer Gold Clusters Protected by Surface-Bound Monolayers of Thiolated Poly(ethylene glycol) Polymer Electrolyte *J. Am. Chem. Soc.* **1998**, *120*, 12696-12697.

(105) Lakowicz, J. R.; Gryczynski, I.; Gryczynski, Z.; Nowaczyk, K.; Murphy, C. J. Time-Resolved Spectral Observations of Cadmium-Enriched Cadmium Sulfide Nanoparticles and the Effects of DNA Oligomer Binding. *Analytical Biochemistry* **2000**, *280*, 128-136.

(106) Peng, X.; Wang, Y. A.; Li, J. J.; Chen, H. Stabilization of Inorganic Nanocrystals by Organic Dendrons *J. Am. Chem. Soc.* **2002**, *124*, 2293-2298.

(107) Mitchell, G. P.; Mirkin, C. A.; Letsinger, R. L. Programmed Assembly of DNA Functionalized Quantum Dots *J. Am. Chem. Soc.* **1999**, *121*, 8122-8123.

(108) Pathak, S.; Choi, S.-K.; Arnheim, N.; Thompson, M. E. Hydroxylated Quantum Dots as Luminescent Probes for in Situ Hybridization *J. Am. Chem. Soc.* **2001**, *123*, 4103-4104.

(109) Zamborini, F. P.; Gross, S. M.; Murray, R. W. Synthesis, Characterization, Reactivity, and Electrochemistry of Palladium Monolayer Protected Clusters *Langmuir* **2001**, *17*, 481-488.

(110) Templeton, A. C.; Wuelfing, W. P.; Murray, R. W. Monolayer-Protected Cluster Molecules *Acc. Chem. Res.* **2000**, *33*, 27-36.

(111) Veinot, J. G. C.; Ginzburg, M.; Pietro, W. J. Surface Functionalization of Cadmium Sulfide Quantum-Confined Nanoclusters. 3. Formation and Derivatives of a Surface Phenolic Quantum Dot. *Chem. Mater.* **1997**, *9*, 2117-2122.

(112) Aldana, J.; Wang, Y. A.; Peng, X. Photochemical Instability of CdSe Nanocrystals Coated by Hydrophilic Thiols *J. Am. Chem. Soc.* **2001**, *123*, 8844-8850.

(113) Flory, P. J. *Principles of Polymer Chemistry*; Cornell University Press: Ithica.

(114) Flory, P. J. Molecular size distribution in three-dimensional polymers. VI. Branched polymer containing A-R-Bf-1-type units. *J. Am. Chem. Soc.* **1952**, *74*, 2718.

(115) Buhleier, E.; Wehner, W.; Voegtle, F. "Cascade"- and "nonskid-chain-like" syntheses of molecular cavity topologies. *Synthesis* **1978**, *2*, 155-158.

(116) Newkome, G. R.; Yao, Z.; Baker, G. R.; Gupta, V. K. Micelles. Part 1. Cascade molecules: a new approach to micelles. A [27]-arborol *J. Org. Chem.* **1985**, *50*, 2003-2004.

(117) Daniel, M.-C.; Ruiz, J.; Nlate, S.; Blais, J.-C.; Astruc, D. Nanoscopic Assemblies between Supramolecular Redox Active Metallodendrons and Gold Nanoparticles: Synthesis, Characterization, and Selective Recognition of H2PO4-, HSO4-, and Adenosine-5'-Triphosphate (ATP2-) Anions *J. Am. Chem. Soc.* **2003**, *125*, 2617-2628.

(118) Ruiz, J.; Lafuente, G.; Marcen, S.; Ornelas, C.; Lazare, S.; Cloutet, E.; Blais, J.-C.; Astruc, D. Construction of Giant Dendrimers Using a Tripodal Building Block *J. Am. Chem. Soc.* **2003**, *125*, 7250-7257.

(119) Bosman, A. W.; Janssen, H. M.; Meijer, E. W. About Dendrimers: Structure, Physical Properties, and Applications *Chem. Rev.* **1999**, *99*, 1665-1688.

(120) Singh, P.; Moll, F., III; ; Lin, S. H.; Ferzli, C.; Yu, K. S.; Koski, R. K.; Saul, R. G.; Cronin, P. Starburst dendrimers: enhanced performance and flexibility for immunoassays. *Clin. Chem.* **1994**, *40*, 1845-1849.

(121) Wiener, E. C.; Brechbiel, M. W.; Brothers, H.; Magin, R. L.; Gansow, O. A.; Tomalia, D. A.; Lauterbur, P. C. Dendrimer Based Metal Chelates. A New Class of Magnetic Resonance Imaging Contrast Agents *Magn. Reson. Med.* **1994**, *31*, 1-8.

(122) Langereis, S.; De Lussanet, Q. G.; Van Genderen, M. H. P.; Backes, W. H.; Meijer, E. W. Multivalent Contrast Agents Based on Gadolinium-Diethylenetriaminepentaacetic Acid-Terminated Poly(propylene imine) Dendrimers for Magnetic Resonance Imaging. *Macromolecules* **2004**, *37*, 3084-3091.

(123) Lui, M.; Fréchet, J. M. J. Designing dendrimers for drug delivery. *Pharm. Sci. Technol. Today* **1999**, *2*, 393-401.

(124) Liu, M.; Kono, K.; Fréchet, J. M. J. Water-soluble dendritic unimolecular micelles:: Their potential as drug delivery agents *J. Controlled Release* **2000**, *65*, 121-131.

(125) Twyman, L. J.; King, A. S. H.; Martin, I. K. Catalysis inside dendrimers. *Chem. Soc. Rev.* **2002**, *31*, 69-82.

(126) Devadoss, C.; Bharathi, P.; Moore, J. S. Energy Transfer in Dendritic Macromolecules: Molecular Size Effects and the Role of an Energy Gradient. *J. Am. Chem. Soc.* **1996**, *118*, 9635-9644.

(127) Xu, Z.; Moore, J. S. Design and synthesis of a convergent and directional molecular antenna. *Acta Polymerica* **1994**, *45*, 83-87.

(128) Wörner, C.; Mülhaupt, R. Polynitrile- and Polyamine-Functional Poly(trimethylene imine) Dendrimers *Angew. Chem., Int. Ed. Engl.* **1993**, *32*, 1306-1311.

(129) De Brabander-Van Den Berg, E. M. M.; Meijer, E. W. Poly(propylenimine) dendrimers: large-scale synthesis via heterogeneously catalyzed hydrogenation. *Angew. Chem., Int. Ed. Engl.* **1993**, *32*, 1308-1311.

(130) Archut, A.; Vögtle, F. Functional cascade molecules. *Chem. Soc. Rev.* **1998**, *27*, 233-240.

(131) Wooley, K. L.; Hawker, C. J.; Fréchet, J. M. J. Hyperbranched macromolecules via a novel double-stage convergent growth approach *J. Am. Chem. Soc.* **1991**, *113*, 4252-4261.

(132) Zeng, F.; Zimmerman, S. C. Dendrimers in Supramolecular Chemistry: From Molecular Recognition to Self-Assembly *Chem. Rev.* **1997**, *97*, 1681-1712.

(133) Hecht, S.; Fréchet, J. M. J. Dendritic encapsulation of function: applying nature's site isolation principle from biomimetics to materials science. *Angew. Chem., Int. Ed.* **2001**, *40*, 74-91.

(134) Lim, Y.-b.; Kim, T.; Lee, J. W.; Kim, S.-m.; Kim, H.-J.; Kim, K.; Park, J.-s. Self-Assembled Ternary Complex of Cationic Dendrimer, Cucurbituril, and DNA: Noncovalent Strategy in Developing a Gene Delivery Carrier *Bioconjugate Chem.* **2002**, *13*, 1181-1185.

(135) Lochmann, L.; Wooley, K. L.; Ivanova, P. T.; Fréchet, J. M. J. Multisite functionalized dendritic macromolecules prepared via metalation by superbases and reaction with electrophiles *J. Am. Chem. Soc.* **1993**, *115*, 7043-7044.

(136) Grayson, S. M.; Fréchet, J. M. J. Convergent Dendrons and Dendrimers: from Synthesis to Applications *Chem. Rev.* **2001**, *101*, 3819-3867.

(137) Peterson, J.; Allikmaa, V.; Subbi, J.; Pehk, T.; Lopp, M. Structural deviations in poly(amidoamine) dendrimers: a MALDI-TOF MS analysis. *Euro. Pol. J.* **2003**, *39*, 33-42.

(138) Terrill, R. H.; Postlethwaite, T. A.; Chen, C.-h.; Poon, C.-D.; Terzis, A.; Chen, A.; Hutchison, J. E.; Clark, M. R.; Wignall, G.; Murray, R. W. Monolayers in Three Dimensions: NMR, SAXS, Thermal, and Electron Hopping Studies of Alkanethiol Stabilized Gold Clusters *J. Am. Chem. Soc.* **1995**, *117*, 12537-12548.

(139) Ingram, R. S.; Hostetler, M. J.; Murray, R. W. Poly-hetero--functionalized Alkanethiolate-Stabilized Gold Cluster Compounds *J. Am. Chem. Soc.* **1997**, *119*, 9175-9178.

(140) Templeton, A. C.; Hostetler, M. J.; Kraft, C. T.; Murray, R. W. Reactivity of Monolayer-Protected Gold Cluster Molecules: Steric Effects *J. Am. Chem. Soc.* **1998**, *120*, 1906-1911.

(141) Fox, M. A.; Whitesell, J. K.; McKerrow, A. J. Fluorescence and Redox Activity of Probes Anchored through an Aminotrithiol to Polycrystalline Gold. *Langmuir* **1998**, *14*, 816-820.

(142) Hostetler, M. J.; Green, S. J.; Stokes, J. J.; Murray, R. W. Monolayers in Three Dimensions: Synthesis and Electrochemistry of -Functionalized Alkanethiolate-Stabilized Gold Cluster Compounds *J. Am. Chem. Soc.* **1996**, *118*, 4212-4213.

(143) Fujihara, H.; Nakai, H. Fullerenethiolate-Functionalized Gold Nanoparticles. A New Class of Surface-Confined Metal-C_{60} Nanocomposite *Langmuir* **2001**, *17*, 6393-6395.

(144) Ding, S.-Y.; Jones, M.; Tucker, M. P.; Nedeljkovic, J. M.; Wall, J.; Simon, M. N.; Rumbles, G.; Himmel, M. E. Quantum Dot Molecules Assembled with Genetically Engineered Proteins *Nano Letters* **2003**, *3*, 1581-1585.

(145) Storhoff, J. J.; Mirkin, C. A. Programmed Materials Synthesis with DNA *Chem. Rev.* **1999**, *99*, 1849-1862.

(146) Lemon, B. I.; Crooks, R. M. Preparation and Characterization of Dendrimer-Encapsulated CdS Semiconductor Quantum Dots *J. Am. Chem. Soc.* **2000**, *122*, 12886-12887.

(147) Fendler, J. H.; Dekany, I. *Nanoparticles in Solids and Solutions*; Kluwer, Dordrecht, Neth.: Amsterdam, 1996; Vol. 18.

(148) Hanus, L. H.; Sooklal, K.; Murphy, C. J.; Ploehn, H. J. Aggregation Kinetics of Dendrimer-Stabilized CdS Nanoclusters *Langmuir* **2000**, *16*, 2621-2626.

(149) Huang, J.; Sooklal, K.; Ploehn, H. J.; Murphy, C. J. Polyamine-Quantum Dot Nanocomposites: Linear versus Starburst Stabilizer Architectures *Chem. Mater.* **1999**, *11*, 3595-3601.

(150) Ispasoiu, R. G.; Balogh, L.; Varnavski, O. P.; Tomalia, D. A.; Goodson, T. G., III; Large Optical Limiting from Novel Metal-Dendrimer Nanocomposite Materials *J. Am. Chem. Soc.* **2000**, *122*, 11005-11006.

(151) Zheng, J.; Petty, J. T.; Dickson, R. M. High Quantum Yield Blue Emission from Water-Soluble Au8 Nanodots. *J. Am. Chem. Soc.* **2003**, *125*, 7780-7781.

(152) Zhao, M.; Crooks, R. M. Intradendrimer Exchange of Metal Nanoparticles *Chem. Mater.* **1999**, *11*, 3379-3385.

(153) Chechik, V.; Crooks, R. M. Monolayers of Thiol-Terminated Dendrimers on the Surface of Planar and Colloidal Gold *Langmuir* **1999**, *15*, 6364-6369.

(154) Daniel, M.-C.; Astruc, D. Gold Nanoparticles: Assembly, Supramolecular Chemistry, Quantum-Size-Related Properties, and Applications toward Biology, Catalysis, and Nanotechnology *Chem. Rev.* **2004**, *104*, 293-346.

(155) Gu, T.; Whitesell, J. K.; Fox, M. A. Energy Transfer from a Surface-Bound Arene to the Gold Core in -Fluorenyl-Alkane-1-Thiolate Monolayer-Protected Gold Clusters *Chem. Mater.* **2003**, *15*, 1358-1366.

(156) Gopidas, K. R.; Whitesell, J. K.; Fox, M. A. Nanoparticle-Cored Dendrimers: Synthesis and Characterization *J. Am. Chem. Soc.* **2003**, *125*, 6491-6502.

(157) Donners, J. J. J. M.; Hoogenboom, R.; Schenning, A. P. H. J.; van Hal, P. A.; Nolte, R. J. M.; Meijer, E. W.; Sommerdijk, N. A. J. M. Fabrication of Organic-Inorganic Semiconductor Composites Utilizing the Different Aggregation States of a Single Amphiphilic Dendrimer *Langmuir* **2002**, *18*, 2571-2576.

(158) Lakowicz, J. R.; Gryczynski, I.; Gryczynski, Z.; Murphy, C. J. Luminescence Spectral Properties of CdS Nanoparticles *J. Phys. Chem. B* **1999**, *103*, 7613-7620.

(159) Zhang, C.; O'Brien, S.; Balogh, L. Comparison and Stability of CdSe Nanocrystals Covered with Amphiphilic Poly(Amidoamine) Dendrimers *J. Phys. Chem. B* **2002**, *106*, 10316-10321.

(160) Guo, W.; Li, J. J.; Wang, Y. A.; Peng, X. Luminescent CdSe/CdS Core/Shell Nanocrystals in Dendron Boxes: Superior Chemical, Photochemical and Thermal Stability *J. Am. Chem. Soc.* **2003**, *125*, 3901-3909.

(161) Balogh, L.; Tomalia, D. A. Poly(Amidoamine) Dendrimer-Templated Nanocomposites. 1. Synthesis of Zerovalent Copper Nanoclusters *J. Am. Chem. Soc.* **1998**, *120*, 7355-7356.

(162) Gopidas, K. R.; Whitesell, J. K.; Fox, M. A. Synthesis, Characterization, and Catalytic Applications of a Palladium-Nanoparticle-Cored Dendrimer *Nano Letters* **2003**, *3*, 1757-1760.

(163) Liu, D.; De Feyter, S.; Cotlet, M.; Stefan, A.; Wiesler, U.-M.; Herrmann, A.; Grebel-Koehler, D.; Qu, J. M., K.;; DeSchryver, F. C. Fluorescence and Intramolecular Energy Transfer in Polyphenylene Dendrimers *Macromolecules* **2003**, *36*, 5918-5925.

(139) Ingram, R. S.; Hostetler, M. J.; Murray, R. W. Poly-hetero--functionalized Alkanethiolate-Stabilized Gold Cluster Compounds *J. Am. Chem. Soc.* **1997**, *119*, 9175-9178.

(140) Templeton, A. C.; Hostetler, M. J.; Kraft, C. T.; Murray, R. W. Reactivity of Monolayer-Protected Gold Cluster Molecules: Steric Effects *J. Am. Chem. Soc.* **1998**, *120*, 1906-1911.

(141) Fox, M. A.; Whitesell, J. K.; McKerrow, A. J. Fluorescence and Redox Activity of Probes Anchored through an Aminotrithiol to Polycrystalline Gold. *Langmuir* **1998**, *14*, 816-820.

(142) Hostetler, M. J.; Green, S. J.; Stokes, J. J.; Murray, R. W. Monolayers in Three Dimensions: Synthesis and Electrochemistry of -Functionalized Alkanethiolate-Stabilized Gold Cluster Compounds *J. Am. Chem. Soc.* **1996**, *118*, 4212-4213.

(143) Fujihara, H.; Nakai, H. Fullerenethiolate-Functionalized Gold Nanoparticles. A New Class of Surface-Confined Metal-C_{60} Nanocomposite *Langmuir* **2001**, *17*, 6393-6395.

(144) Ding, S.-Y.; Jones, M.; Tucker, M. P.; Nedeljkovic, J. M.; Wall, J.; Simon, M. N.; Rumbles, G.; Himmel, M. E. Quantum Dot Molecules Assembled with Genetically Engineered Proteins *Nano Letters* **2003**, *3*, 1581-1585.

(145) Storhoff, J. J.; Mirkin, C. A. Programmed Materials Synthesis with DNA *Chem. Rev.* **1999**, *99*, 1849-1862.

(146) Lemon, B. I.; Crooks, R. M. Preparation and Characterization of Dendrimer-Encapsulated CdS Semiconductor Quantum Dots *J. Am. Chem. Soc.* **2000**, *122*, 12886-12887.

(147) Fendler, J. H.; Dekany, I. *Nanoparticles in Solids and Solutions*; Kluwer, Dordrecht, Neth.: Amsterdam, 1996; Vol. 18.

(148) Hanus, L. H.; Sooklal, K.; Murphy, C. J.; Ploehn, H. J. Aggregation Kinetics of Dendrimer-Stabilized CdS Nanoclusters *Langmuir* **2000**, *16*, 2621-2626.

(149) Huang, J.; Sooklal, K.; Ploehn, H. J.; Murphy, C. J. Polyamine-Quantum Dot Nanocomposites: Linear versus Starburst Stabilizer Architectures *Chem. Mater.* **1999**, *11*, 3595-3601.

(150) Ispasoiu, R. G.; Balogh, L.; Varnavski, O. P.; Tomalia, D. A.; Goodson, T. G., III; Large Optical Limiting from Novel Metal-Dendrimer Nanocomposite Materials *J. Am. Chem. Soc.* **2000**, *122*, 11005-11006.

(151) Zheng, J.; Petty, J. T.; Dickson, R. M. High Quantum Yield Blue Emission from Water-Soluble Au8 Nanodots. *J. Am. Chem. Soc.* **2003**, *125*, 7780-7781.

(176) Boden, E. P.; Keck, G. E. Proton-transfer steps in Steglich esterification: a very practical new method for macrolactonization *J. Org. Chem.* **1985**, *50*, 2394-2395.

(177) Goossen, L. J.; Ghosh, K. Palladium-Catalyzed Synthesis of Aryl Ketones from Boronic Acids and Carboxylic Acids or Anhydrides *Angew. Chem., Int. Ed.* **2001**, *40*, 3458-3460.

(178) Kim, S.; Lee;, J. I.; Kim;, Y. C. A simple and mild esterification method for carboxylic acids using mixed carboxylic-carbonic anhydrides *J. Org. Chem.* **1985**, *50*, 560-565.

(179) Marshall, J. L.; Erickson, K. C.; Folsom, T. K. Esterification of carboxylic acids using a boron trifluoride-etherate-alcohol reagent. *Tetrahedron Letters* **1970**, *11*, 4011-4012.

(180) Kadaba, P. K. Esterification of heterocyclic carboxylic acids using a boron trifluoride etherate-alcohol reagent. *Synthesis* **1972**, *11*.

(181) Kadaba, P. K. New compounds. Convenient selective esterification of aromatic carboxylic acids bearing other reactive groups using a boron trifluoride etherate-alcohol reagent. *Journal of Pharmaceutical Sciences* **1974**, *63*, 1333-1335.

(182) Sachleben, J. R.; Wooten, E. W.; Emsley, L.; Pines, A.; Colvin, V. L.; Alivisatos, A. P. NMR studies of the surface structure and dynamics of semiconductor nanocrystals *Chem. Phys. Lett.* **1992**, *198*, 431-436.

(183) Zhang, H.; Ma, X.; Ji, Y.; Xu, J.; Yang, D. Single crystalline CdS nanorods fabricated by a novel hydrothermal method. *Chem. Phys. Lett.* **2003**, *377*, 654-657.

(184) Ma, Y.; Qi, L.; Ma, J.; Cheng, H.; Shen, W. Synthesis of Submicrometer-Sized CdS Hollow Spheres in Aqueous Solutions of a Triblock Copolymer. *Langmuir* **2003**, *19*, 9079-9085.

(185) Bao, H.; Gong, Y.; Li, Z.; Gao, M. Enhancement Effect of Illumination on the Photoluminescence of Water-Soluble CdTe Nanocrystals: Toward Highly Fluorescent CdTe/CdS Core-Shell Structure. *Chem. Mater.* **2004**, *16*, 3853-3859.

(186) Omotowa, B. A.; Keefer, K. D.; Kirchmeier, R. L.; Shreeve, J. n. M. Preparation and Characterization of Nonpolar Fluorinated Carbosilane Dendrimers by APcI Mass Spectrometry and Small-Angle X-ray Scattering. *J. Am. Chem. Soc.* **1999**, *121*, 11130-11138.

(187) Wankhede, M. E.; Haram, S. K. Synthesis and Characterization of Cd-DMSO Complex Capped CdS Nanoparticles. *Chemistry of Materials* **2003**, *15*, 1296-1301.

(188) Li, Y.; Liao, H.; Fan, Y.; Li, L.; Qian, Y. A solvothermal synthetic route to CdE (E = S, Se) semiconductor nanocrystalline. *Materials Chemistry and Physics* **1999**, *58*, 87-89.

(189) Peng, X.; Zhang, J.-Y.; Wang, X.-Y.; Xiao, M.; Qu, L. Lattice contraction in free-standing CdSe nanocrystals. *Appl. Phys. Lett.* **2002**, *81*, 2076-2078.

(190) Aldana, J.; Lavelle, N.; Wang, Y.; Peng, X. Size-Dependent Dissociation pH of Thiolate Ligands from Cadmium Chalcogenide Nanocrystals. *J. Am. Chem. Soc.* **2005**, *127*, 2496-2504.

(191) Wuister, S. F.; De Donega, C.; Meijerink, A. Influence of thiol capping on the exciton luminescence and decay kinetics of CdTe and CdSe quantum dots. *J. Phys. Chem. B* **2004**, *108*, 17393-17397.

(192) Trindade, T.; O'Brien, P.; Zhang, X.-m. Synthesis of CdS and CdSe Nanocrystallites Using a Novel Single-Molecule Precursors Approach *Chem. Mater.* **1997**, *9*, 523-530.

(193) Malik, M. A.; Revaprasadu, N.; O'Brien, P. Air-Stable Single-Source Precursors for the Synthesis of Chalcogenide Semiconductor Nanoparticles *Chem. Mater.* **2001**, *13*, 913-920.

(194) Dalba, G.; Fornasini, P.; Grisenti, R.; Pasqualini, D.; Diop, D.; Monti, F. Anharmonicity effects on the extended x-ray-absorption fine structure: The case of cadmium selenide *Phys. Rev. B* **1998**, *58*, 4793-4802.

(195) Rockenberger, J.; Troger, L.; Rogach, A. L.; Tischer, M.; Grundmann, M.; Eychmuller, A.; Weller, H. The contribution of particle core and surface to strain, disorder and vibrations in thiol-capped CdTe nanocrystals *J. Chem. Phys.* **1998**, *108*, 7807-7815.

(196) Marcus, M. M.; Flood, W.; Steigerwald, M.; Brus, L.; Bawendi, M. G. Structure of Capped CdSe Clusters by EXAFS *J. Phys. Chem.* **1991**, *95*, 1572-1576.

(197) Rasheed, K.; Warkentin, J. D. Reactions of S,S'-[2,2'-dithiobis(nitrophenyl)] bis(N,N-dimethylcarbamothioates) with hydroxide and hydrosulfide anions. A synthesis of nitrobenzotrithioles. *J. Org. Chem.* **1980**, *45*, 4806-4807.

(198) Lim, B. B.; Hosmane, R. S. Reagents for bioorganic synthesis. 2. Methyl N-(dicarbomethoxymethyl)methanimidate. *J. Org. Chem.* **1985**, *50*, 5111-5115.